UNIVERSITY OF CALIFORNIA SAN DIEGO

Soil structure interaction of Chilean medium-rise residential building

A Thesis submitted in partial satisfaction of the requirements
for the degree Master of Science

in

Structural Engineering

by

Felipe Bedecarratz

Committee in charge:

Professor José I. Restrepo, Chair
Professor Ahmed Elgamal
Professor Georgios Tsampras

2023

The Thesis of Felipe Bedecarratz is approved, and it is acceptable in quality and form for publication on microfilm and electronically.

University of California San Diego

2023

TABLE OF CONTENTS

LIST OF FIGURES

LIST OF TABLES

ABSTRACT OF THE THESIS

Soil structure interaction of Chilean medium-rise residential building

by

Felipe Bedecarratz

Master of Science in Structural Engineering

University of California San Diego, 2023

Professor José Restrepo, Chair

Soil-structure interaction (SSI) corresponds to the phenomenon that occurs when seismic waves coming from the soil affect the response of a structure and then, the response of the structure affects the response of the soil. It is often thought that the soil-structure interaction is beneficial for the behavior of the structure since it increases the period of the structure and incorporates additional damping due to the radiation of energy into the soil. For this reason, in practice, SSI is either not included when modeling the structure or is replaced by increased viscous damping.

In models developed to perform nonlinear time-history analyses of 3D structures, the soil nonlinearity and radiation damping are often represented by a series of springs and dashpots placed along the height of the piles in two orthogonal directions. This thesis shows that such array results in bias in the response, and an improved array of the p-y springs is discussed.

A case study performed on a typical Chilean mid-rise building founded on piles is presented. To compare the effects of SSI on the building's response, nonlinear fixed-base and on pile models were developed in ETABS 20 and subjected to the strong input ground motion recorded during the 27 February 2010 Mw 8.8 Maule earthquake. The SSI effects resulted in a slight increase in demands of key engineering response parameters, but the increase did not justify the incorporation of SSI in the analysis.

1 INTRODUCTION

Earthquake induced waves travel through the ground dynamically exciting the soil and built infrastructure in its path. The response of the soil to this excitation affects the response of the structures and the response of the structures affects the response of the soil. This is known as soil-structure interaction (SSI). This interaction has two fundamental effects: kinematic and inertial. The kinematic effect depends on the propagation of waves in the structure and in the soil. The ground motion induces deformations in the structure and the structure constrains the ground motion, i.e., the free-field motion of the soil is modified near the structure. The inertial effect is caused by the inertial forces generated by accelerating the mass of the structure.

Considering soil-structure interaction can be important when evaluating the seismic response of a structure. For this there are direct and discrete methods of analysis (Figure 1-1). The direct methods use finite elements to model the soil as a continuum and interface elements between the soil and the foundation. The discrete methods model the interaction between the soil and the structure by means of springs and dampers. Whereas the former is the preferred method of choice in the analyses of dams and tunnels, the latter is the most commonly accepted method in the analyses of large structural engineering building and bridge projects in practice.

For the interaction between the soil and the structure, an indirect method considering vertical and horizontal nonlinear springs, linear springs and dampers is considered. Discrete methods are more applicable in practice due to the fact that direct methods are computationally very expensive. The indirect method also allows to visualize the different components of the interaction separately. However, when using springs in the 3D model there is a problem that is

important to consider. Typically, the springs configuration used considers only 2 springs connected orthogonally, so that one spring is aligned with the X- and the other with Y-direction of analysis. The problem that is generated is that when using nonlinear springs, if the load is applied diagonally (45 degrees) and both springs start yielding, an overestimation of the force is generated since the resultant of the spring force is 1.41 times the yield force of one spring. This report analyzes different spring configurations in three dimensions and compares their behavior.

In addition, a discrete SSI model is implemented for the case of a 23-story concrete building with pre-drilled concrete pile foundations. The results obtained with SSI are compared with the results of a fixed-base model typically used in practice.

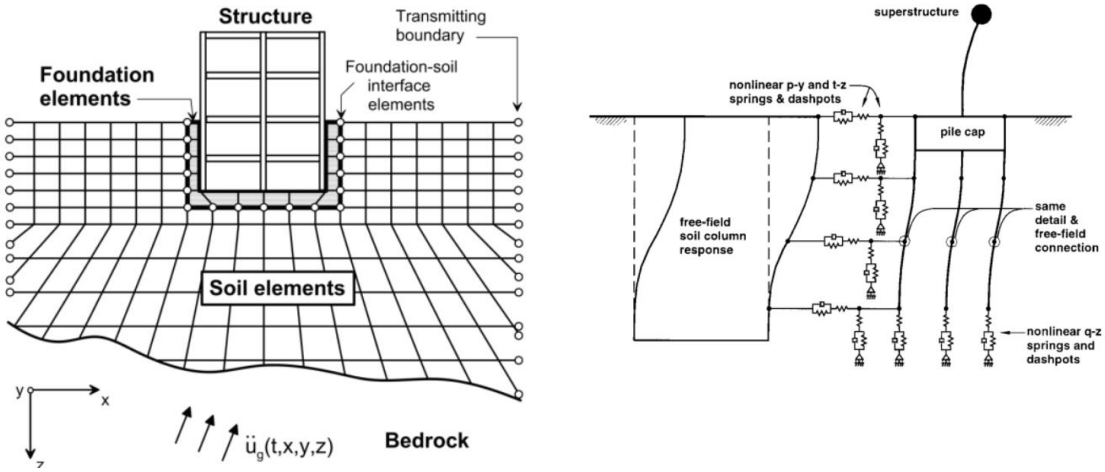

a) Direct Model, NIST (2012) **b) Discrete Model, Curras et al. (2001)**

Figure 1-1: Model types

1.1 PROBLEM DESCRIPTION

In the past ten years there has been an increase in the use of nonlinear time-history structural analysis, especially for performance-based design. Some of the buildings analyzed

using this method are founded in deep foundations and in these cases the piles need to be properly modeled to carry out performance-based design. There are different ways to perform this modeling, but they can be divided into two categories: continuum modeling, for example the model developed by Elgamal et al. (2008), and discrete modeling, for example the model described by Boulanger et al. (1999). The discrete models are an accepted approximation to the continuum but less expensive computationally. The discrete modeling for piles is typically done using p-y springs. When performing a 3D model, in practice, an L Shape (orthogonal) configuration of springs has been accepted but as shown here, such modeling assumption can be questionable.

The purpose of this thesis is to 1) critically evaluate the behavior of different configurations of p-y springs in 3D simple structures and 2) to perform a 3D model of a building with piles foundations designed using Chilean standards and compare the response with and without incorporating soil-structure interaction.

1.2 OBJECTIVES

The objectives of this thesis are the following:

- Perform a literature review of soil-structure interaction modelling.
- Evaluate the performance on different spring configurations to generate a discrete model including SSI.
- Estimate the behavior of a pile-supported medium-height building of complex geometry using a nonlinear numerical finite element model incorporating soil-structure

interaction. To the knowledge of the author, this is the first time that such type of analysis has ever been conducted.

- Compare results of the nonlinear model with soil-structure interaction with a fixed-base nonlinear model.

1.3 OUTLINE

This thesis is divided into six chapters. The first chapter presents the introduction to the subject, the problem to be studied and the objectives of the work. In the second chapter, a review of the literature is done incorporating the studies that have been carried out on SSI and the types of modeling that can be used for the analysis. In addition, the provisions of international codes on the subject are reviewed. The third chapter defines the model considered in this thesis to incorporate SSI in the analysis and studies different springs configurations that can be used. The fourth chapter presents the building to be analyzed and the nonlinear model generated with and without SSI. The fifth chapter presents the analysis of the results obtained for the building and how the inclusion of SSI in the nonlinear model affects it. Finally, the sixth chapter presents the conclusions and final remarks of the work.

2 LITERATURE REVIEW

2.1 HISTORY OF SOIL-STRUCTURE INTERACTION

According to Roësset (2013), the first approach to seismic soil-structure interaction was made by Okabe (1926), and Mononabe and Matsuo (1929) studying the seismic effects of soil on a retaining wall. However, the first time the seismic soil-structure interaction effects were mentioned in the United States was by Martel (1940) reporting observations from the 1933 Long Beach earthquake. During the 60s and 70s research on the subject increased considerably because of the design of new nuclear plants. Biggs (1964) presents a simple model with elastic foundations using constant stiffness springs to simulate the foundation stiffness. Whitman (1970) presents for the first time the soil-structure interaction in seismic design, specifically related to nuclear plants, and also introduces for the first time the terms inertial and kinematic interaction effects. The first models that incorporated soil nonlinearity (using equivalent linearization) were those of Kausel and Roesset (1974) and Lysmer et al. (1974). These models were idealized cases analyzed in the frequency domain without considering nonlinearities in the structure. Luco (1974) presents a more realistic model with a layered half space soil.

With respect to SSI with piles, one of the pioneers in analyzing these effects was Priestley (1974) for static lateral loading. It is worth mentioning the work done by Cox and Reese (1974) who were the first to introduce the concept of p-y springs. The p-y springs represent the lateral resistance of the soil by generating a relation between the lateral pile force on the soil p and the lateral displacement of the pile y. The p-y springs resemble Winkler springs (1867) used in the analysis of continuous foundation beams, which introduce the concept of subgrade modulus developed by Terzaghi (1955). The dynamic stiffness of a single pile was

first studied by Novak (1974). Then, Kaynia and Kausel (1982) and Gomez (1982) studied the dynamic stiffness of pile groups. There is still controversy on this subject, especially in the definition of group factors for dynamically loaded piles and it is still a subject of research.

To this day there is much to be done regarding the study of SSI. However, the books published by Wolf (1985, 1988) present the theory and basis of the phenomenon in a rigorous and comprehensive manner. A detailed review of the early stages of soil-structure interaction is presented by Roesset (2013) and Kausel (2010). Also, Anand and Kumar (2018) review the state of the art in this subject.

2.2 METHODS OF ANALYSIS

Soil-structure interaction (SSI) is defined as the process of soil response influencing the movement of a structure and vice versa. SSI has generally been considered beneficial to seismic response of a structure but there is evidence that this is not always the case as Mylonakis and Gazetas (2000) pointed out. There is a need for design guidelines to take this phenomenon into account. In general, it is mentioned in the codes but there is no detailed procedure for its incorporation.

SSI is composed of the free field response, the kinematic effect, and the inertial effect. The free field corresponds to the response of the soil when no structure is present, i.e., only the soil. The kinematic effects are associated with the diffraction of the incident waves on the foundation when it is fixed and weightless. Inertial effects correspond to the influence of the vibration of the structure on the foundation soil.

There has been a lack of consensus among researchers about the effects of SSI when a structure is dynamically excited via earthquake induced input ground motions. Traditionally, it is assumed that the incorporation of SSI is beneficial to the structure because it reduces the stiffness of the system, increases the predominant period, and the effective damping ratio. Therefore, in design, in order to consider the effect of SSI, the seismic coefficient is usually reduced, or SSI is simply ignored. However, Miranda and Bertero (1994) noted that in soft soil there is an increase in the ductility demand with an increase of the predominant period by 20%, which indicates a detrimental nature of the SSI. Also, Gazetas and Mylonakis (2001) evidenced that SSI played a role in the collapse of structures in the 1994 Kobe earthquake. Gazetas and Mylonakis (2000) concluded that SSI effects can be detrimental in some cases and assuming that SSI is always beneficial is an oversimplification which leads to unsafe designs.

Several parametric studies on the influence of SSI have been conducted and some of these are mentioned below. Van Nguyen et al. (2016) analyzed the effect of the size of shallow foundations noting that larger foundations can moderate lateral deflection amplification and that larger foundations attract larger inertial forces. With respect to piles, Van Nguyen et al. (2017) concluded that the type and size of piles influence the dynamic characteristics and seismic response of the building due to SSI. Saez et al. (2013) investigated the influence of inelastic dynamic soil-structure interaction in frame buildings noting that in saturated soils the SSI effects were favorable or negligible. Jarernprasert et al. (2013) noted that incorporating SSI generated higher ductility demands and larger displacements in one-story structures. In addition

to those mentioned above are the analyses by Ciampoli and Pinto (1995), De Carlo et al. (2000), Raychowdhury (2011), Hassani et al. (2018), among others.

Regarding the study of SSI, efforts have been made to obtain solutions from the analytical and experimental point of view. On the analytical side, it is worth mentioning the general formulation for the dynamic response of piles and pile groups in stratified soil using Green's functions by Kaynia and Kausel (1991). On the experimental side, one can point out the shaking table tests performed by Gazetas and Stokoe (1991), the soil shaking table tests with embedded piles by Durante et al. (2016), the geotechnical centrifuge experiments by Hussien et al. (2016) of the kinematic and experimental effects of soil-pile-structure interaction, the dynamic centrifuge tests of Martakis et al. (2017), the full-scale dynamic test of Zangeneh et al. (2018) of SSI of a railway bridge. Finally, it is important to note the dynamic centrifuge tests of Boulanger et al. (1999) for the validation of the dynamic p-y spring pile model which is used in the present work.

There are different ways of modeling soil-structure interaction but in general they can be divided into 2 categories: discrete modeling and continuous modeling. In discrete modeling, springs and dampers are used for the interface elements, some examples are the Winkler model (1867), the Filonenko-Borodich model (1940), Hetenyi's model (1946), Kerr model (1965), and the beam-column analogy developed by Horvath (1993). On the other hand, in continuous modeling, finite elements or boundary elements are used to model the interface. NIST (2012) provides some comparisons using different types of models and provides some design guidelines.

Another way to differentiate model types is whether these are linear models or not. The nonlinearity in the model can be included in interface elements such as p-y and t-z springs, in the materials of the structure, in the soil (e.g., considering liquefaction), with geometric nonlinearity or using gap elements between the foundation and the soil. Some examples are Ciampoli and Pinto (1995), Mylonakis and Gaztetas (2000) that incorporate nonlinearity in the structure. Raychowdhury and Hutchinson (2009) incorporated the BNWF (beam on nonlinear Winkler foundation) model in OpenSees to consider nonlinear foundation and soil. Other models such as PBM (plasticity based macro-element) developed by Nova and Montrasio (1991) or CIM (contact interface model) developed by Gajan and Kutter (2009) include nonlinearity in soil and through gap elements, respectively. Soil degradation curves are also part of the nonlinearity of the model, these curves represent the variation of soil stiffness and damping as a function of its deformation, among the most used curves are the curves of Idriss and Seeds (1970) and those of Darandeli (2001).

Also, a model can be categorized depending on whether it is performed in the frequency domain or in the time domain. In general, the models in the frequency domain are simplified and, to solve the equations of motion, the fast Fourier transformation is used, and linearity is required. On the other hand, in the time domain, the incorporation of nonlinearities described above is allowed.

2.3 DESIGN CODES

Currently, due to the lack of consensus on the subject, the design codes, although they mention SSI, in general, do not give details on how to incorporate it in the models or what criteria should be considered; there are no detailed design guidelines. The ATC3-06 (1978) model code stated that soil-structure interaction is an issue, and suggested decrease in the base shear and an increase in the equivalent viscous damping as a way to incorporate SSI effects, i.e., tacitly assuming SSI is always beneficial. Then, the ASCE7-10 standard (2010) incorporates constraints on the base shear reduction when incorporating SSI. NEHRP FEMA (2015) includes functions relating base shear reduction to modifying factors. The ASCE7-16 standard (2016) allows for a dynamic linear analysis using a modified general design response spectrum due to SSI and also allows for using a site-specific design spectrum to be evaluated by the engineer.

Other countries also mention SSI. In Europe, Eurocode 8, EN 1998-5 (2004) suggests performing a dynamic SSI analysis on slender structures but does not provide guidance in this regard. In India, IS 1893-3 (2014) and IS 1893-4 (2015) suggest considering SSI in some special cases. In Japan, JSCE 15 (2007) leave it to the designer's discretion whether to incorporate SSI. In New Zealand, NZS 1170.5 (2004) does not provide guidance in this regard but includes a structural performance factor.

In general, current design codes do not provide design guidelines indicating how SSI should be incorporated. NIST (2012) suggests some checklists that can be performed for modeling. Companies such as ARUP are using software (e.g., LS-DYNA) to perform

continuum models of the structure incorporating structure, foundations, and soil in both 2D and 3D models (Shao, 2022). In general, these models are used for checking structures designed considering fixed-base.

2.4 CONCLUSIONS

In this chapter, a general review of the literature on soil-structure interaction and its modeling was carried out. According to the review, to the date there have been no publications on 3D nonlinear analysis of complex geometry buildings with piles, so this work would be the first effort to perform such analysis. For this, a discrete model is considered due to its simplicity compared to a continuous model. Specifically, the SSI model for piles proposed by Boulanger et al. (1999) and Curras et al. (2001) is implemented. This model uses one-dimensional springs to represent the p-y curves and one-dimensional dampers to incorporate the radiation damping in the soil. The analysis is performed in the time domain and incorporates nonlinearity in the materials of the structure and in the soil springs. The details of the modeling and analysis are described in the following chapters.

3 MODELING PILES FOR 3D NONLINEAR TIME-HISTORY ANALYSIS OF BUILDING VIA SOIL SPRINGS

3.1 SOIL SPRINGS DEFINITION

Boulanger et al. (1999) proposed a nonlinear model to analyze the seismic soil-pile-structure interaction based on the work done by Wang et al. (1998). The model developed for an individual pile corresponds to a dynamic beam in a nonlinear Winkler foundation, also referred to as a "dynamic p-y" model. In other words, this model consists of a frame element to represent the pile and nonlinear p-y springs distributed vertically along the pile to represent the lateral soil reaction. The superstructure is represented by an extension of the pile above ground level and a mass at the top. The model input corresponds to the free-field response of the soil column. The displacements of the soil column are transmitted through the p-y springs along the pile. A schematic of the model of Boulanger et al. (1999) is presented in the Figure 3-1.

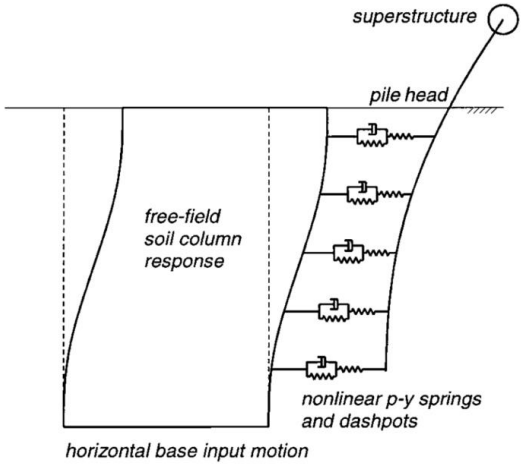

Figure 3-1: Schematic Boulanger et al. (1999) model

Curras et al. (2001), considering the model of Boulanger et al. (1999), proposed a model for a group of piles. In this case, in addition to the lateral resistance springs (p-y springs), it is also necessary to incorporate vertical springs to account for the interaction of the pile with the soil due to the generation of rocking motions of the system. The vertical springs are the t-z and q-z sprigns to represent the vertical frictional resistance and vertical tip resistance, respectively. In addition, it is necessary to include a group factor (p-multiplier) that modifies the lateral response of the pile. In this case, an average value for this parameter equal to 0.7 is assumed to simplify the model.

Therefore, for the soil-structure interaction, p-y springs, t-z springs, and q-z springs are considered to represent lateral soil resistance, vertical frictional resistance, and vertical tip resistance, respectively. These three elements are composed of a plastic part and an elastic part connected in series. The plastic part is a nonlinear spring that allows incorporating the hysteretic response (near field element). The elastic part consists of a linear spring and a viscous damper connected in parallel (far field element). The viscous damper in the elastic part is included to account for radiation damping. Figure 3-2 shows the typical soil spring. The term p-y springs, t-z springs or q-z springs refers to the element composed of the plastic and elastic parts.

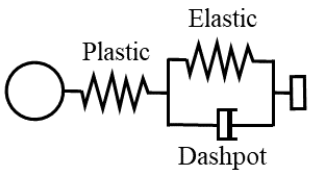

Figure 3-2: Soil spring

The p-y and t-z springs are connected to each pile node. In the model, coupling between p-y and t-z springs is not considered. The q-z springs are connected to the end of the piles. For the backbone curves of the p-y springs, the American Petroleum Institute (API, 2000) recommendation for sands is considered:

$$P = A \cdot p_u \cdot \tanh\left(\frac{k \cdot H}{A \cdot p_u} \cdot y\right) \tag{3-1}$$

A is a factor considering the cyclic condition (equal to 0.9), p_u is the ultimate bearing capacity at height H. k is the initial modulus of subgrade reaction, y is the lateral deflection, and H is the depth. The calculation process to obtain the p-y curves is shown in Appendix 1.

The ultimate skin friction resistance of the t-z springs is calculated using:

$$f_s = K\sigma_v' \tan(\delta) \tag{3-2}$$

K is the effective earth pressure coefficient, σ_v' is the effective vertical stress y δ is the soil-pile friction angle. The ultimate resistance in compression of the q-z springs is:

$$q_u = N_q^* \sigma_{v,t}' \tag{3-3}$$

N_q^* is the Meyerhof's theory factor associated with the angle of soil firming and $\sigma_{v,t}'$ is the effective vertical stress at the tip elevation. In tension, a minimum capacity is assumed for the q-z springs. The initial stiffness of the t-z and q-z springs is based on the recommendations

of Randolph (1991). The yield displacement is 0.5% of the pile diameter for t-z springs and 2.5% for q-z springs. Figure 3-3 shows typical hysteresis curves for the different soil springs.

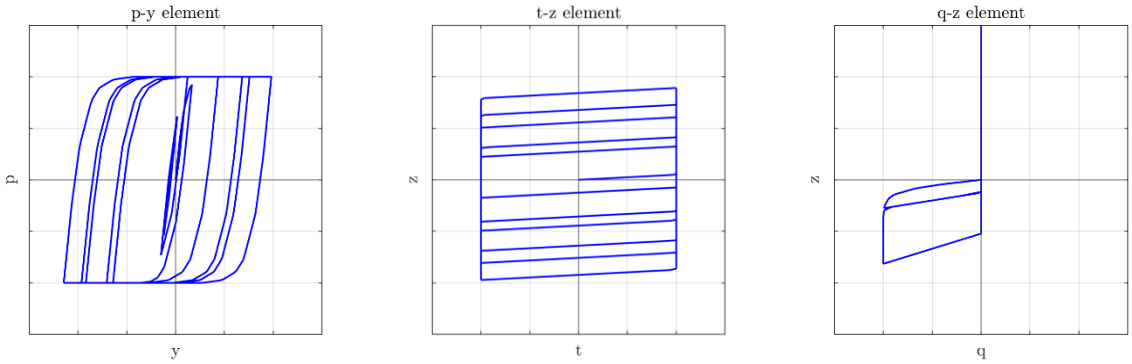

a) p-y spring **b) t-z spring** **c) q-z spring**

Figure 3-3: Typical spring hysteresis

The radiation damping is considered by means of a linear viscous damper connected in parallel to the elastic part of the soil springs. According to Berger et al. (1977), for the p-y springs the damping coefficient is calculated as $c = 2B\rho(V_p + V_s)$, for the t- z springs, $c = 4B\rho V_s$, and for the q-z springs, $c = (B/2)^2\pi\rho V_p$. B is the pile diameter, ρ is the soil density, V_s is the soil shear wave velocity, and V_p is the soil compressive wave velocity. This model is used due to its simplicity (see Figure 3-4). Other more rigorous damping models could be used as the one proposed by Novak et al. (1978) or the model proposed by Gazetas and Dobry (1984).

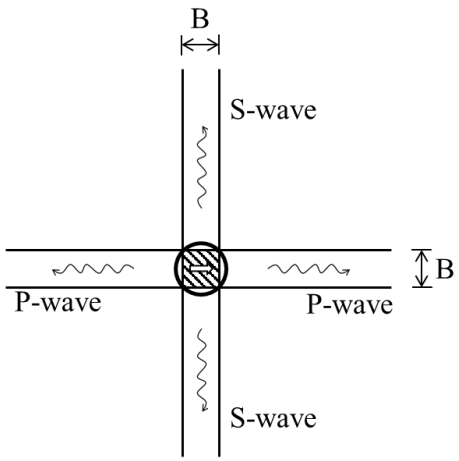

Figure 3-4: Model of Berger et al. (1977) for radiation damping plan view.

3.2 LATERAL SPRINGS CONFIGURATION

Typically for a 3D model, p-y springs are in two orthogonal directions with uncoupled interaction between them (L Shape), see Figure 3-5a. However, in this case, the lateral springs are nonlinear and when the system is loaded diagonally and yielding occurs in the springs, results in an overestimated force, as discussed by Blandon (2007). To reduce this problem, three springs every 60 degrees (Delta Shape), see Figure 3-5b, are considered. It is possible to consider five springs at 36 degrees (Penta Shape), see Figure 3-5c, and further reduce the error.

Each of the spring models were loaded at angles between 0 and 360 degrees. The overstrength ratio is defined as the maximum force obtained divided by the theoretical yield force. Figure 3-6 shows the overstrength ratio for each one of the configurations. It can be noted that for the L Shape springs configuration an overstrength ratio of 1.41 is obtained at a loading angle of 45 degrees (this ratio corresponds to the square root of 2).

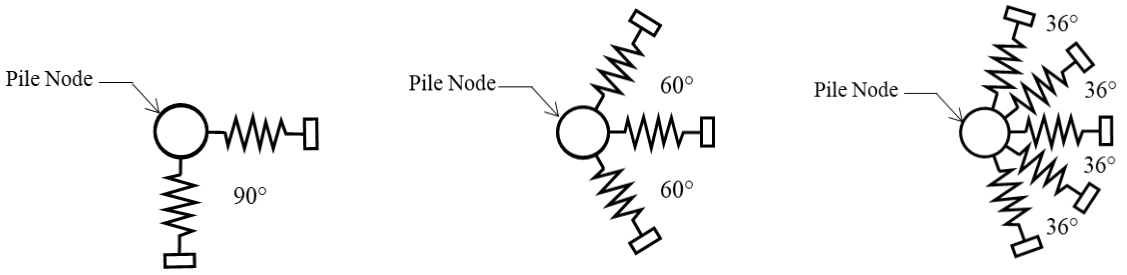

a) L Shape **b) Delta Shape** **c) Penta Shape**

Figure 3-5: Horizontal soil springs configuration

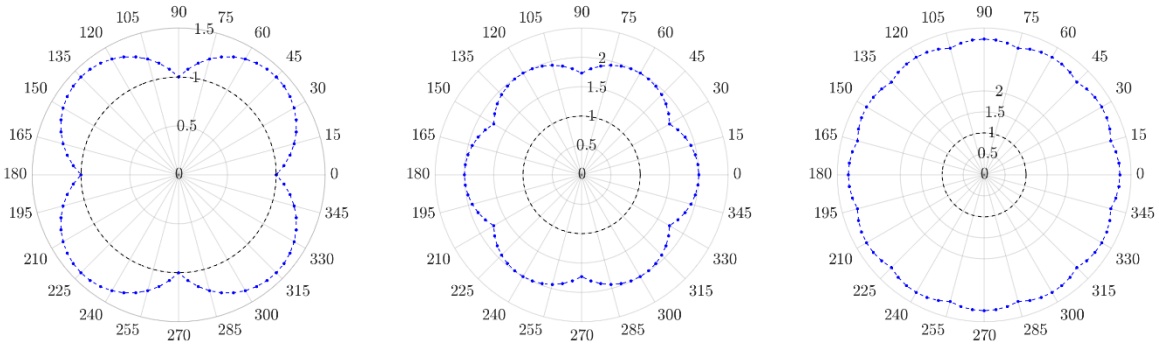

a) L Shape **b) Delta Shape** **c) Penta Shape**

Figure 3-6: Overstrength ratio

It is necessary to apply a force factor to adjust the response of the springs and obtain a force ratio close to unity independent of the direction in which the springs configuration is loaded. Blandon (2007) proposes the reduction factors indicated in Table 3-1. In this way, the responses of Figure 3-7 are obtained.

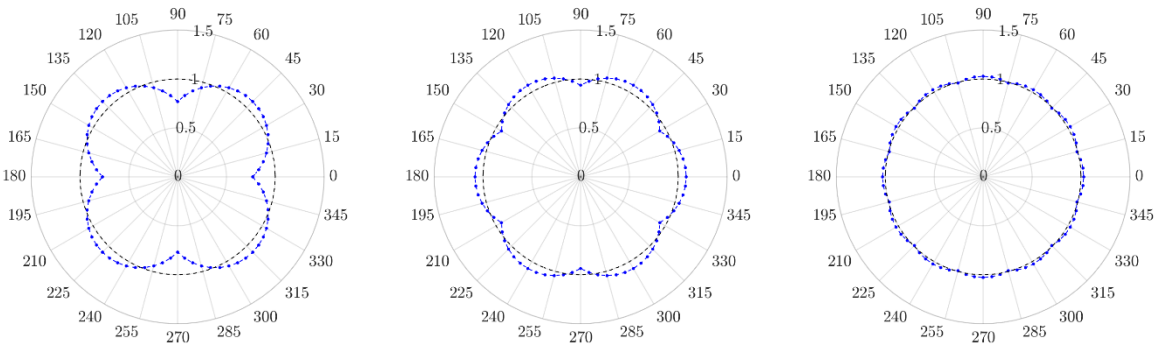

a) L Shape **b) Delta Shape** **c) Penta Shape**

Figure 3-7: Overstrength ratio with force reduction factors

In addition to the force reduction factor, it is necessary to apply a stiffness reduction factor. For example, when the system is elastic and we are loading a Delta Shape springs configuration (at any angle), the force obtained will be 1.5 times the expected force. This value is accurate and valid for any loading angle. If the springs are linear and the stiffness reduction factors are used, the response would be exact regardless of the configuration used. The error occurs when the springs are nonlinear.

Table 3-1: Force and stiffness reduction factors, Blandon (2007)

Configuration	Strength Factor	Stiffness Factor
L Shape	1.30	1.0
Delta Shape	1.85	1.5
Penta Shape	3.10	2.5

The L Shape, Delta Shape, and Penta Shape models were tested considering a bilinear elastic perfectly plastic spring constitutive relationship (Figure 3-8a) and considering the p-y curve proposed by API for sands (Figure 3-8b).

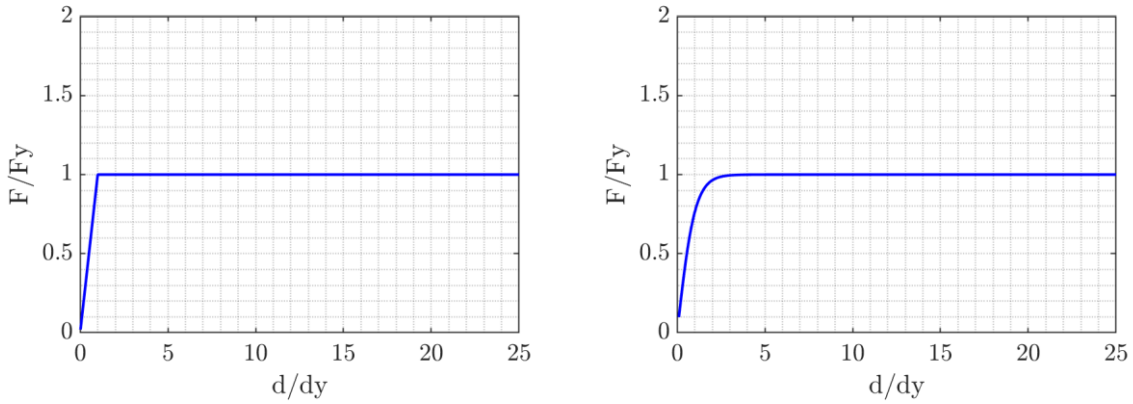

a) Bilinear **b) API**

Figure 3-8: Spring constitutive curves

It can be noted from Figure 3-7 that in the L Shape springs configuration the critical angles are 0 and 45 degrees since for these angles the greatest difference in forces is generated. In the case of the Delta Shape spring configuration these critical angles are 0 and 30 degrees, and for the Penta Shape springs configuration the critical angles are 0 and 18 degrees.

In Figure 3-9, for the L Shape springs configuration without using force reduction factors, when plotting the force ratio, corresponding to the resultant force (F) divided by the expected theoretical force (F_e), as a function of displacement, it is observed that at the beginning, independent of the angle, the force ratio is equal to 1 because the system is completely linear. As the displacement increases, the nonlinear springs begin to yield, and the curves begin to diverge depending on the load angle. When the springs are in a yielding state the force ratio for a load angle of 0 degrees is equal to 1, but for 45 degrees angle it is equal to 1.41. That is, depending on the angle at which this system is loaded, the resultant force load can be up to 1.41 times the theoretical force. The range of the force ratio is 0.41 for this configuration. This behavior occurs when considering a bilinear elastic perfectly plastic spring

constitutive relationship and a p-y curve proposed by API. The bilinear constitutive allows us to appreciate the point at which the springs start yielding.

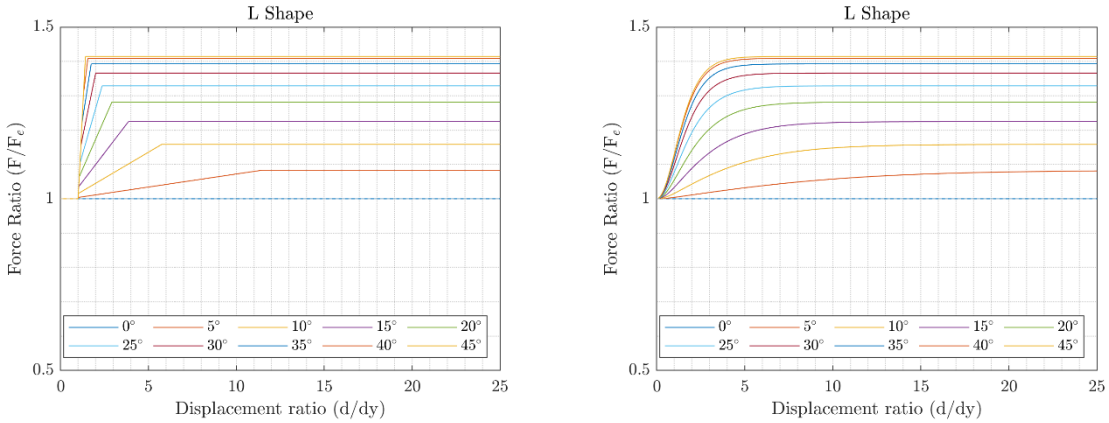

a) Bilinear **b) API**

Figure 3-9: L Shape force ratio against displacement

In Figure 3-10, the L Shape (c) configuration is considered, which incorporates the reduction factors proposed by Blandon (2007). It is obtained that for an angle of 0 degrees the force ratio at complete yielding is 0.77 and for an angle of 45 degrees it is 1.09. The range of the force ratio is 0.32 for this configuration.

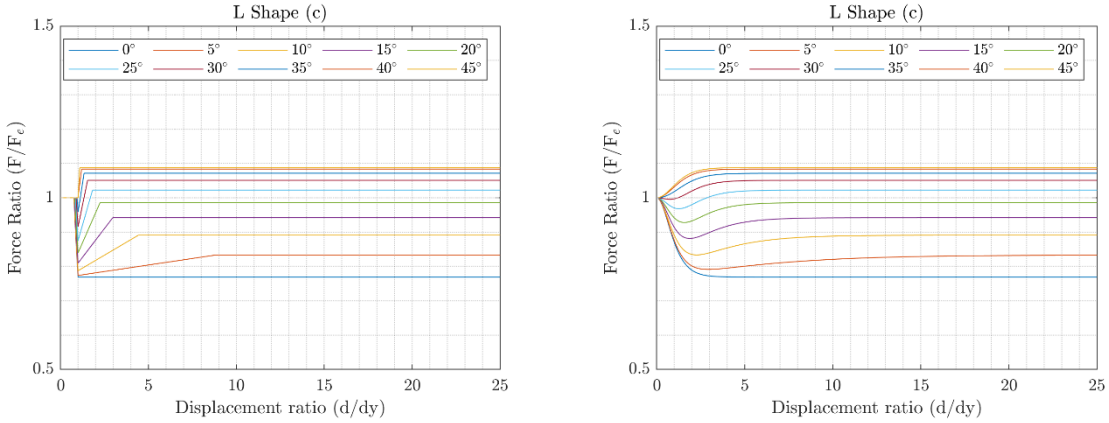

a) Bilinear **b) API**

Figure 3-10: L Shape (c) force ratio against displacement

Performing the analysis for the Delta Shape springs configuration in Figure 3-11, incorporating the reduction factors proposed by Blandon (2007), for an angle of 0 degrees, the force ratio at complete yielding is 1.08 and for an angle of 30 degrees is 0.94. The range of the force ratio is 0.14 for this configuration.

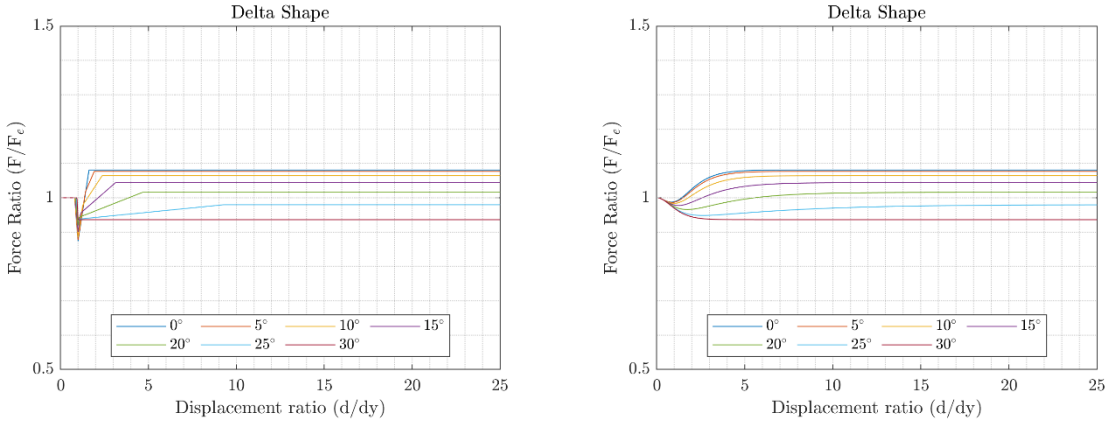

a) Bilinear **b) API**

Figure 3-11: Delta Shape force ratio against displacement

The range obtained for the Delta Shape configuration is smaller compared to the L Shape configuration. This implies that the resultant force obtained in a nonlinear analysis will vary less depending on the loading angle when using the Delta Shape configuration than when using an L Shape or an L Shape (c) configuration.

Finally, the Penta Shape springs configuration is analyzed using the reduction factors proposed by Blandon (2007) in Figure 3-12. For an angle of 0 degrees the force ratio at complete yielding is 1.03 and for an angle of 18 degrees is 0.98. The range of the force ratio is 0.05 for this element.

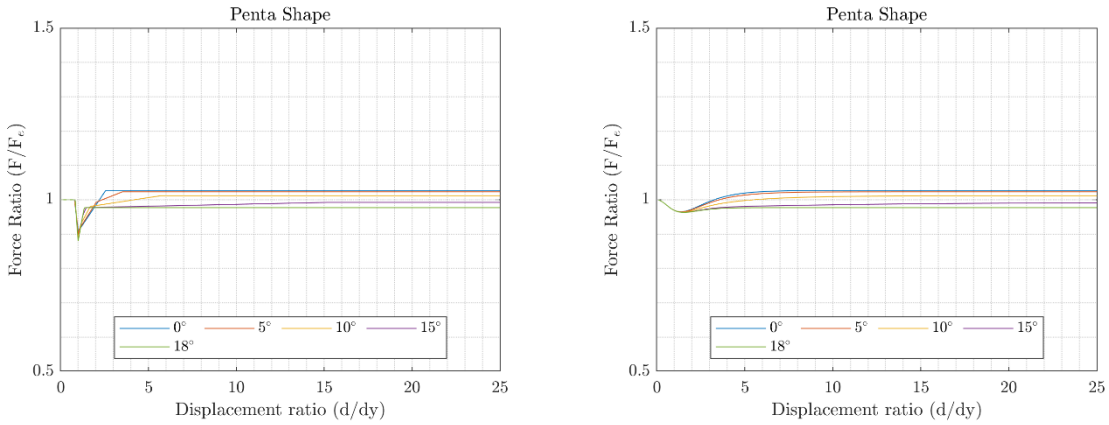

a) Bilinear **b) API**

Figure 3-12: Penta Shape force ratio against displacement

It can be noted that the Penta Shape springs configuration is even less affected by load directionality than the Delta Shape springs configuration. However, because the Penta Shape presents greater modeling complexities, it was decided to consider only L Shape and Delta Shape in the subsequent analyses. In the following, the elements are evaluated considering L Shape and Delta Shape configurations with a single pile and a group of 4 piles, all within two horizontal components of dynamic excitation.

3.3 SINGLE PILE

3.3.1 Single pile general description

A model of a single pile of 0.6 m diameter, embedded 10 m and with a cantilever of 2 m above ground level is generated (see Figure 3-13). A mass M of 200 tons is assigned above the structure. The pile material is concrete H35 (f'_c=30 MPa).

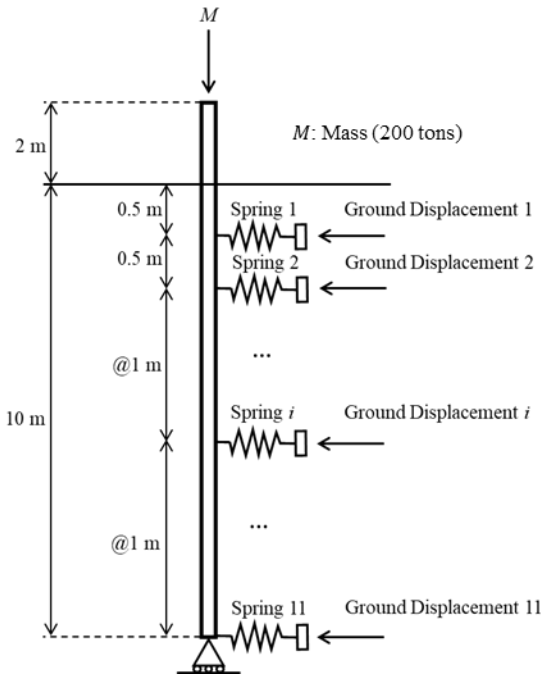

Figure 3-13: Single pile model

3.3.2 Soil profile description

The soil profile considered in the analysis corresponds to the soil described in the soil mechanics study report performed by Sanhueza and Verdugo (2010). The profile is composed of four layers of sandy soil (see Figure 3-14). The water table is 4 m depth. The characteristics of each of the layers are shown below, including compression wave velocity (V_p), shear wave velocity (V_s), internal friction angle (ϕ), and specific weight (γ').

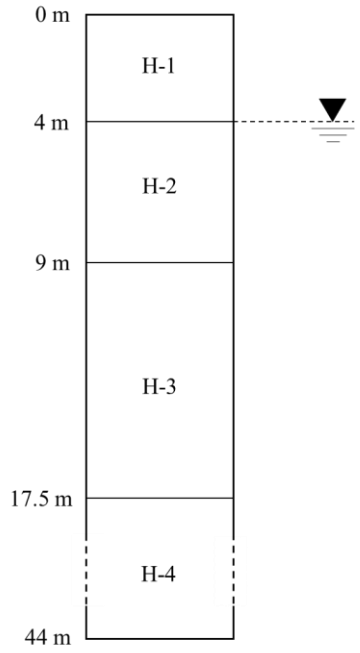

Layer	Thickness (m)	V_p (m/s)	V_s (m/s)		ϕ (°)	γ' (kN/m^3)
H-1	4	520	133	Sand	37	17
H-2	5	950	181	Sand	37	9
H-3	8.5	1430	217	Sand	37	9
H-4	26.5	1504	260	Sand	37	9

Figure 3-14: Soil profile

It can be noted that the soil profile is composed only of sand. In this case it is assumed that no liquefaction occurs in any of the soil layers. The average shear wave velocity for the top 30 m of soil (V_{s30}) is equal to 207 m/s. This soil could be classified as class D according to ASCE7-16 (2016).

3.3.3 Ground motion input

The seismic record considered corresponds to the CONZ station record of the M_w 8.8 Maule earthquake of February 27, 2010 (see Figure 3-15 to Figure 3-20).

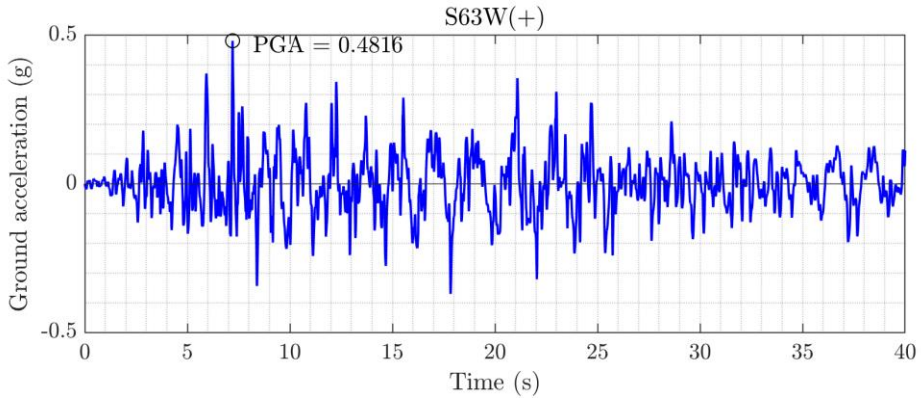

Figure 3-15: Ground acceleration record, component S63W (+)

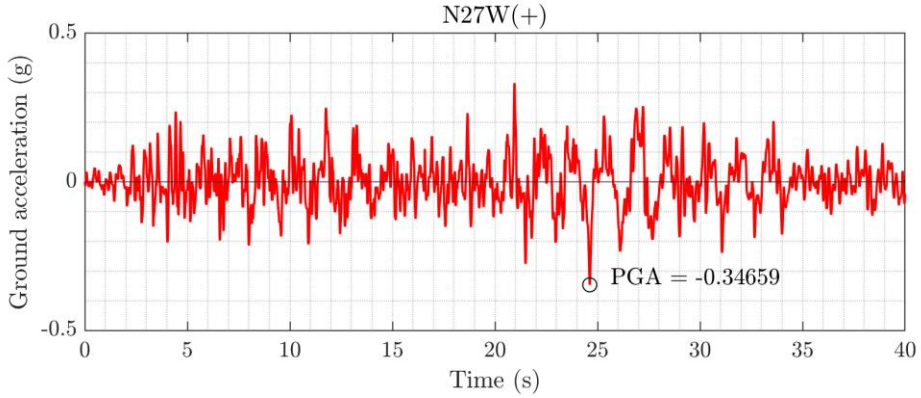

Figure 3-16: Ground acceleration record, component N27W (+)

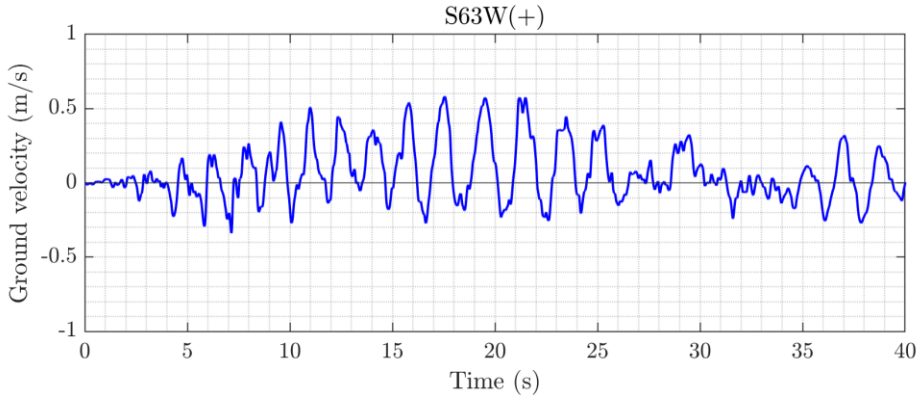

Figure 3-17: Ground velocity, component S63W (+)

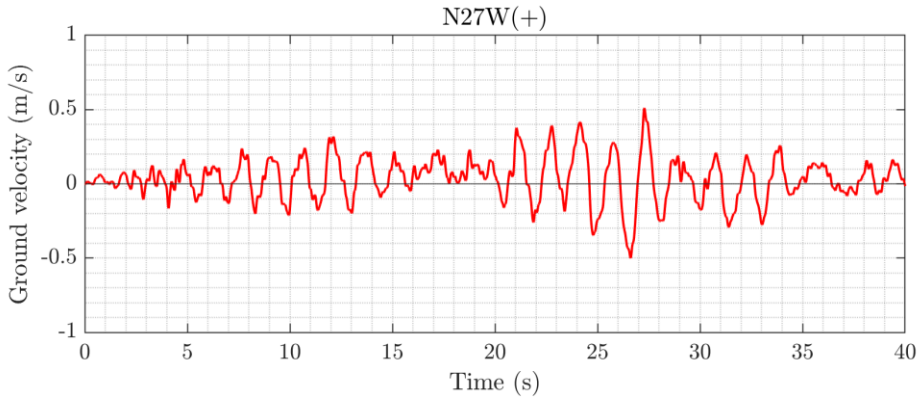

Figure 3-18: Ground velocity, component N27W (+)

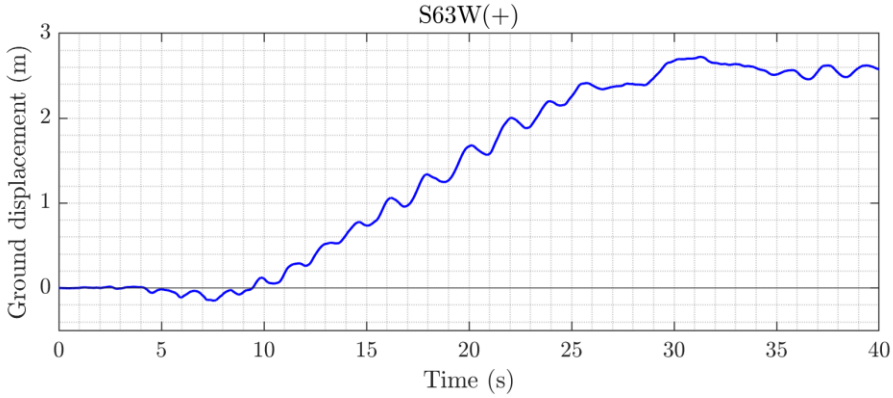

Figure 3-19: Ground displacement, component S63W (+)

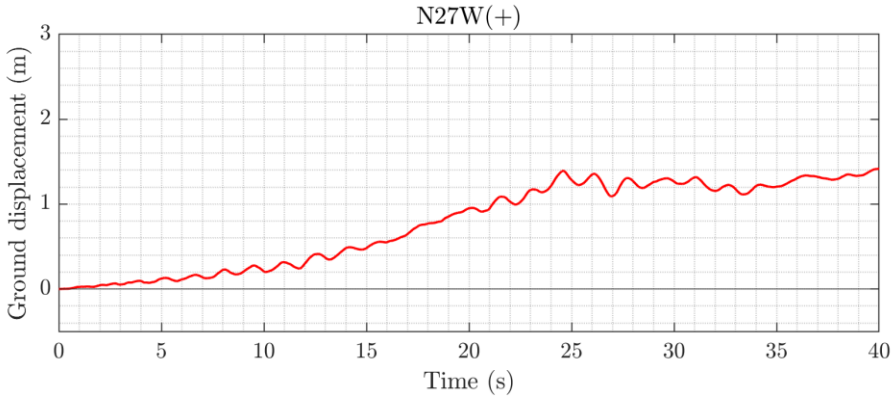

Figure 3-20: Ground displacement, component N27W (+)

The strong component of the ground motion was assessed as 40 seconds long, although the full record is 180 seconds. However, the elastic response spectrum when considering the 40-second recording is equal to that obtained using the full 180-second recording. With this

criterion, it was decided to consider the 40-second recording in the analysis. The peak ground acceleration (PGA) of the record is 0.48g in the S63W (+) component and 0.35g in the N27W (+) component. The resonance period of the Concepción basin can be noted, which is around 2 seconds. This ground motion has a residual displacement of 2.59 m in the S63W (+) component and 1.41 m in the N27W (+) component.

The pseudo-acceleration and displacement response spectra for linear response of both components of the record considering a damping ratio of 5% are shown below (Figure 3-21 and Figure 3-22).

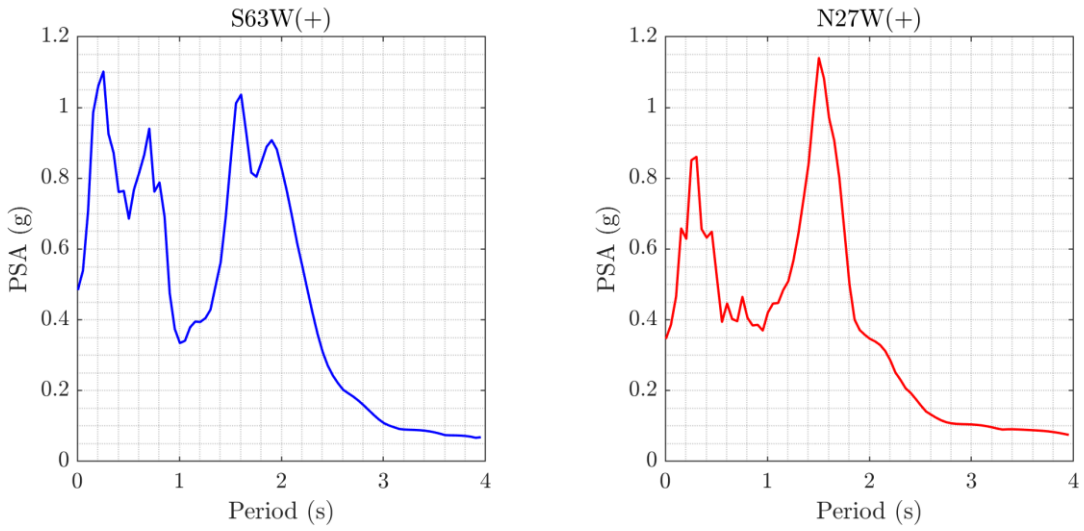

a) Component S63W (+) **b) Component N27W (+)**

Figure 3-21: CONZ ground motion pseudo-acceleration spectra

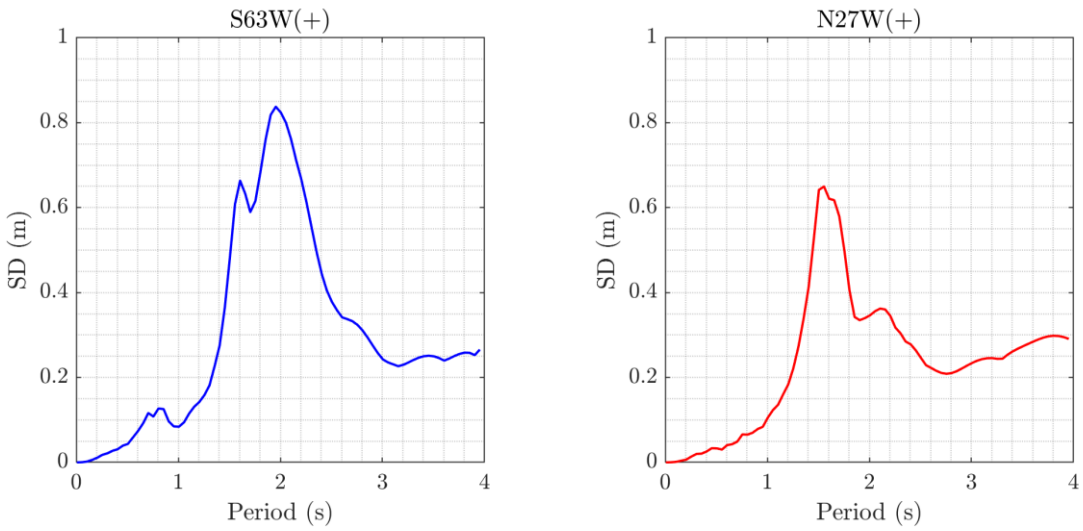

a) Component S63W (+) **b) Component N27W (+)**

Figure 3-22: CONZ ground motion spectral displacement

It can be noticed in the acceleration spectrum that there are two peaks. At periods close to 1 second, a low energy zone can be observed and as the period increases the spectral pseudo-acceleration increases considerably. If a structure with a fundamental period close to 1 second enters the nonlinear range during this earthquake, its period will increase, and it would enter the high energy zone of the spectrum which would imply large forces on the structure.

3.3.4 Single pile model

An ETABS 20 model of the pile was developed using an elastic frame element. The SSI was modeled with p-y springs distributed along the pile spaced 1 m apart. Vertical support was provided at the base to allow for horizontal displacements. The fundamental period of the system is 1.125 seconds, a damping ratio of 0.5% in the first mode and 10% at 20 Hz was considered as Rayleigh damping.

The input is applied as a time-history of displacement in each of the p-y springs. To obtain the soil displacements at different depths a model is performed in DeepSoil v7 (2020). This is a 1D model that allows us to obtain the free-field response of a soil column. Since the ground motion considered was recorded at ground level, it is necessary to perform a deconvolution of the response, i.e., from the accelerations at the surface it is possible to obtain the displacements at different depths. DeepSoil v7 (2020) has this function, but it does not allow a nonlinear model, so an equivalent linear model of the soil is considered. This restriction is due to the fact that in a nonlinear system it is very complex to solve the response in inverse form (deconvolution) and this is solved using the linearized model. The soil layers previously mentioned are defined and the stiffness degradation curves, and the damping curves proposed by Darandelli (2001) are considered. In this analysis, the earthquake scaled by 0.50, 1.00, and 1.25 is considered. Then, the results obtained with DeepSoil v7 (2020) are entered as displacements input in the nonlinear model of ETABS 20. The analysis process is shown in Figure 3-23.

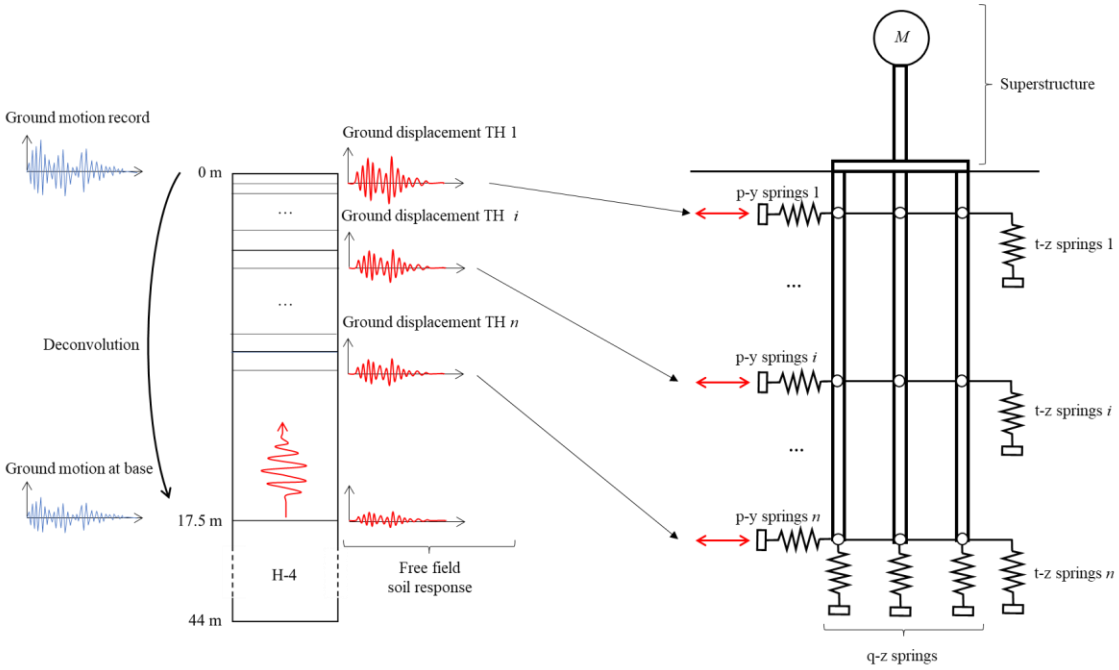

Figure 3-23: Single pile with discrete SSI model process of analysis

3.3.5 Single pile analysis results: S23W (+) component

In order to analyze the directionality of the L Shape (with and without correction factors) and Delta Shape configurations, first, the case is analyzed considering only the S23W (+) component of the ground motion in such a way that it is comparable with a 2D model of the pile. In this way, the 2D model is considered as the benchmark behavior (see Figure 3-24) and is compared with the results using L Shape, L Shape (c) and Delta Shape configurations rotated at their critical angles (see Figure 3-25).

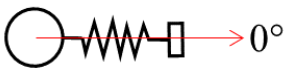

Figure 3-24: 2D spring (Benchmark behavior)

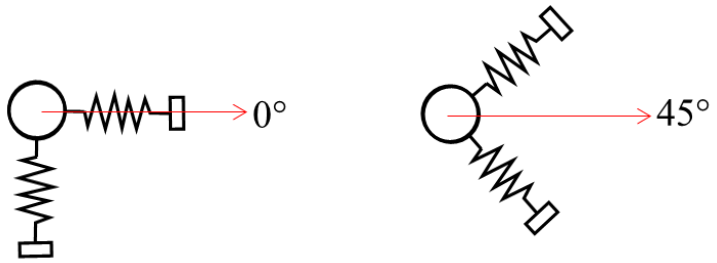

a) L Shape and L Shape (c) 0° **b) L Shape and L Shape (c) 45°**

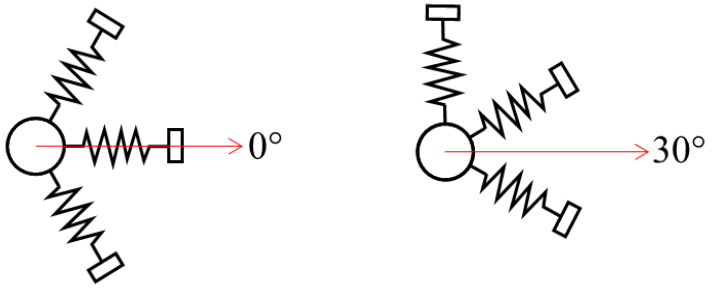

c) Delta Shape 0° **d) Delta Shape 30°**

Figure 3-25: L Shape, L Shape (c) and Delta Shape rotated in their critical angles.

To include these configurations in ETABS, link elements are considered. The plastic part of the soil spring is modeled using a multilinear plastic element incorporating the backbone curve obtained using the p-y curve equation proposed by API. The viscoelastic part of the soil spring is modeled with a linear link element with constant stiffness and damping. In order for the displacement input to be applied to all the springs composing each configuration (L Shape and Delta Shape), the springs are linked together using rigid elements and the displacement is applied at a master node. Thus, by displacing the master node, the displacement is transmitted to all the springs without the need to decompose the displacement input in different directions and assign it to each spring individually. The modeling performed in ETABS for each configuration is shown schematically in Figure 3-26 and Figure 3-27.

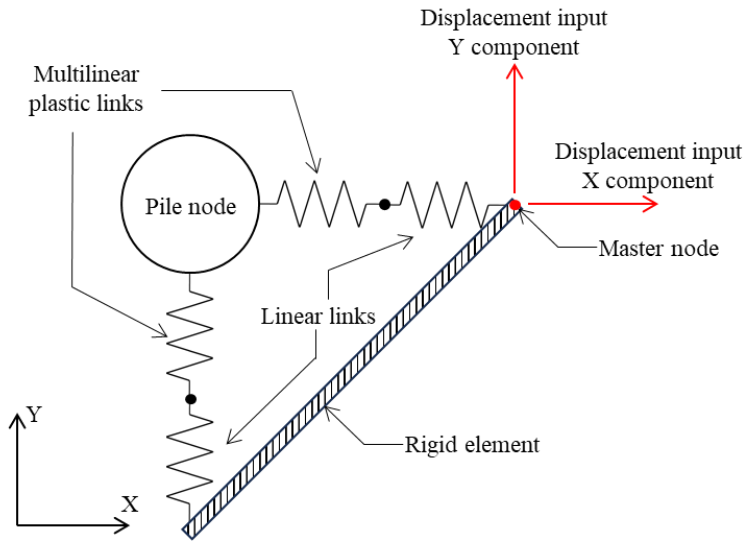

Figure 3-26: L Shape soil springs configuration ETABS modeling

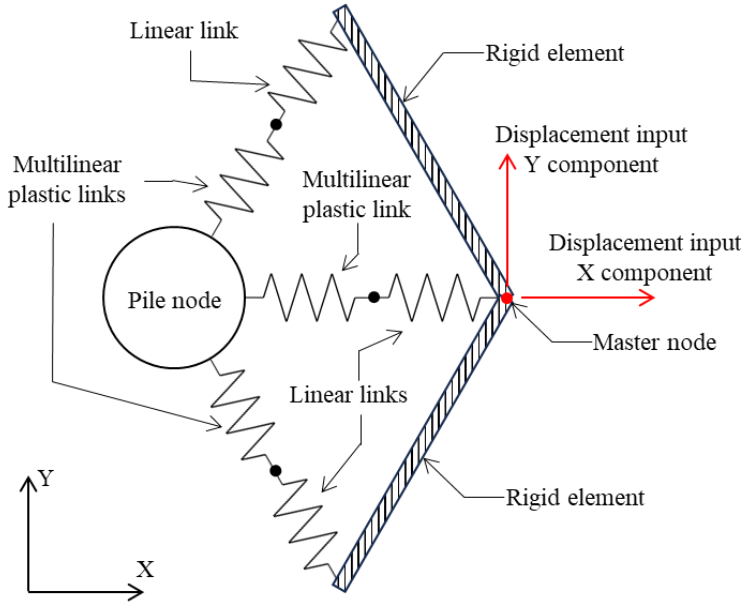

Figure 3-27: Delta Shape soil springs configuration ETABS modeling

The time-history of the relative displacement with respect to the ground surface of the mass *M* are presented for each case (Figure 3-28 to Figure 3-30), considering the described configurations. It should be noted that in this case, where only one component is considered,

the response obtained with the L Shape configuration loaded at 0 degrees is the same as the response obtained with the 2D benchmark spring. This changes if we rotate this configuration 45 degrees or if we include the reduction factors.

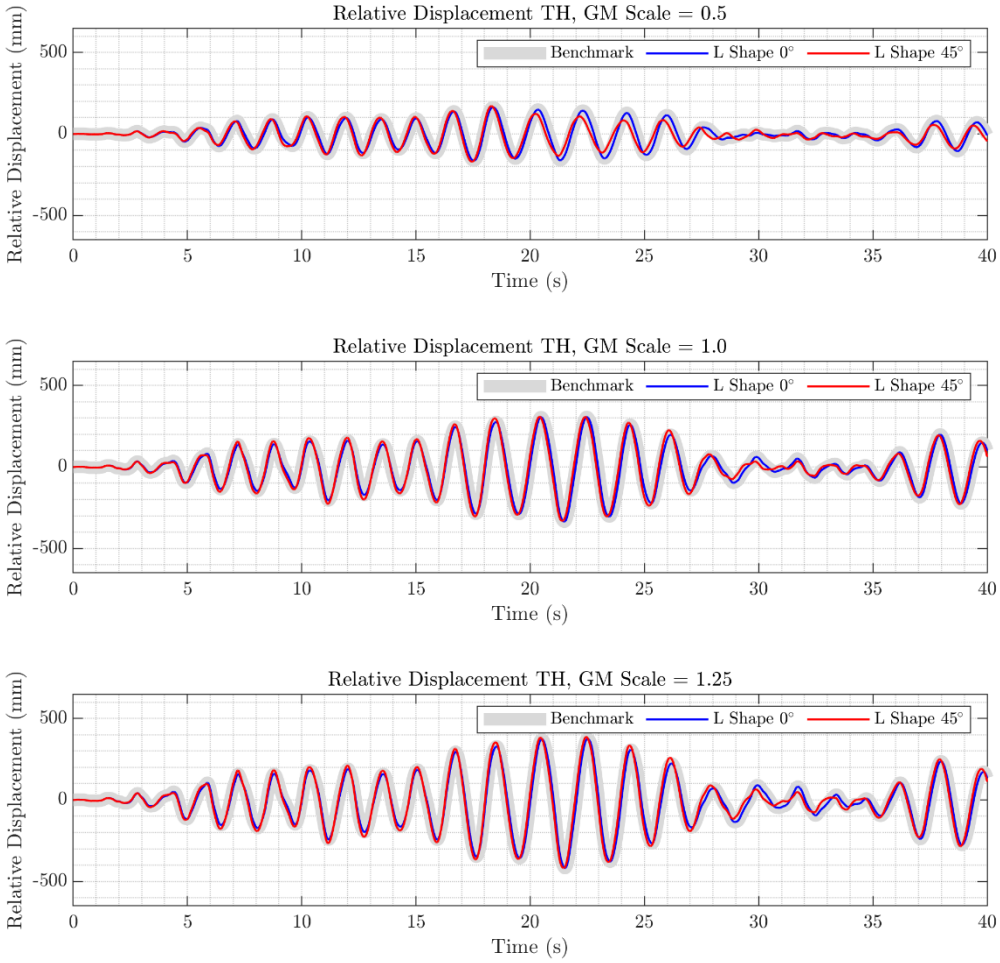

Figure 3-28: Single pile with L Shape configuration. Relative displacement TH. S63W (+).

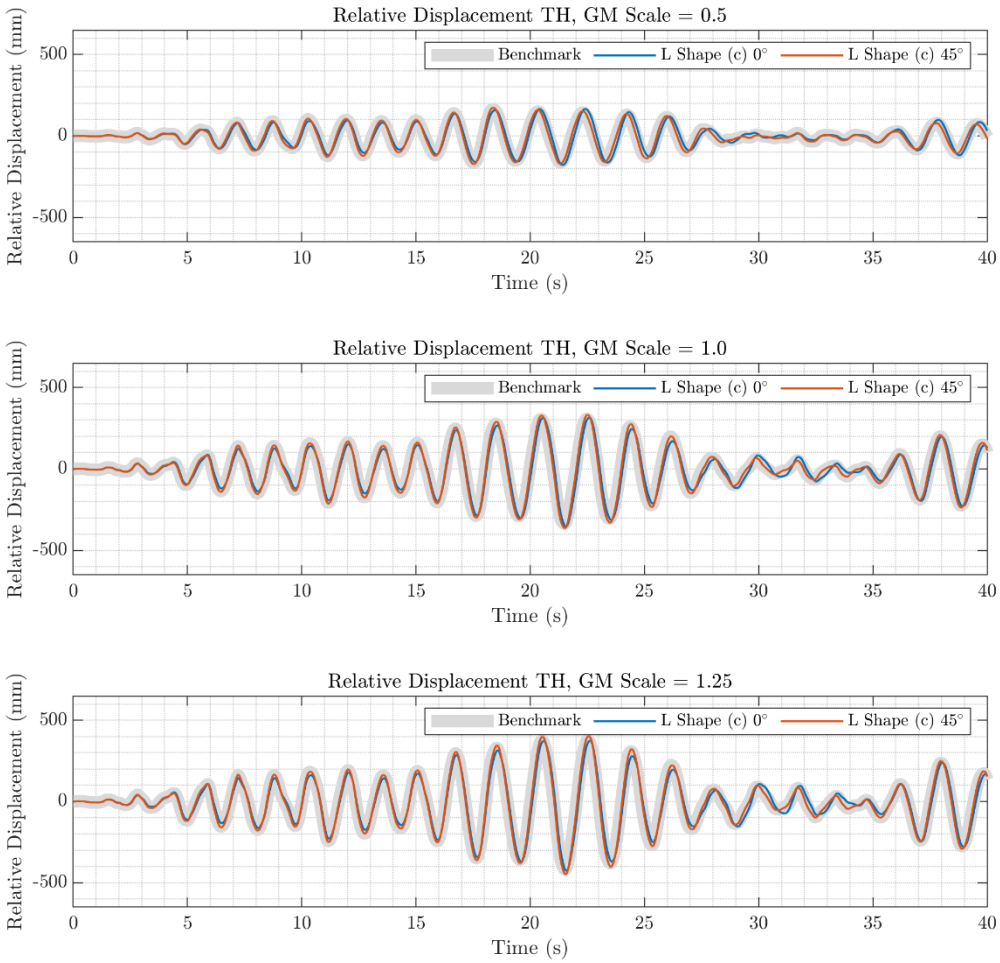

Figure 3-29: Single pile with L Shape (c) configuration. Relative displacement TH. S63W (+).

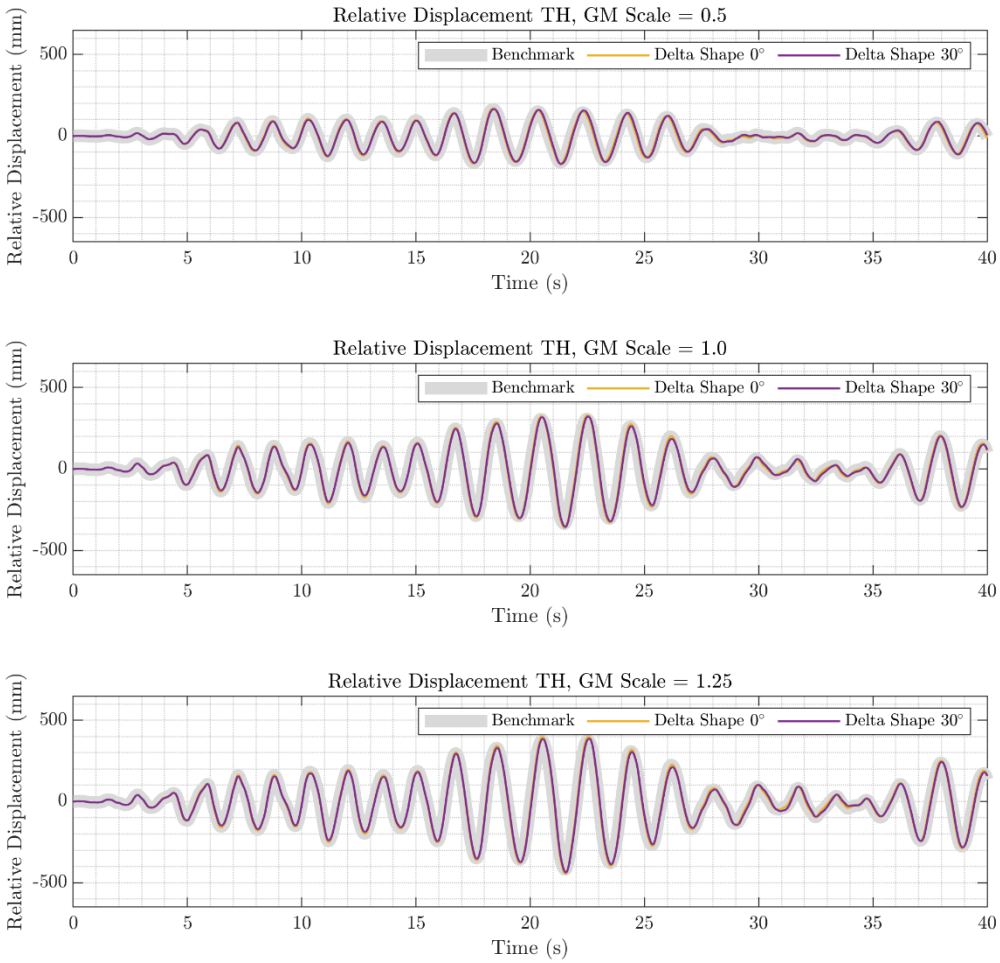

Figure 3-30: Single pile with Delta Shape configuration. Relative displacement TH. S63W (+).

In the relative displacement plots of the system subjected to the S23W (+) ground motion, it can be seen that when using L Shape and L Shape (c) configurations there are evident bias when loaded at 0 degrees or 45 degrees, which is an indicator of directionality present in this configuration. In addition, a shifting of the response can be noticed in some sections as the peaks do not occur at exactly the same time. On the other hand, when using Delta Shape configuration, the curves are practically superimposed, which indicates a low directionality. The figures show the errors obtained with each configuration when comparing the responses with the 2D model (benchmark behavior). It should be noted that at the beginning of the

response, the curves are exactly the same regardless of the configuration, this is due to the fact that for an elastic system, the response is exact, and bias occurs when yielding occurs.

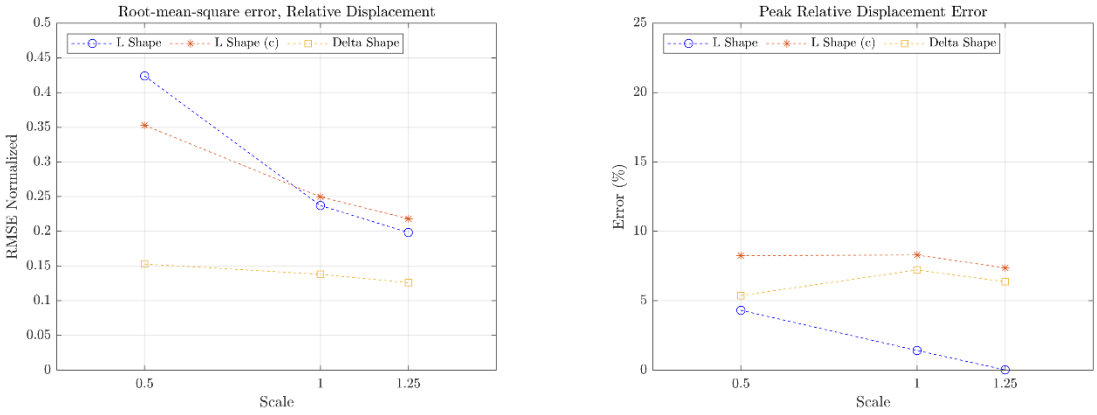

a) RMSE normalized **b) Peak relative displacement error**

Figure 3-31: Error for relative displacement single pile S23W (+)

The root-mean-square error (RMSE) is calculated as:

$$RMSE = \left[\frac{\sum_{i=1}^{N}\left(z_{fi} - z_{oi}\right)^2}{N}\right]^{\frac{1}{2}} \quad (3\text{-}4)$$

Where z_{fi} corresponds to the values obtained using the analyzed configurations, z_{oi} are the values obtained with the 2D model (benchmark) and N is the total amount of data. In this way, it is possible to analyze how well the results obtained with each configuration fit the behavior benchmark. To make the values comparable, the RMSE is normalized by the elastic spectral displacement of the system (T_1=1.125s) subjected to each of the scaled records.

Looking at Figure 3-31, it can be seen that the fit achieved with the Delta Shape springs configuration is considerably better than when using the L Shape configurations. One can note that there is no substantial difference when using L Shape or the L Shape configurations using the Blandon (2007) reduction factors. As the ground motion scale increases, the RSME values tend to decrease. This can be understood to mean that the configurations perform better as the system enters a more nonlinear range. However, this may be because as the scale increases, the spectral displacement increases linearly, but the nonlinear response does not change in the same way. As for the peak relative displacements, there is no clear trend to indicate that one configuration is better than the other.

Next, the same analysis is performed considering the absolute acceleration response of the system mass for each of the configurations (see Figure 3-32 to Figure 3-34).

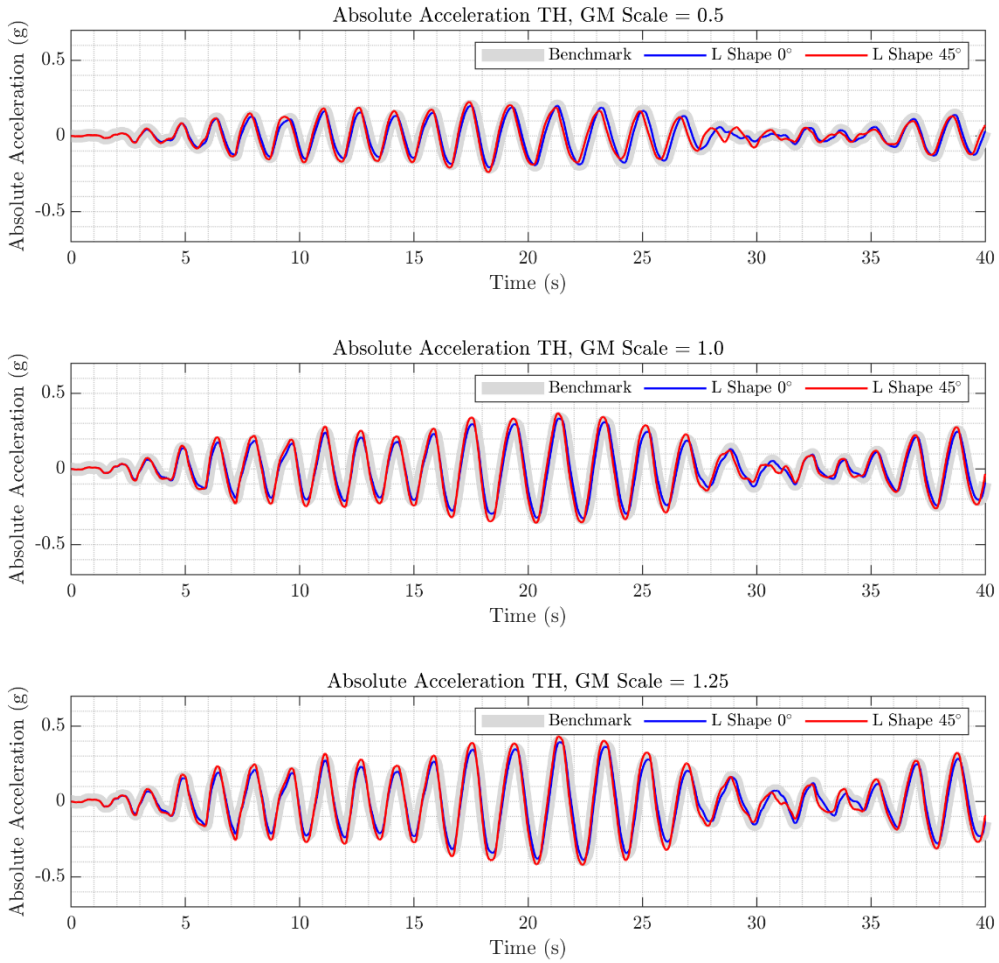

Figure 3-32: Single pile with L Shape configuration. Absolute acceleration TH. S63W (+).

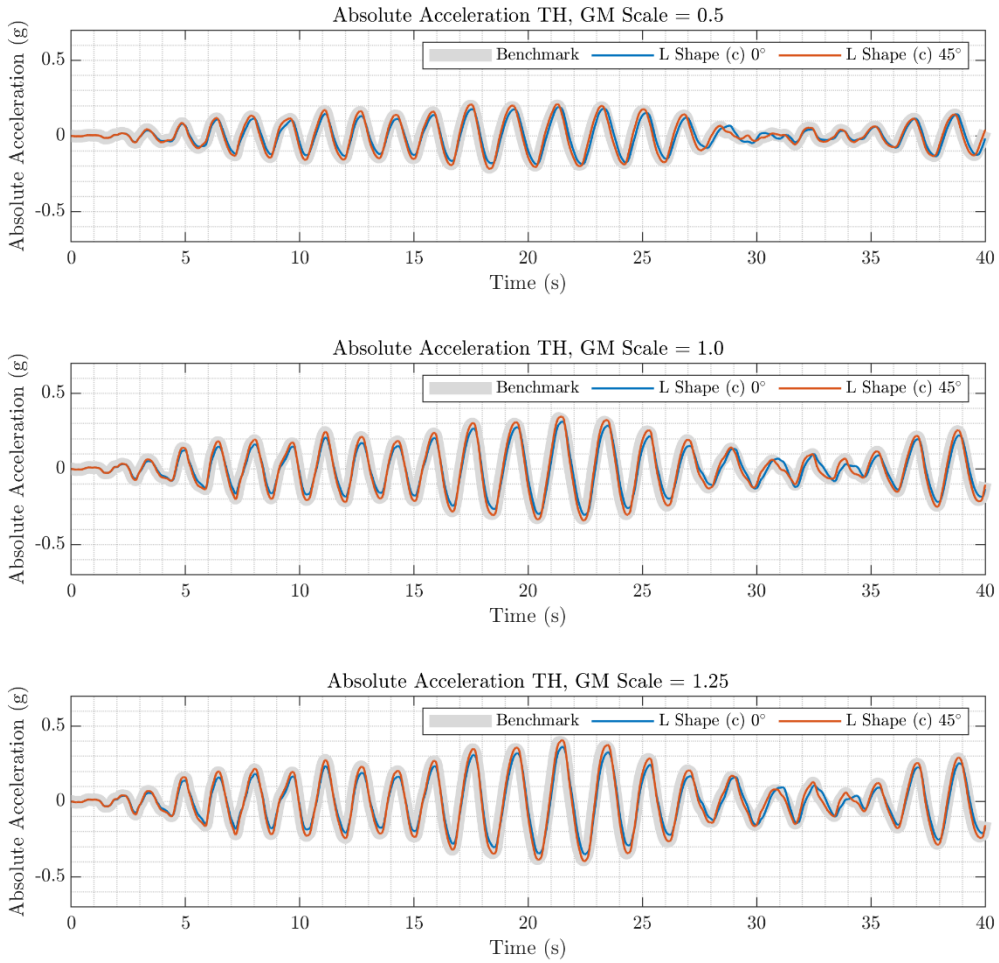

Figure 3-33: Single pile with L Shape (c) configuration. Absolute acceleration TH. S63W (+).

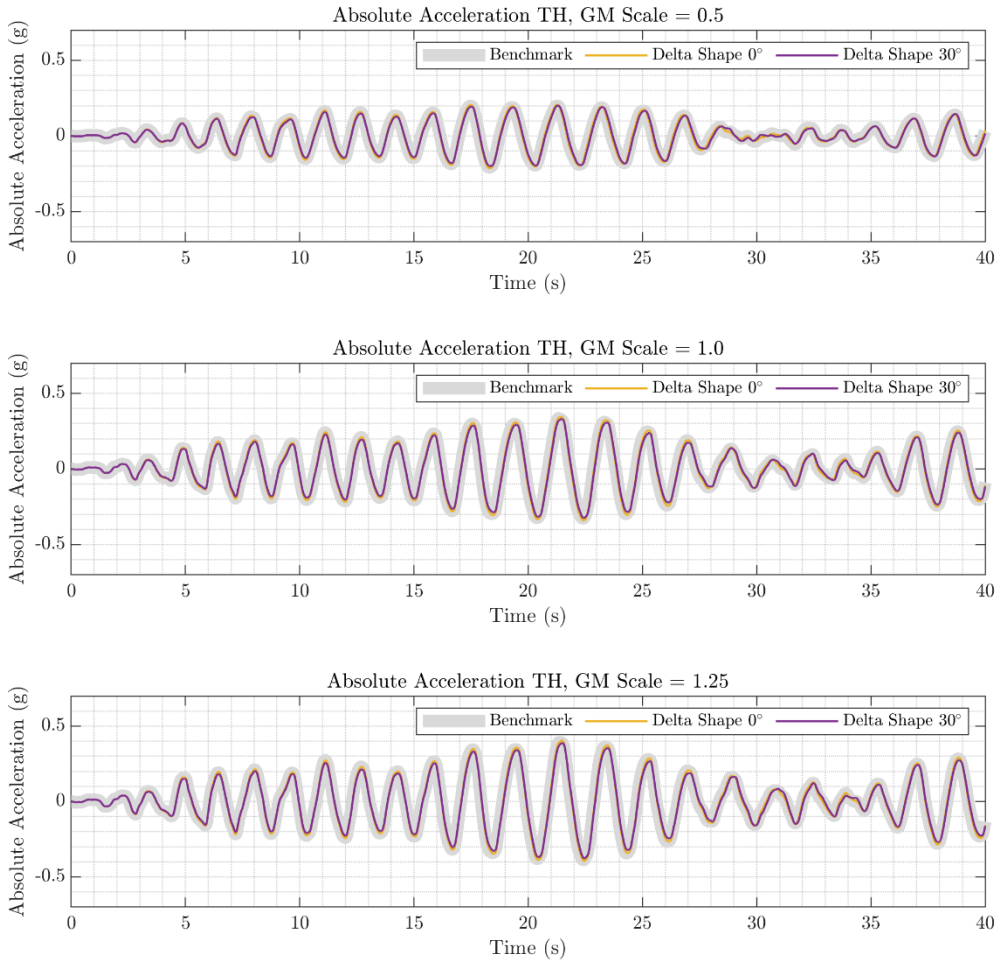

Figure 3-34: Single pile with Delta Shape configuration. Absolute acceleration TH. S63W (+).

Like the case of relative displacement, there is evident directionality when using the L Shape configurations and also a shift in the response. In the case of the Delta Shape configuration the response is much better adjusted and does not present a noticeable directionality.

The Figure 3-35a presents the RMSE normalized by the elastic spectral pseudo-acceleration of the system subjected to the scaled logs. The Figure 3-35b shows the errors obtained for the absolute acceleration peaks.

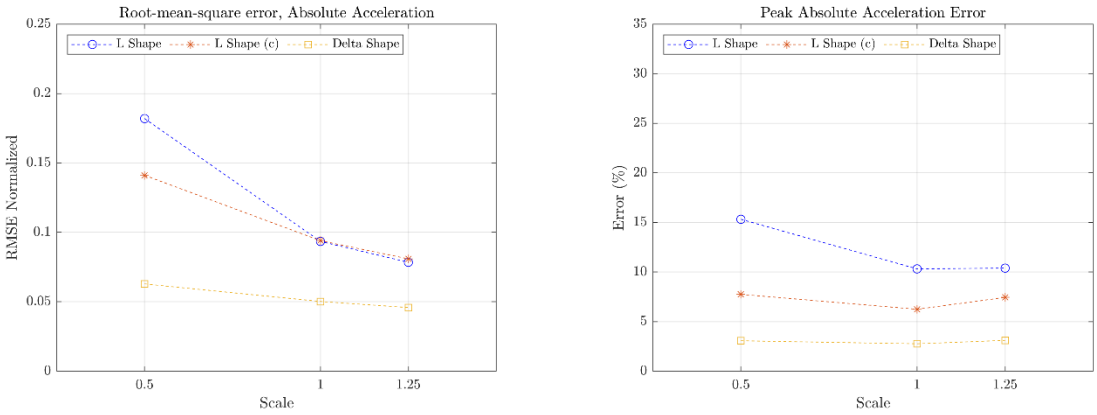

a) RMSE normalized **b) Peak absolute acceleration error**

Figure 3-35: Error for absolute acceleration single pile S63W (+)

Again, it can be seen that the Delta Shape configuration has a better fit than the L Shape configurations. In this case, when observing the peak absolute acceleration error graph, it can be seen that the Delta Shape has the smallest bias compared with the rest and that the uncorrected L Shape has the worst fit.

3.3.6 Single pile analysis results: N27W (+) component

Now we perform the same analysis, but considering the other component of the log, i.e., considering the N27W (+) component.

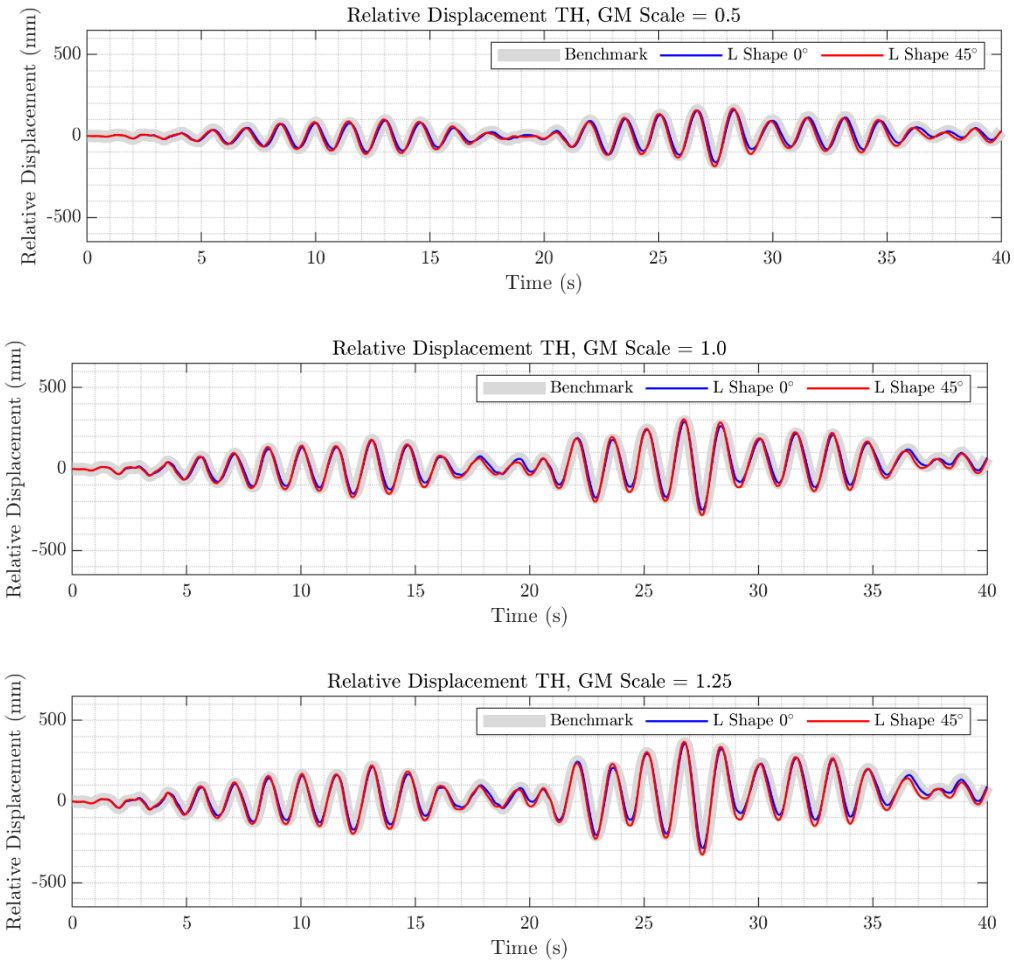

Figure 3-36: Single pile with L Shape configuration. Relative displacement TH. N27W (+).

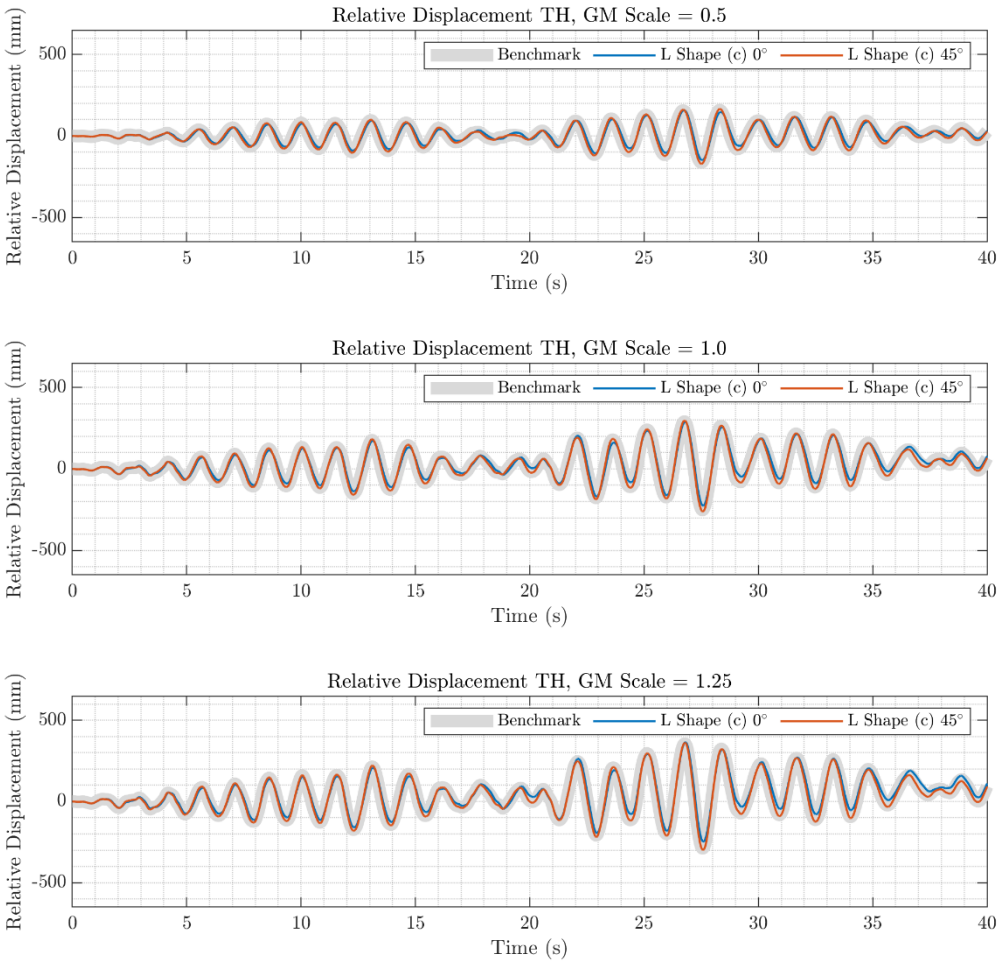

Figure 3-37: Single pile with L Shape (c) configuration. Relative displacement TH. N27W (+).

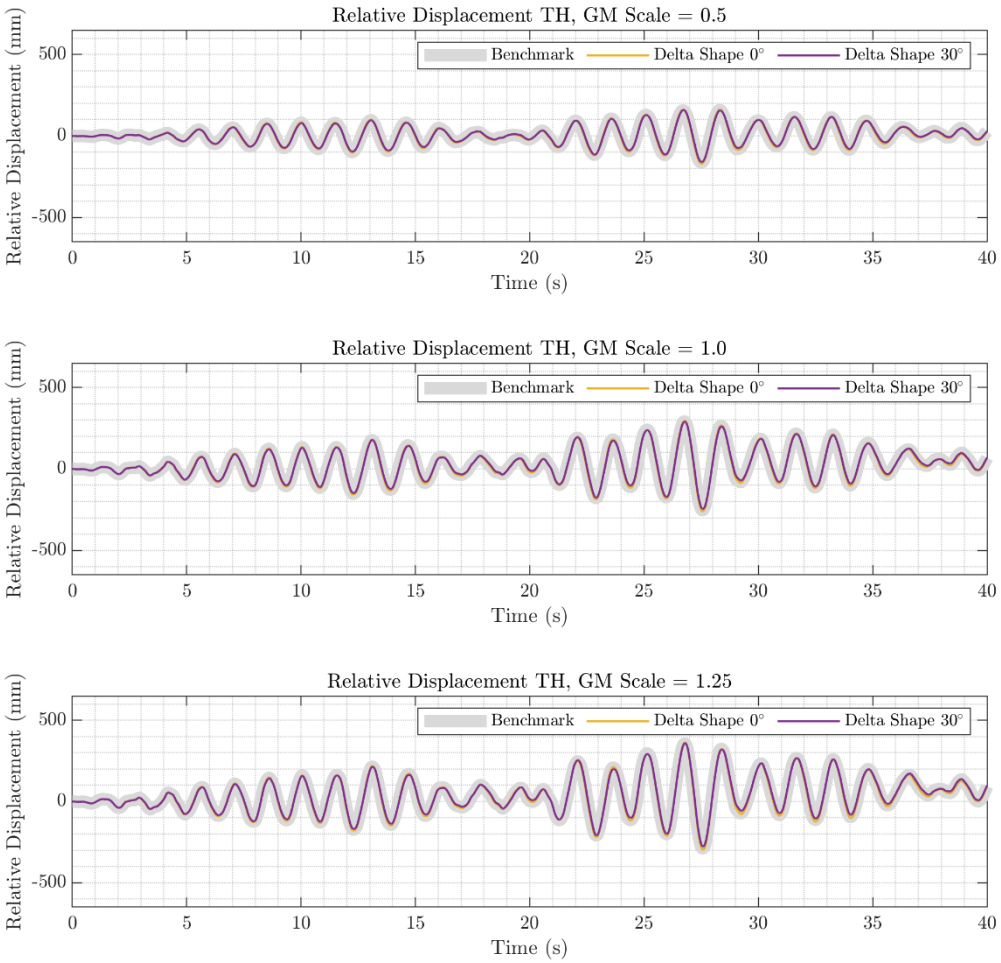

Figure 3-38: Single pile with Delta Shape configuration. Relative displacement TH. N27W (+).

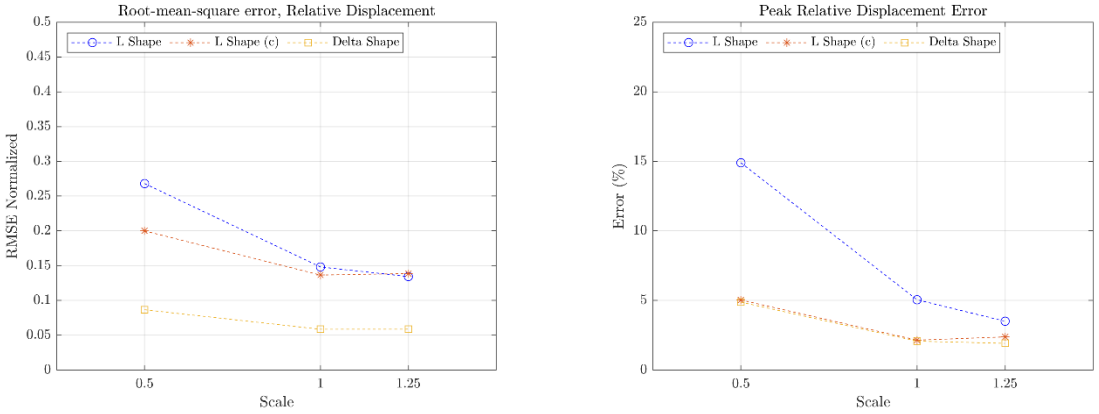

a) RMSE normalized **b) Peak relative displacement error**

Figure 3-39: Error for relative displacement single pile N27W (+)

The results obtained for relative displacement show considerable directionality when using L Shape configurations, but no clear shift in the response is observed. Using the Delta Shape configuration shows better behavior. The RMSE plot reaffirms the better fit obtained using the Delta Shape configuration and that there is no significant difference between using L Shape or L Shape (c) configurations. The absolute acceleration responses for the scaled N27W (+) log are presented below (see Figure 3-40 to Figure 3-42).

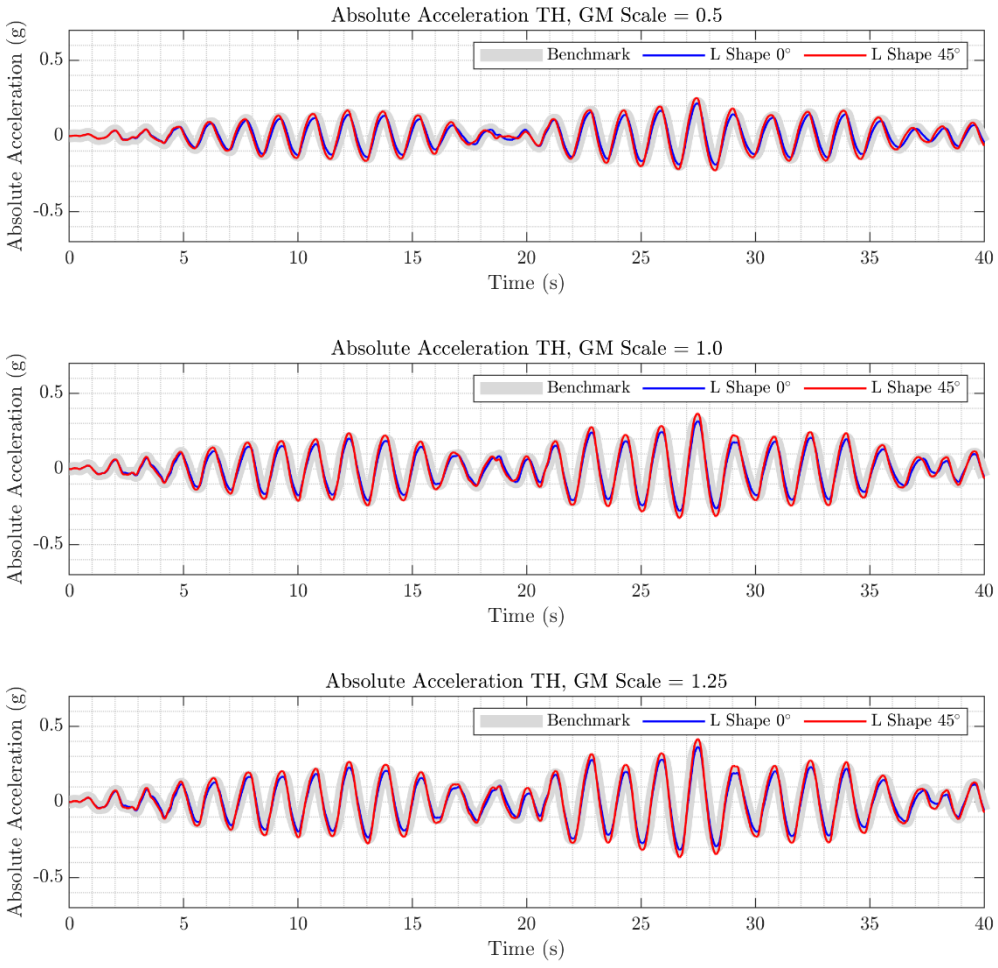

Figure 3-40: Single pile with L Shape configuration. Absolute acceleration TH. N27W (+).

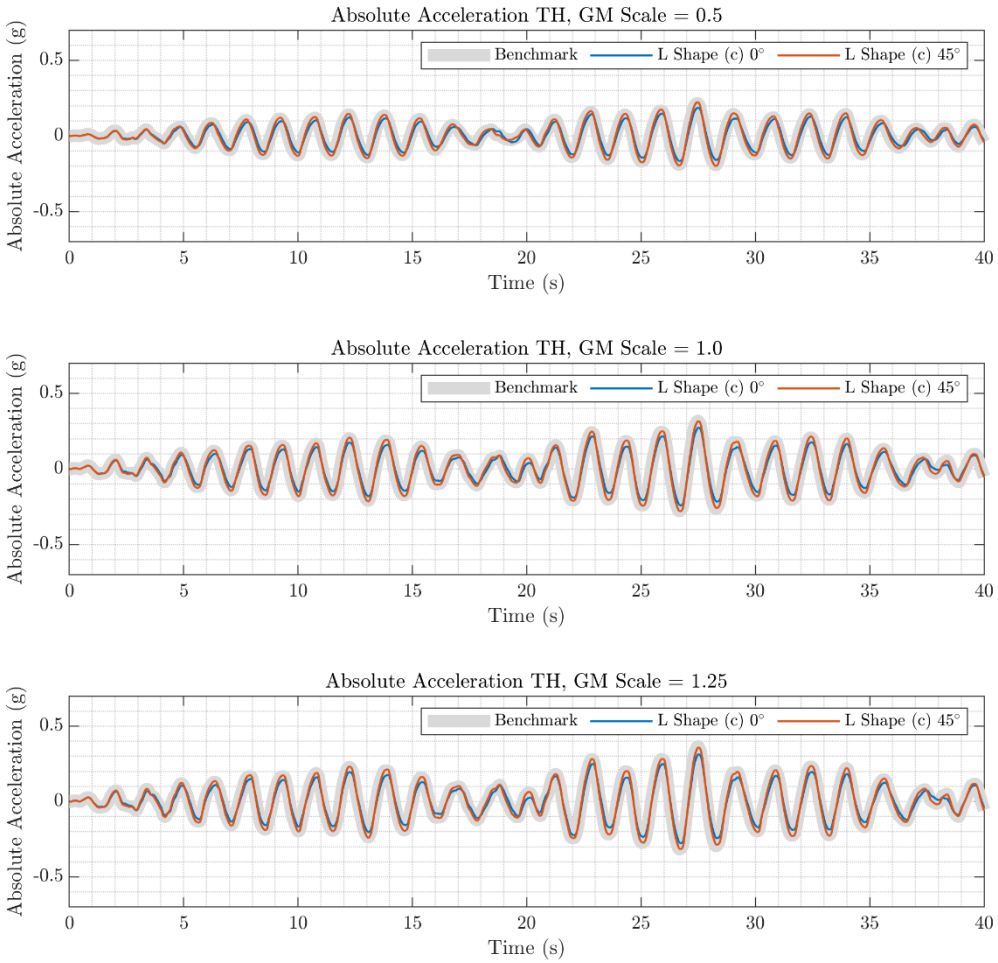

Figure 3-41: Single pile with L Shape (c) configuration. Absolute acceleration TH. N27W (+).

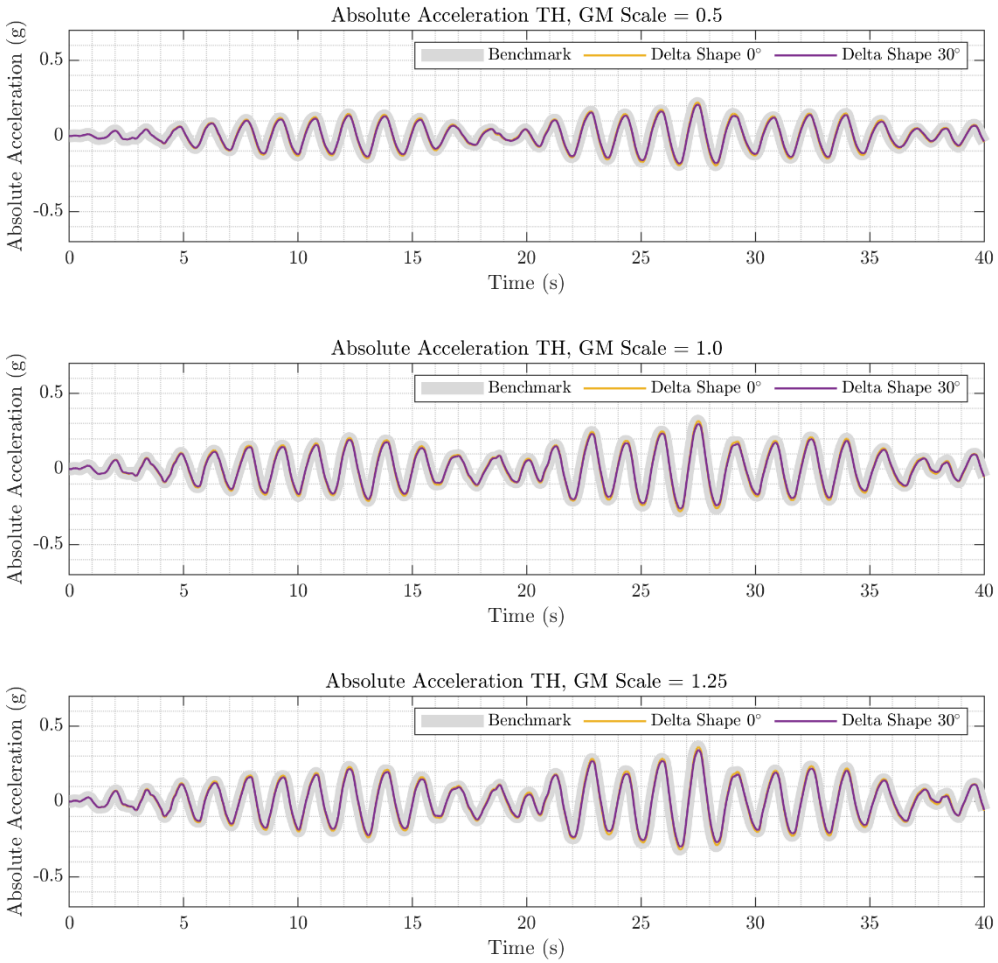

Figure 3-42: Single pile with Delta Shape configuration. Absolute acceleration TH. N27W (+).

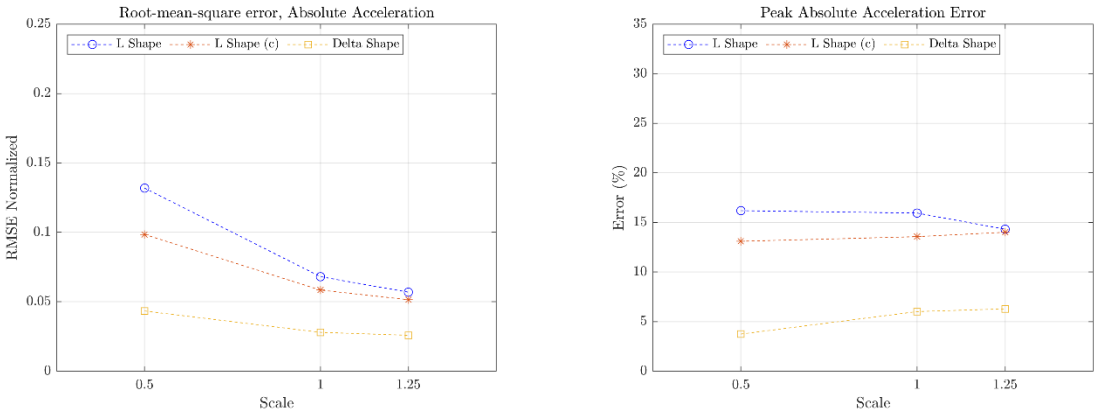

a) RMSE normalized **b) Peak absolute acceleration error**

Figure 3-43: Error for absolute acceleration single pile N27W (+)

Again, the Delta Shape configuration performs better than the Delta Shape configuration. The L Shape configuration has higher directionality than the Delta Shape configuration, which is confirmed by looking at the RMSE (see Figure 3-43a) and Peak absolute acceleration error (Figure 3-43b) plots. Surprisingly, the L Shape (c) configuration does not perform better than the uncorrected L Shape configuration.

For the records considered, an improvement can be noted when using the Delta Shape, configuration especially in terms of directionality. In terms of displacement peaks obtained, no improvement can be seen. It would be important to perform this analysis with a larger number of logs and piles of other dimensions in order to have a more complete database and to be able to compare the configurations in general.

3.3.7 Single pile analysis results: Bending moment envelopes

The flexural moment evolutions along the pile for each configuration are shown below. First, the results for S63W (+) are presented in Figure 3-44 to Figure 3-46.

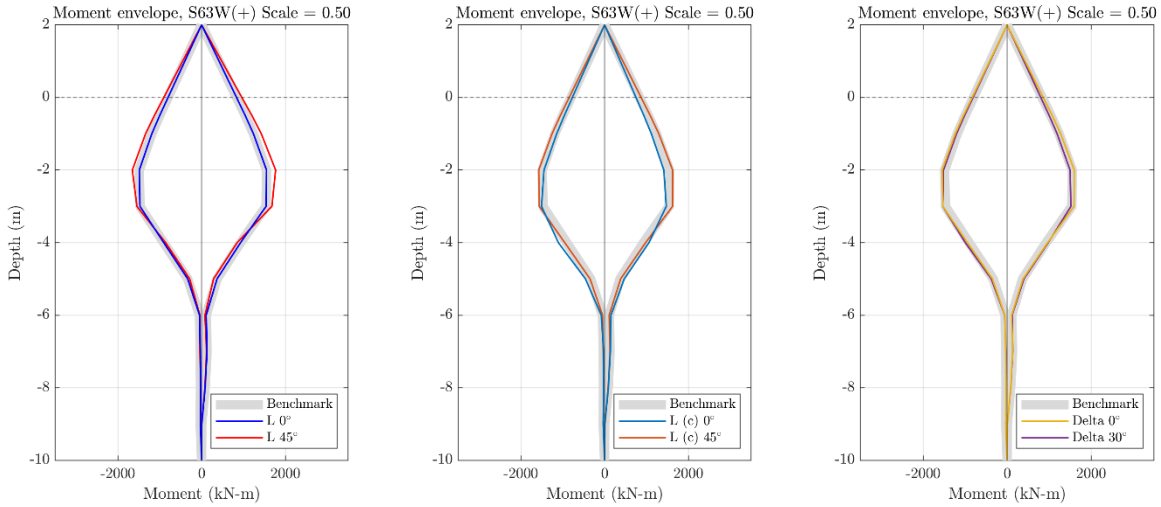

Figure 3-44: Bending moment envelopes. S63W (+) scale =0.50

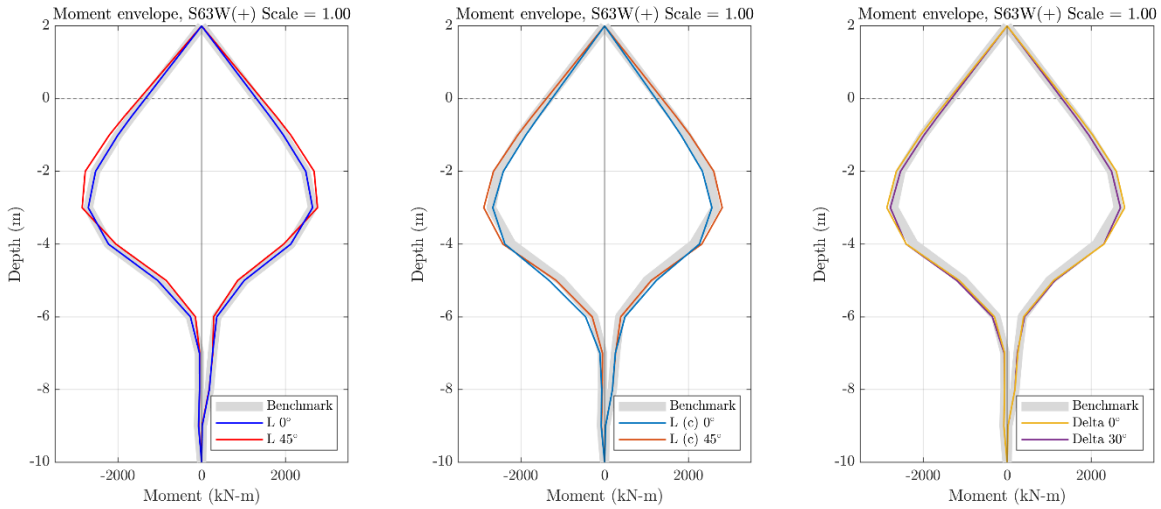

Figure 3-45: Bending moment envelopes. S63W (+) scale =1.00

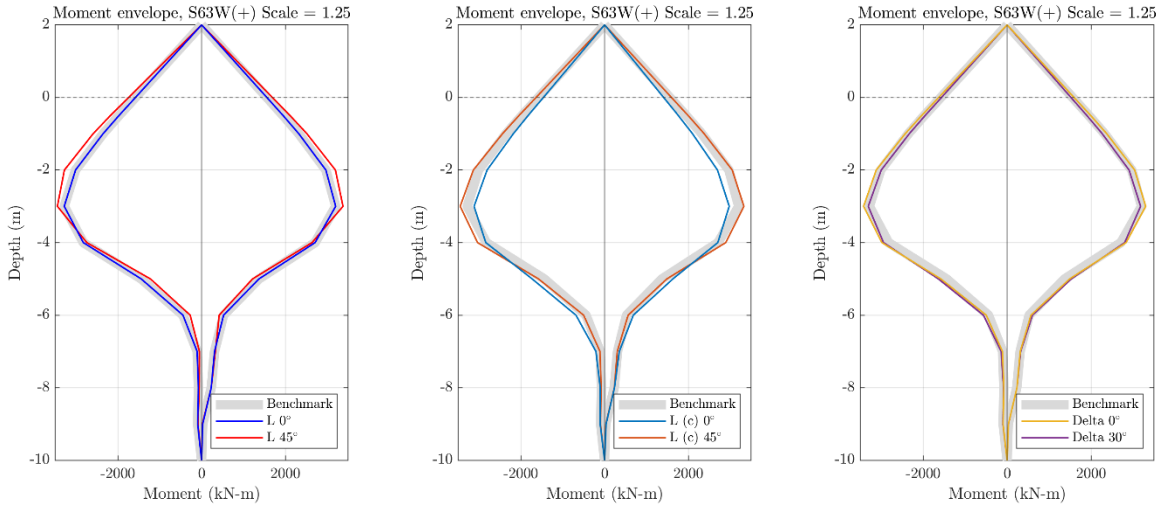

Figure 3-46: Bending moment envelopes. S63W (+) scale =1.25

As in the time-history, it can be noted that the Delta configuration has less directionality than the L configuration. As for the error at the peak moment along the pile, with the L Shape configuration a maximum error of 14.0% is obtained, with L Shape (c) configuration the maximum error is 7.8% and with Delta Shape configuration it is 5.8%.

The same analysis is performed for record N27W (+) (see Figure 3-47 to Figure 3-49).

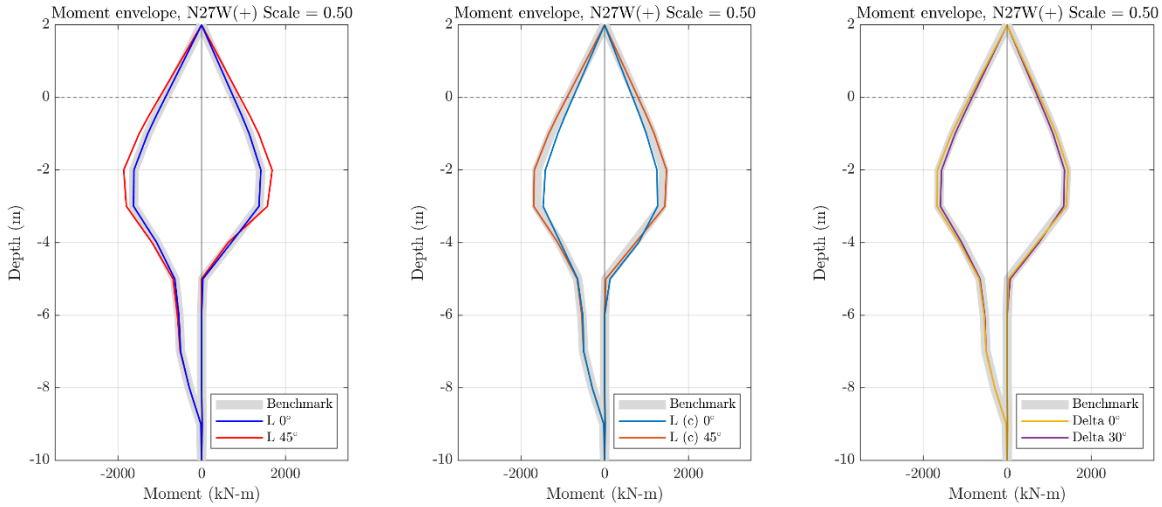

Figure 3-47: Bending moment envelopes. N27W (+) scale =0.50

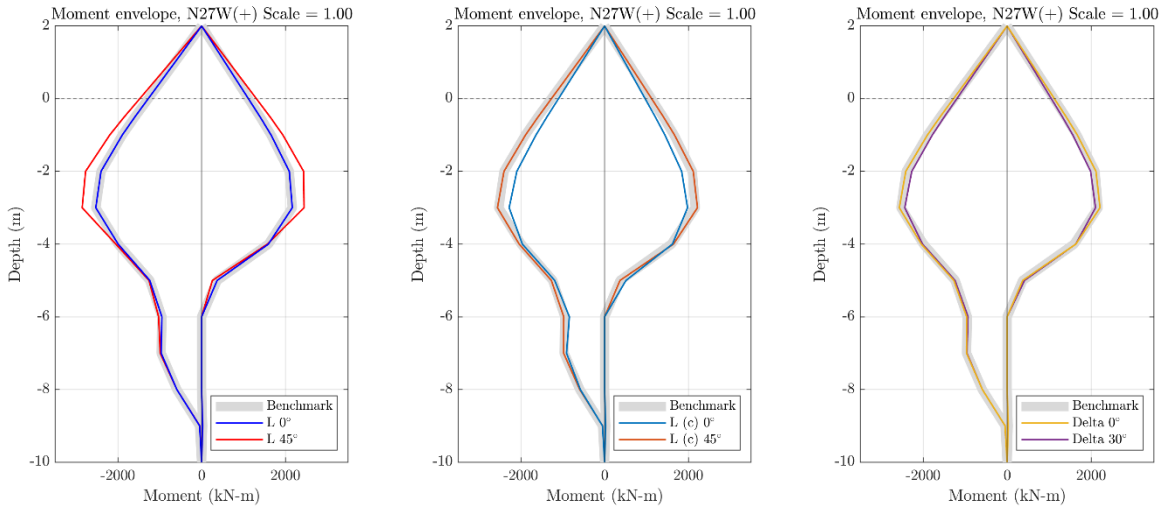

Figure 3-48: Bending moment envelopes. N27W (+) scale =1.00

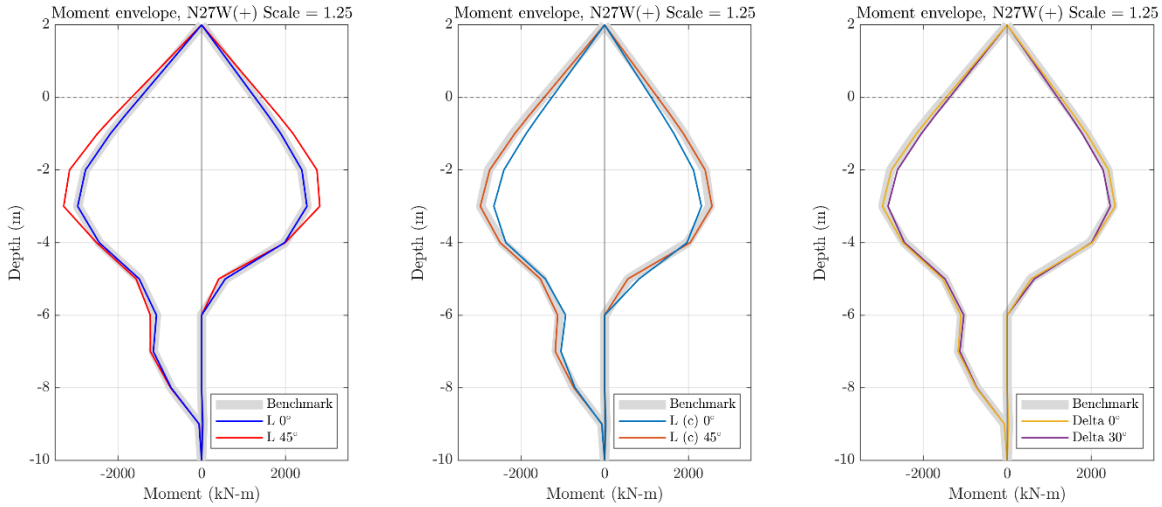

Figure 3-49: Bending moment envelopes. N27W (+) scale =1.25

It can be noted that the Delta configuration has less directionality than the L configuration. As for the error in the peak moment along the pile, with the L Shape configuration a maximum error of 19.1% is obtained, with L Shape (c) configuration the maximum error is 10.6% and with Delta Shape configuration it is 4.1%. For this log it is clearer the superiority of Delta Shape configuration compared to L Shape configuration if higher accuracy in the internal forces along the pile is desired.

3.3.8 Single pile analysis results: 2 components

Having analyzed the pile in one direction, we now analyze the response of the pile subjected to the full log, i.e., considering the S63W (+) component in the X-direction of analysis and the N27W (+) component in the Y-direction of analysis. In this case it is not possible to compare the response with a benchmark behavior, but it is important to analyze the directionality presented (see Figure 3-50 to Figure 3-52).

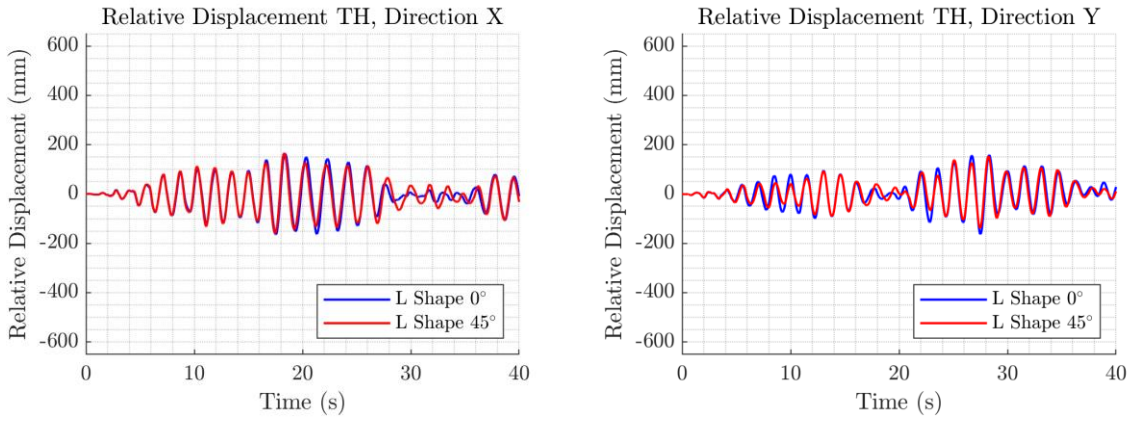

a) Scale = 0.50

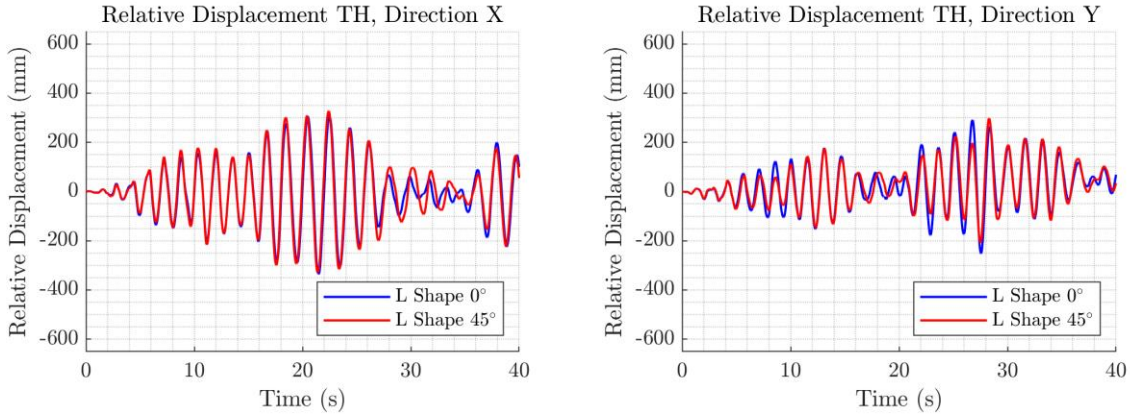

b) Scale = 1.00

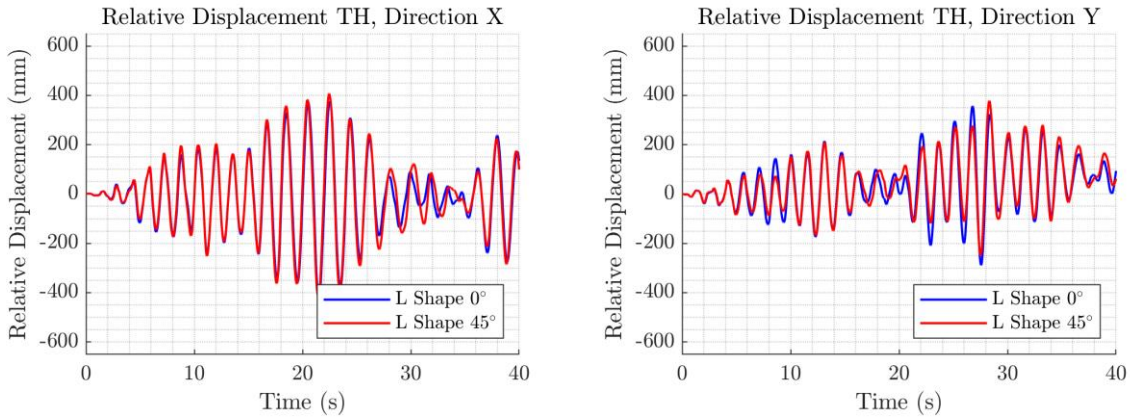

c) Scale = 1.25

Figure 3-50: Single pile with L Shape configuration. Relative displacement TH. 2 components.

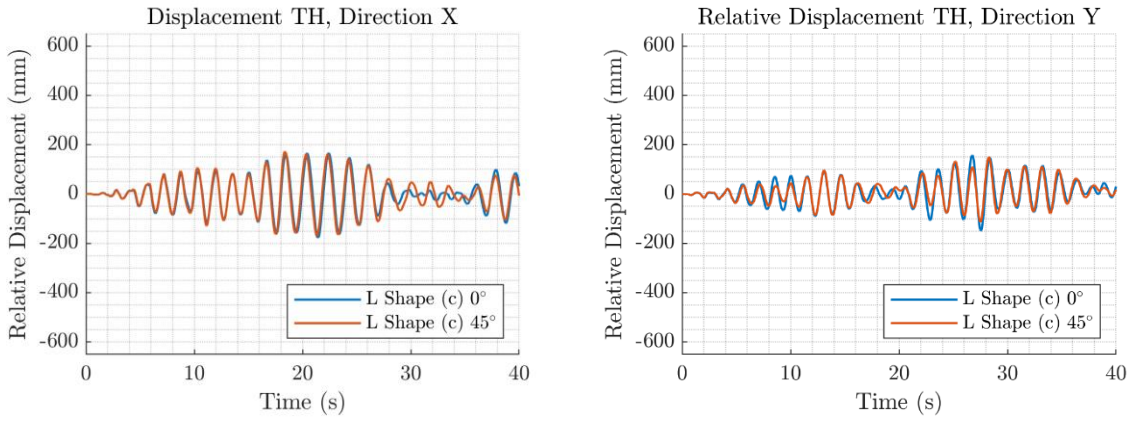

a) Scale = 0.50

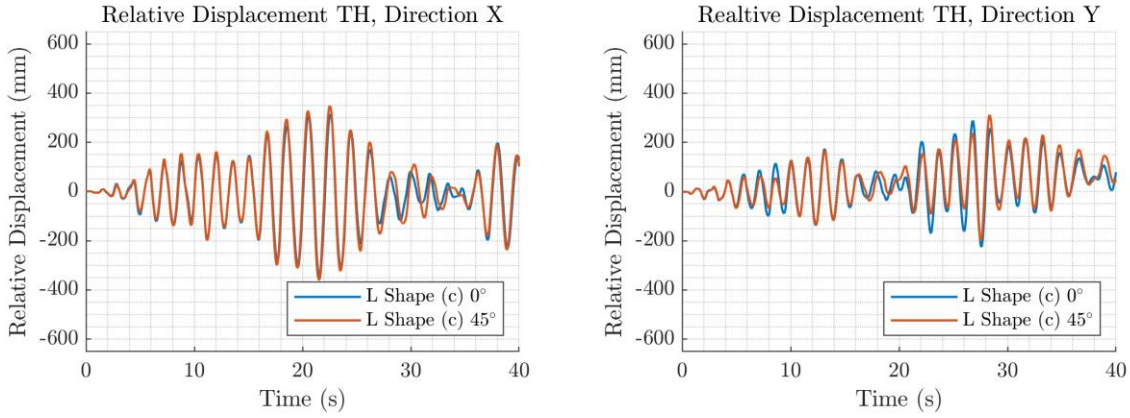

b) Scale = 1.00

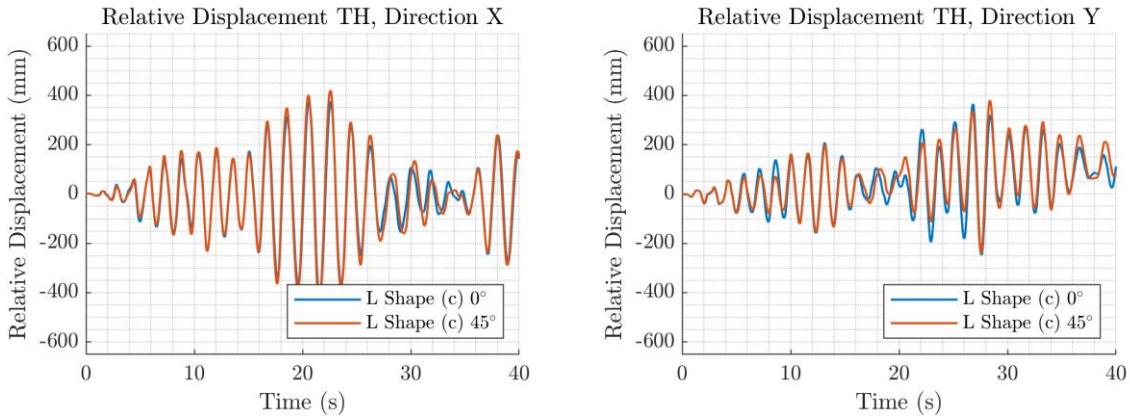

c) Scale = 1.25

Figure 3-51: Single pile with L Shape (c) configuration. Relative displacement TH. 2 components.

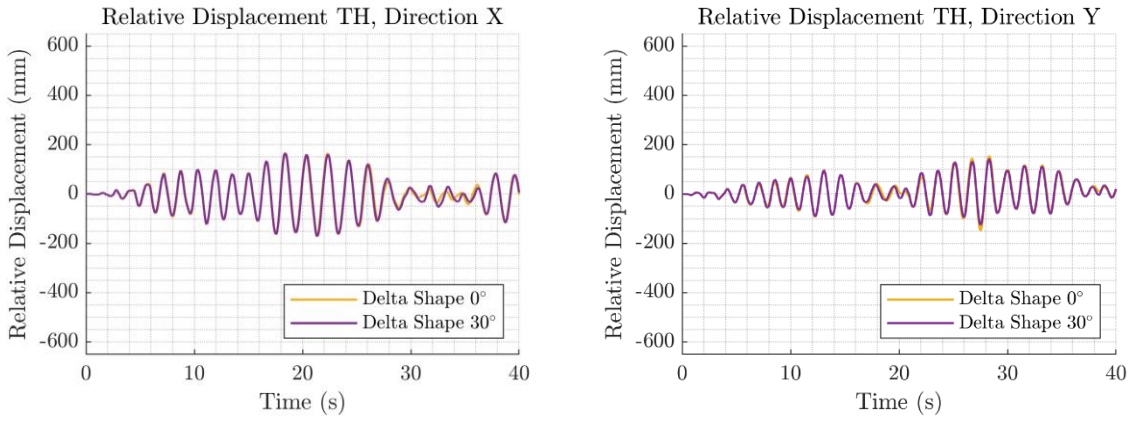

a) Scale = 0.50

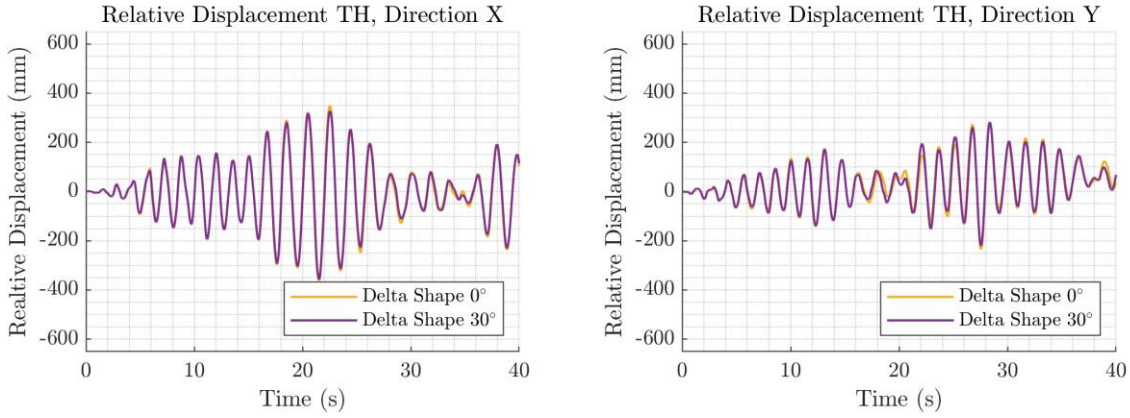

b) Scale = 1.00

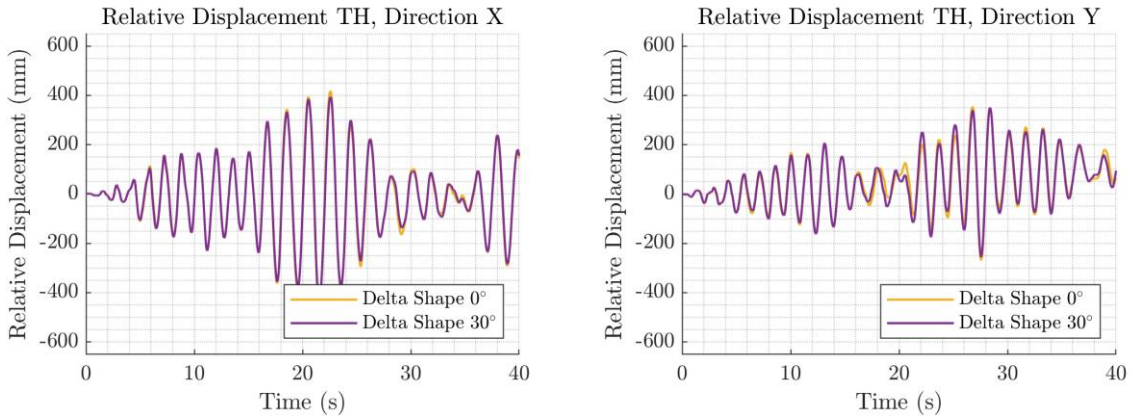

c) Scale = 1.25

Figure 3-52: Single pile with Delta Shape configuration. Relative displacement TH. 2 components.

In this case it is not possible to calculate an error in the response, but the root-mean-square deviation (RMSD) can be calculated to buy the responses as the angle varies. The RMSD is calculated as:

$$RMSD = \left[\frac{\sum_{i=1}^{N}\left(z_{fi} - z_{gi}\right)^2}{N}\right]^{\frac{1}{2}} \tag{3-5}$$

Where z_{fi} corresponds to the values obtained using the configuration with the first critical angle, z_{gi} are the values obtained using the configuration with the second critical angle and N is the total amount of data. In this way, it is possible to analyze the directionality of the configurations, the lower the RMSD the lower the directionality of the configuration. To make the values comparable, the RMSD is normalized by the elastic spectral displacement of the system ($T_1 = 1.125$s) subjected to each of the scaled records.

The RMSD and ratio between the relative displacement peaks for each TH are presented in Figure 3-53.

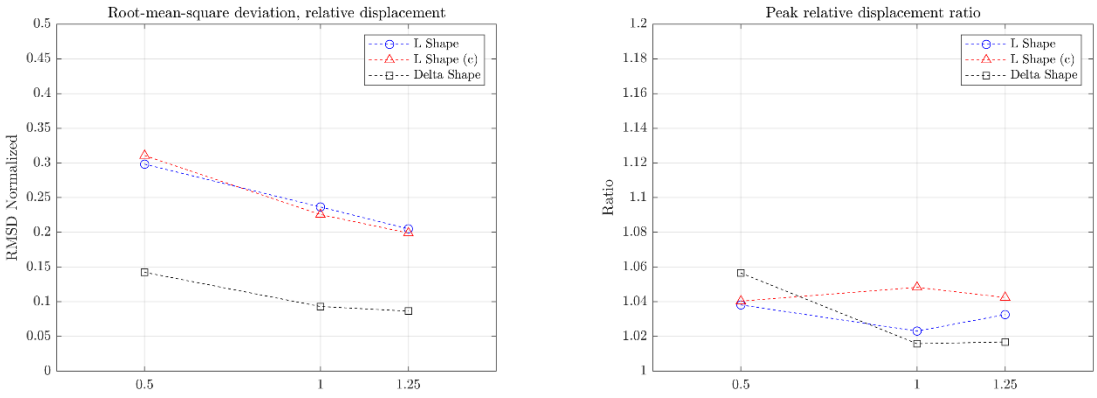

a) RMSD normalized **b) Peak relative displacement ratio**

Figure 3-53: Deviation for relative displacement single pile both components

Both the RMSD and TH plots show that the Delta configuration has lower directionality. As for the displacement peaks, there is no trend indicating the superiority of one configuration over the others.

The same analysis is performed with the absolute acceleration TH in Figure 3-54 to Figure 3-57.

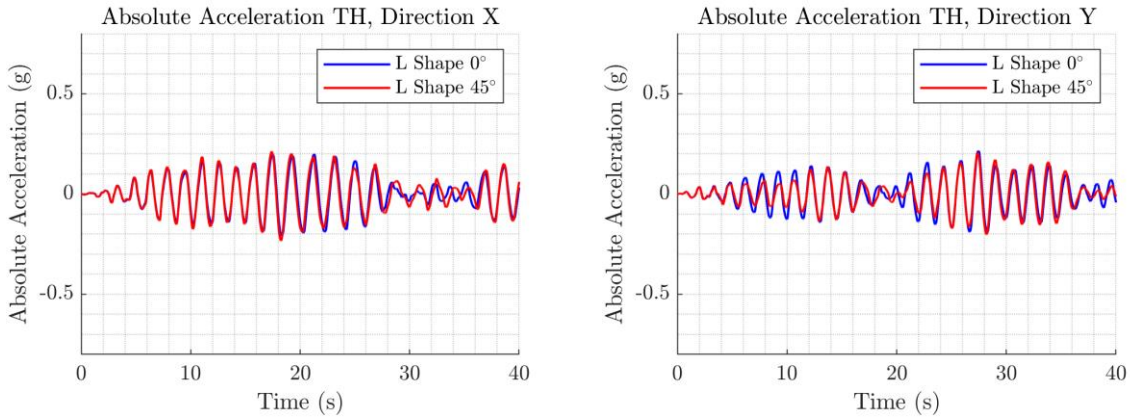

a) Scale = 0.50

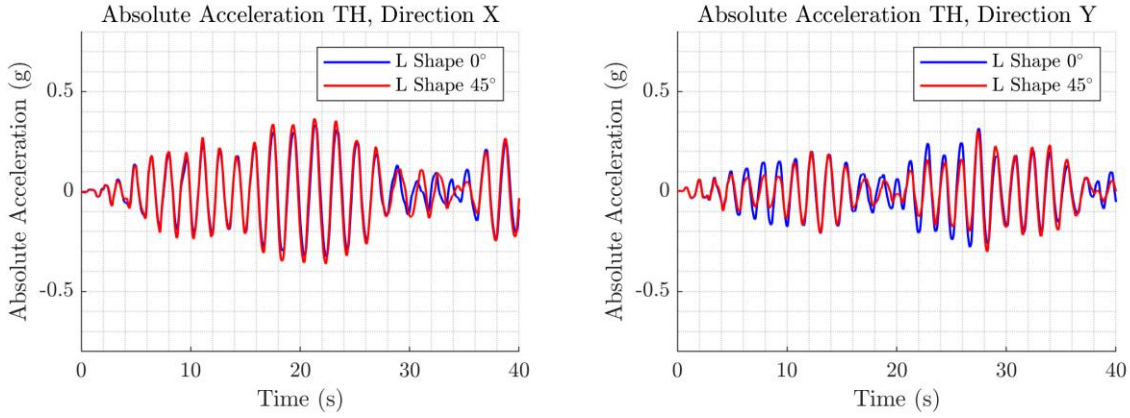

b) Scale = 1.00

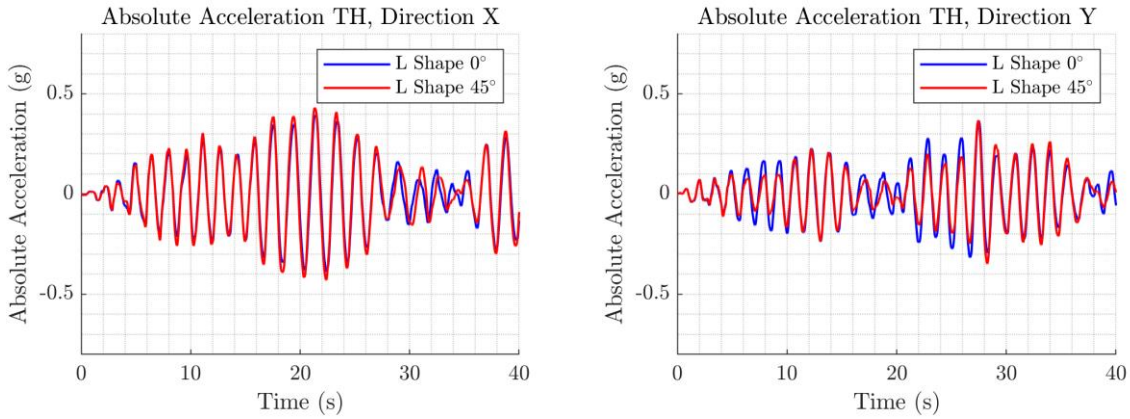

c) Scale = 1.25

Figure 3-54: Single pile with L Shape configuration. Absolute acceleration TH. 2 components.

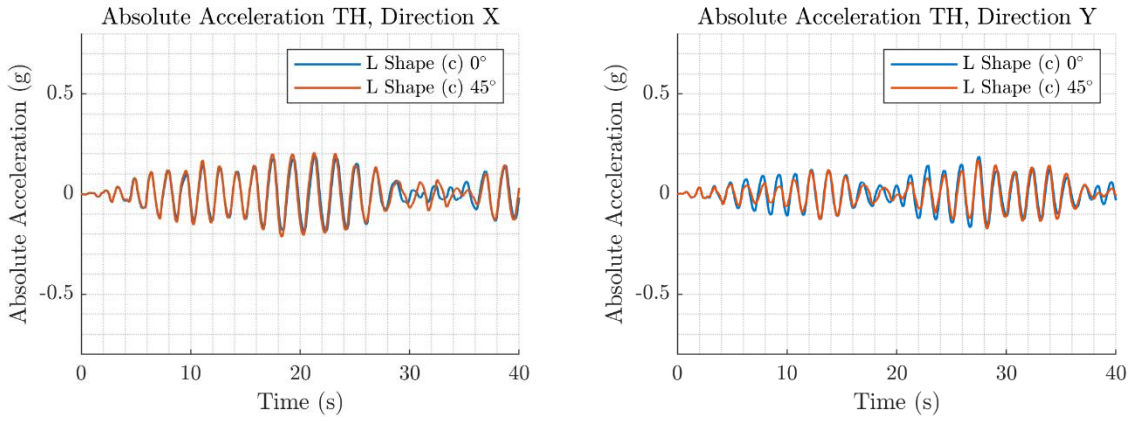

a) Scale = 0.50

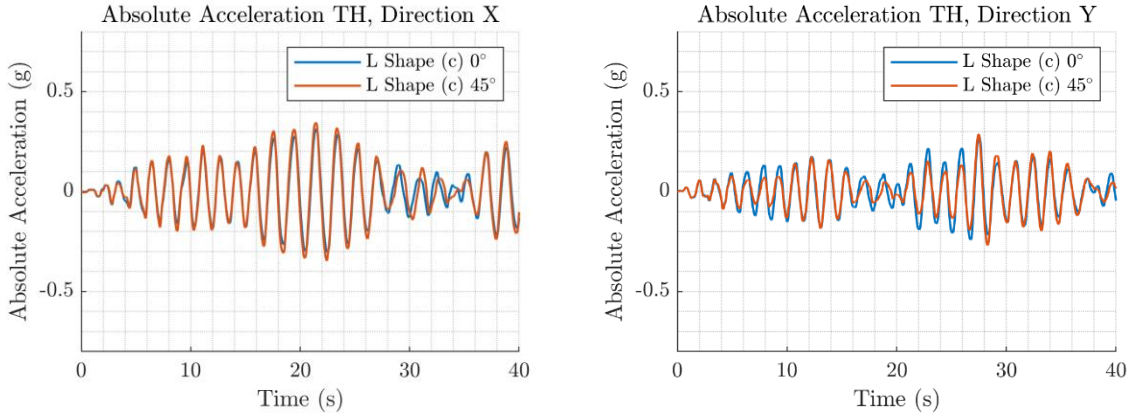

b) Scale = 1.00

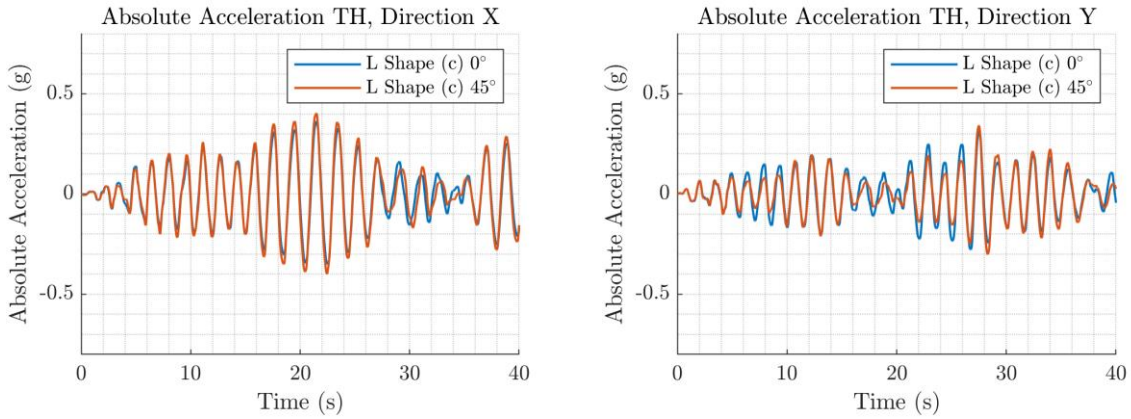

c) Scale = 1.25

Figure 3-55: Single pile with L Shape (c) configuration. Absolute acceleration TH. 2 components.

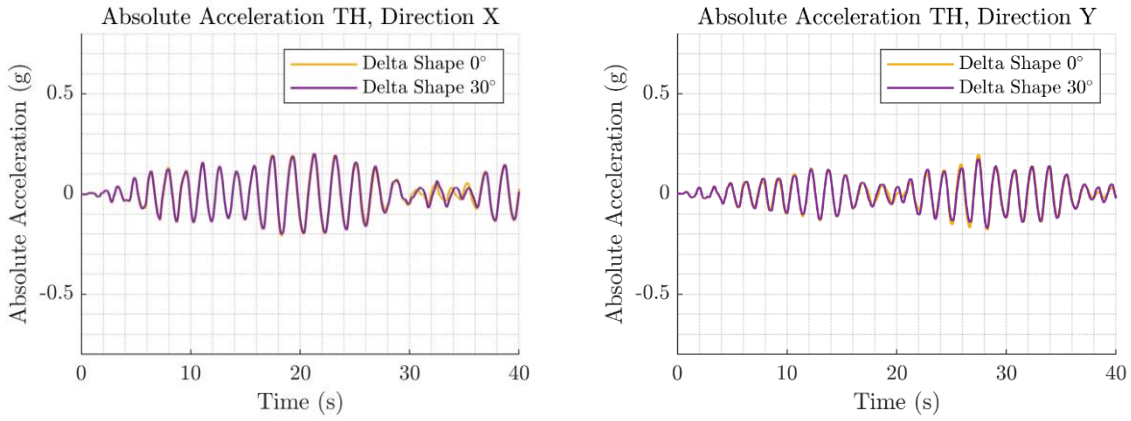

a) Scale = 0.50

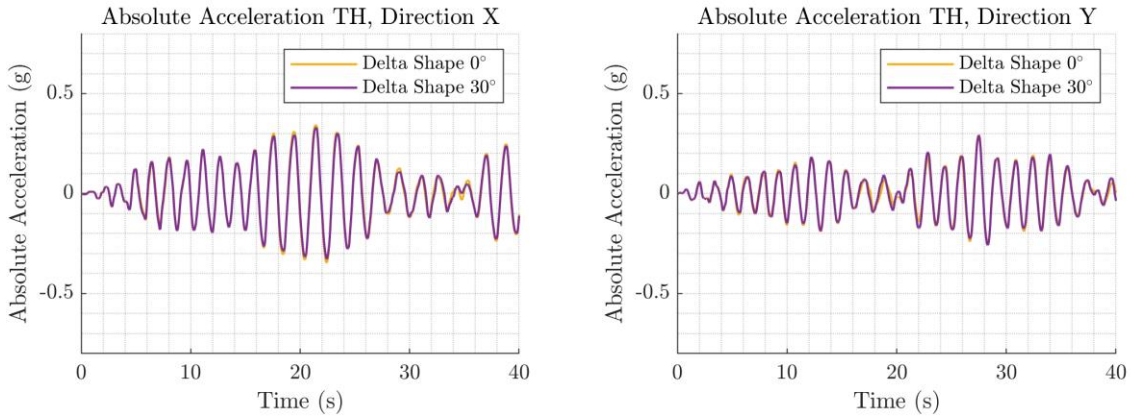

b) Scale = 1.00

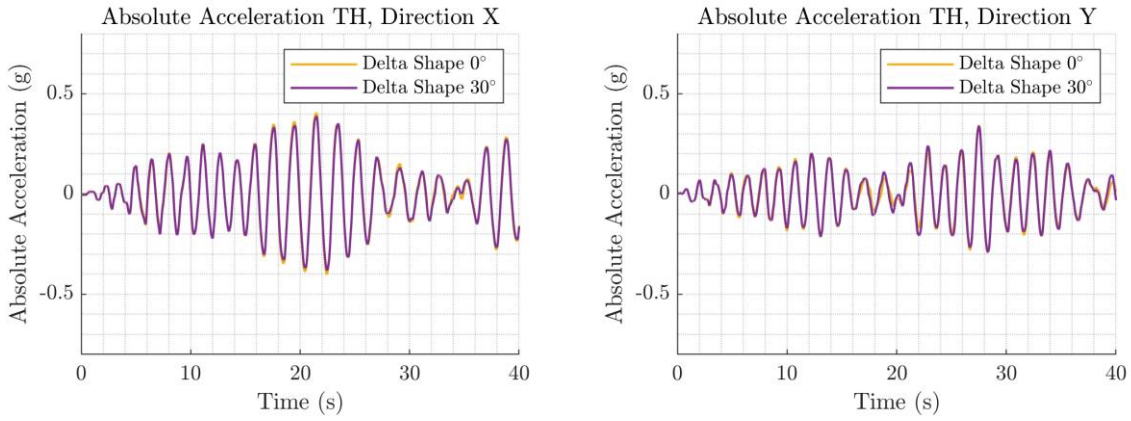

c) Scale = 1.25

Figure 3-56: Single pile with Delta Shape configuration. Absolute acceleration TH. 2 components.

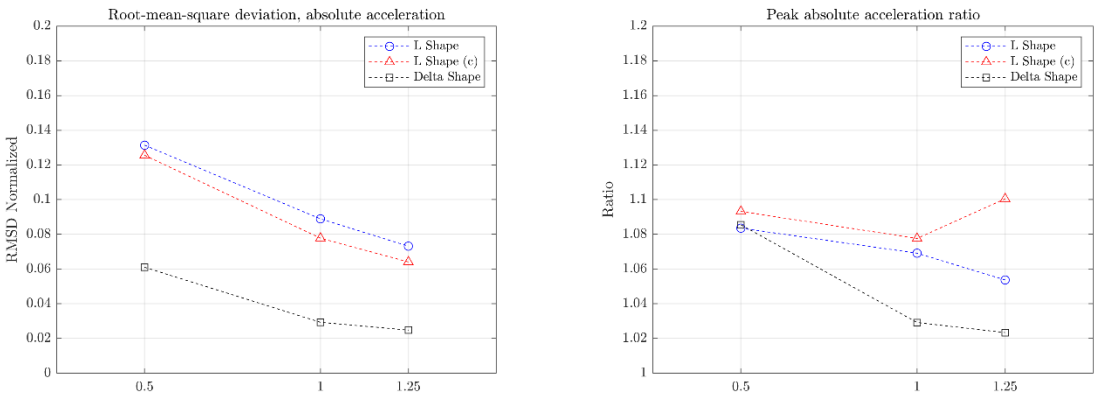

a) RMSD normalized **b) Peak absolute acceleration ratio**

Figure 3-57: Deviation for absolute acceleration single pile both components

The results obtained have the same trends noted previously. The Delta Shape configuration presents a lower directionality, but no advantage in the prediction of the peak absolute acceleration response. The differences between using L Shape and L Shape (c) configurations are practically negligible.

From the results, it can be seen that the Delta Shape configuration performs better than the L Shape configuration. In order to make more general conclusions, a larger number of analyses should be performed considering other ground motions.

3.4 GROUP OF 4 PILES

3.4.1 Group of piles model

After the analysis performed for a single pile, we proceed to the analysis of a structure with 4 piles. This structure consists of 4 piles of 600 mm diameter embedded 10 m and 4 m long above ground level (see Figure 3-59). In the plan view the structure measures 4 m wide by 4 m long (see Figure 3-58). The piles are elastic frame elements and are connected to each

other at their upper end by rigid frame elements. The fundamental period of the structure is 1.056s. The nonlinear analysis is performed considering a damping ratio equal to 0.5% in the first mode and 10% at 20Hz. Each pile is assigned a mass M of 200 tons at its top node.

In this case, because the structure may be rocking, it is necessary to incorporate the t-z and q-z springs in the model to represent the vertical soil-structure interaction.

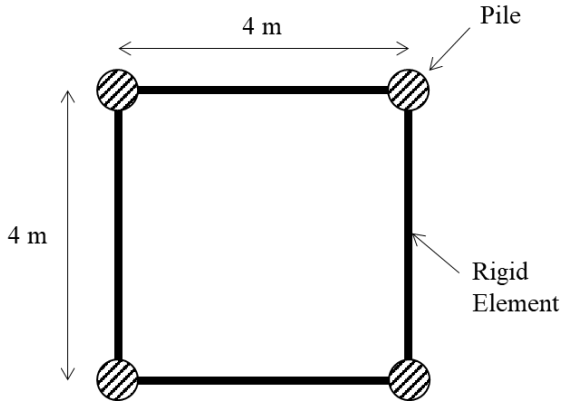

Figure 3-58: 4 piles supported structure plan view.

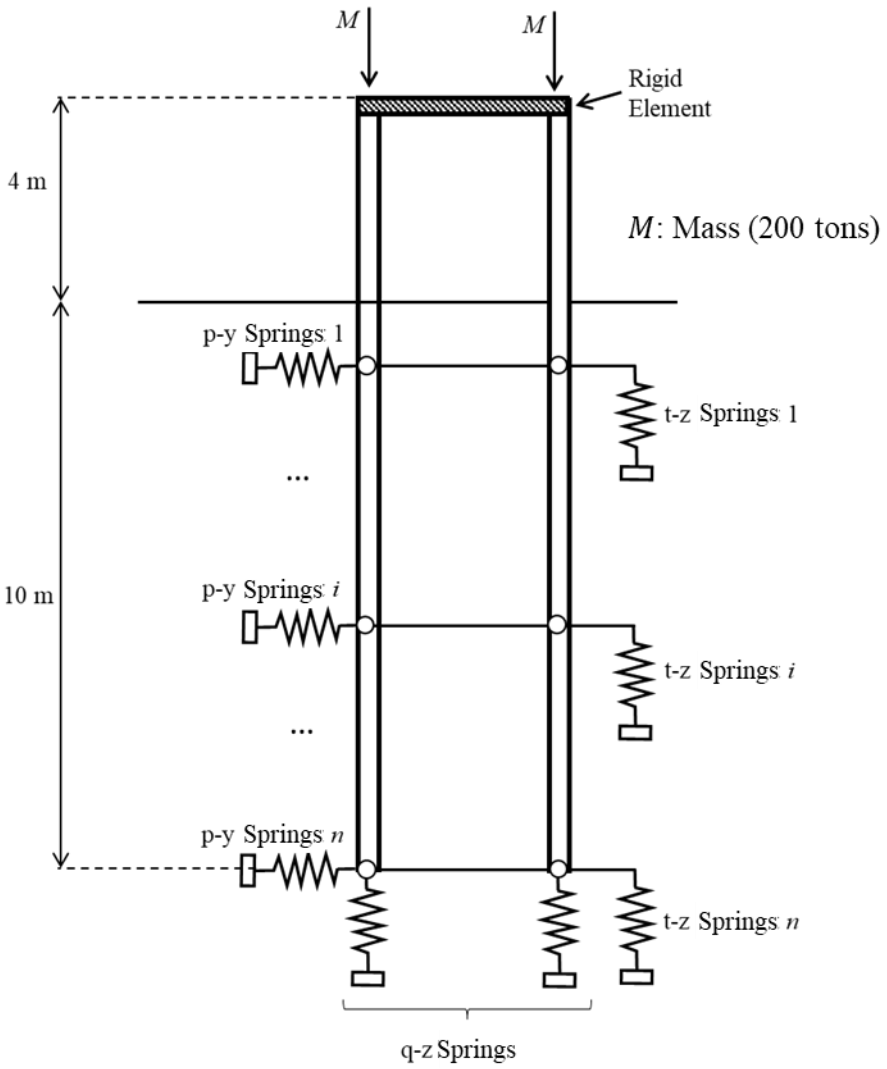

Figure 3-59: 4 piles supported structure elevation.

3.4.2 Group of piles analysis results

The input and soil profile considered are the same as those considered for the single pile. The TH obtained for the relative displacement of the center of gravity of the structure are presented in Figure 3-60 to Figure 3-62.

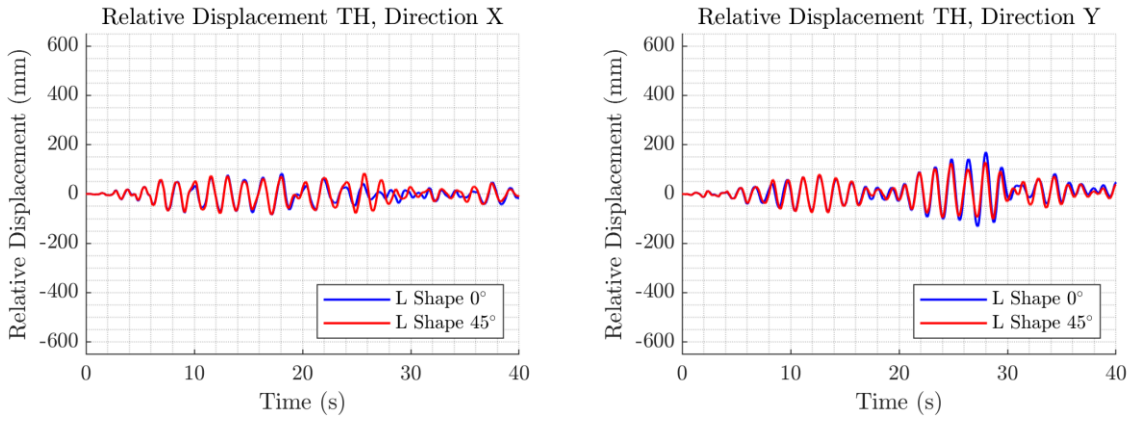

a) Scale = 0.50

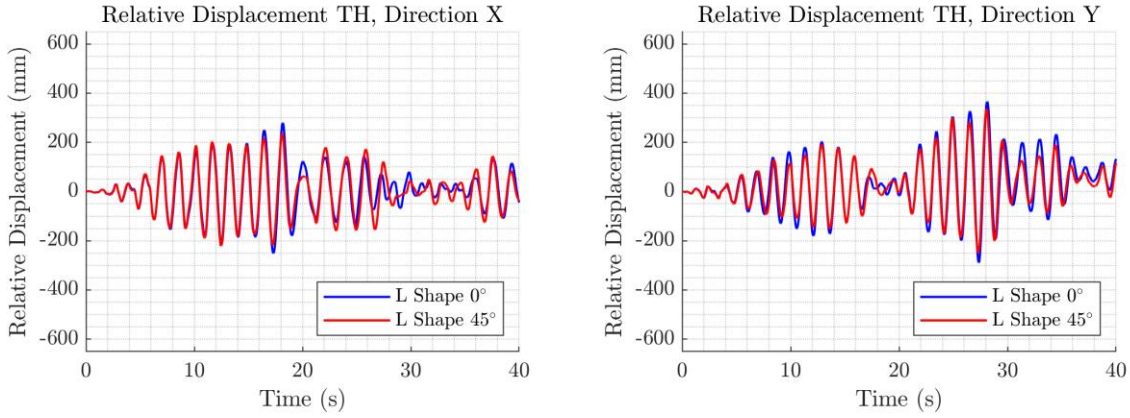

b) Scale = 1.00

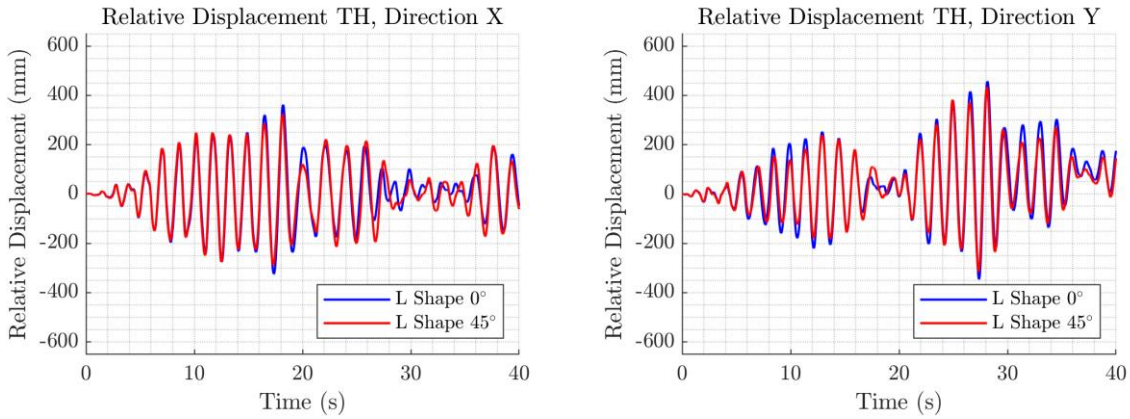

c) Scale = 1.25

Figure 3-60: 4 piles with L Shape configuration. Relative displacement TH.

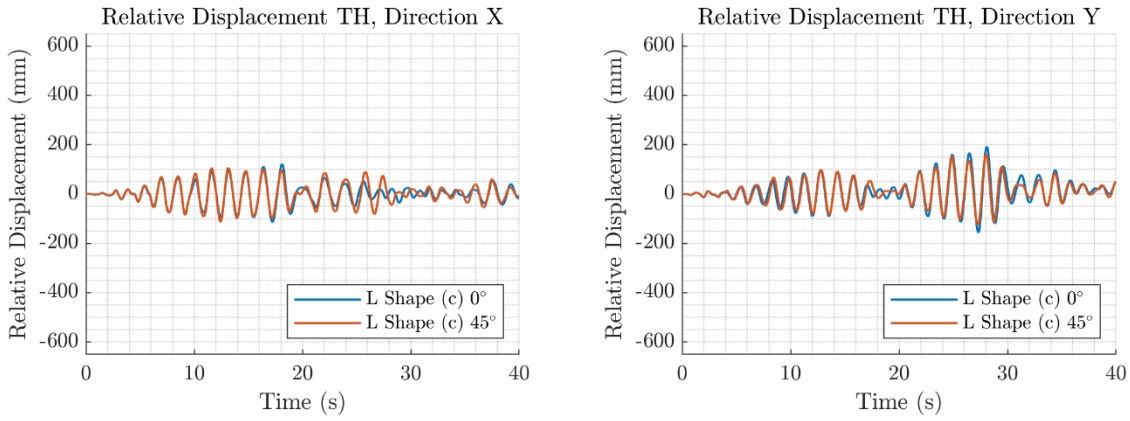

a) Scale = 0.50

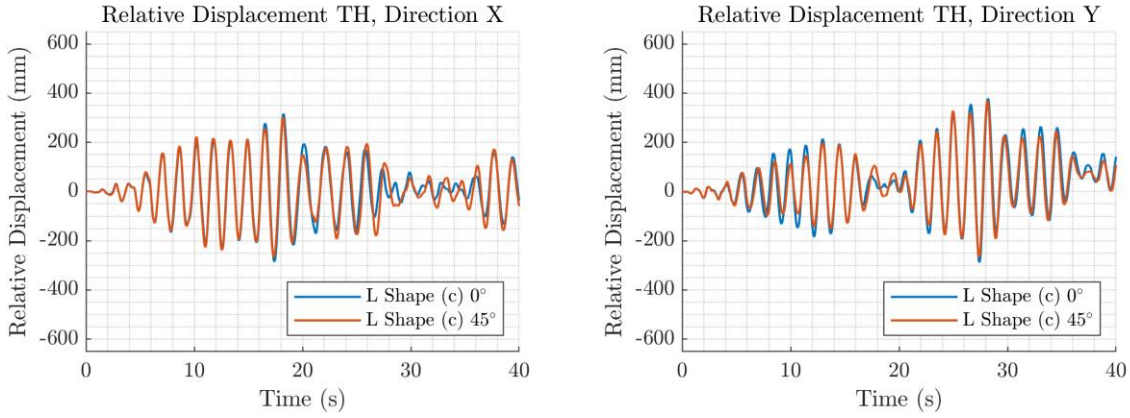

b) Scale = 1.00

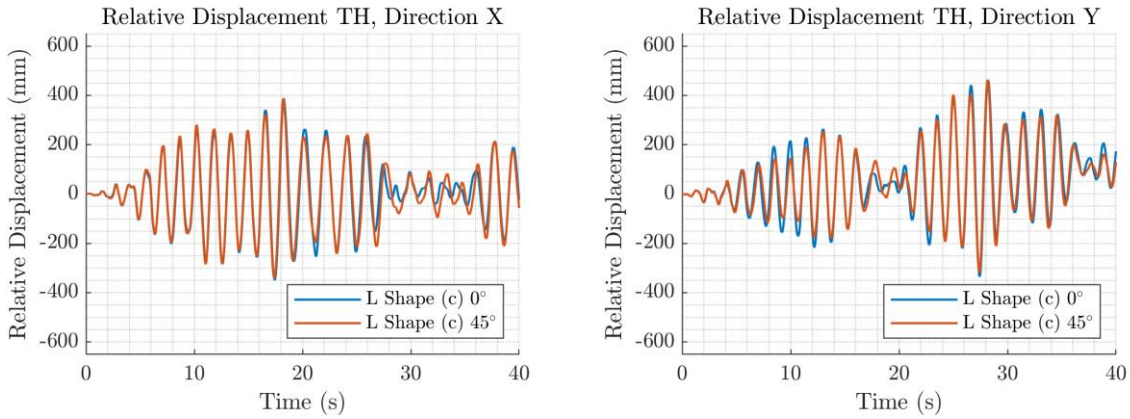

c) Scale = 1.25

Figure 3-61: 4 piles with L Shape (c) configuration. Relative displacement TH.

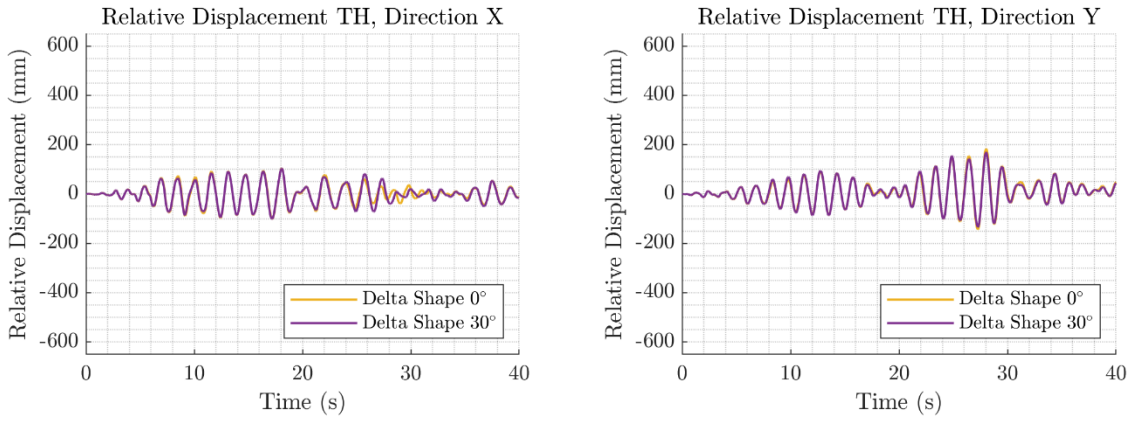

a) Scale = 0.50

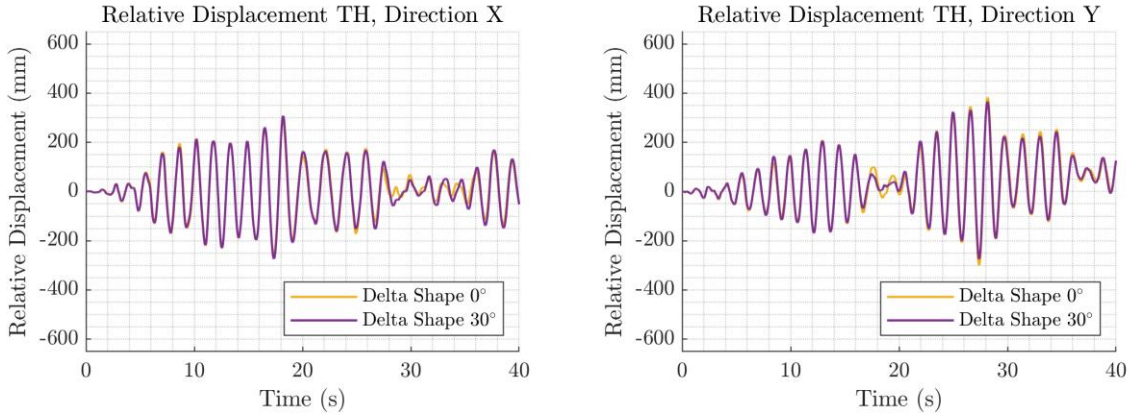

b) Scale = 1.00

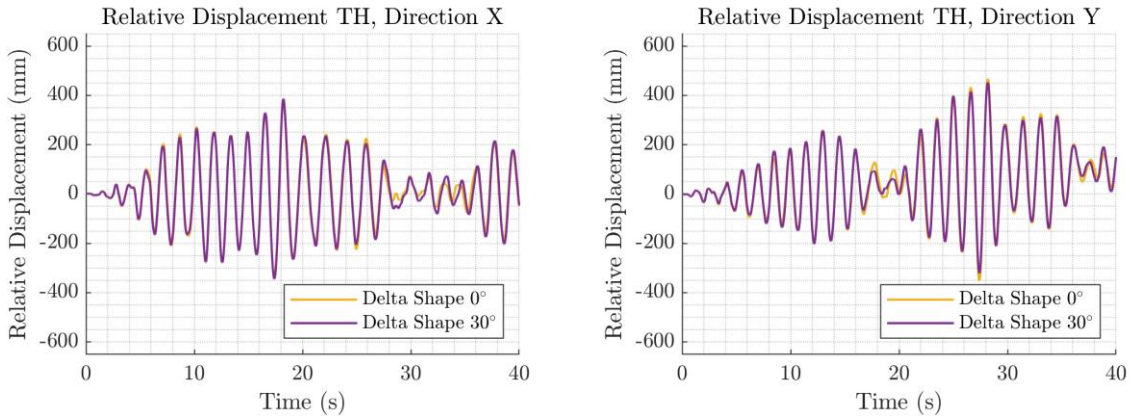

c) Scale = 1.25

Figure 3-62: 4 piles with Delta Shape configuration. Relative displacement TH.

As in the case of the single pile, less directionality is seen when considering the Delta Shape configuration. It can be seen that a residual displacement is obtained in the Y direction. The RMSD and peak relative displacement ratios are shown in Figure 3-63.

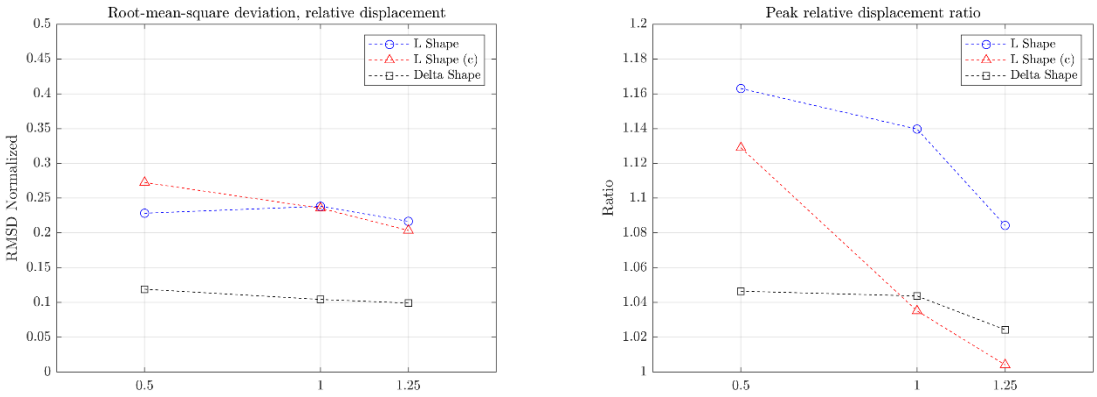

a) RMSD normalized **b) Peak relative displacement ratio**

Figure 3-63: Deviation for relative displacement group of piles

It is reaffirmed that Delta Shape p-y spring configuration has a better performance in terms of directionality, being the Delta Shape configuration that is practical and nearly omnidirectional. As for peak relative displacement, the uncorrected L Shape configuration shows the greatest directionality bias but there is no clear advantage of any of the configurations over the others.

Next, the analysis is repeated but for the absolute acceleration of the center of gravity of the structure (see Figure 3-64 to Figure 3-67).

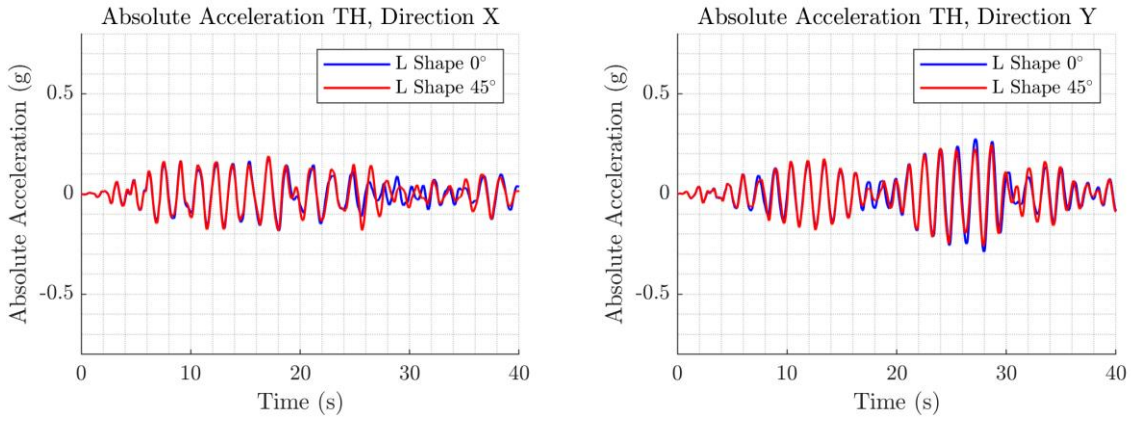

a) Scale = 0.50

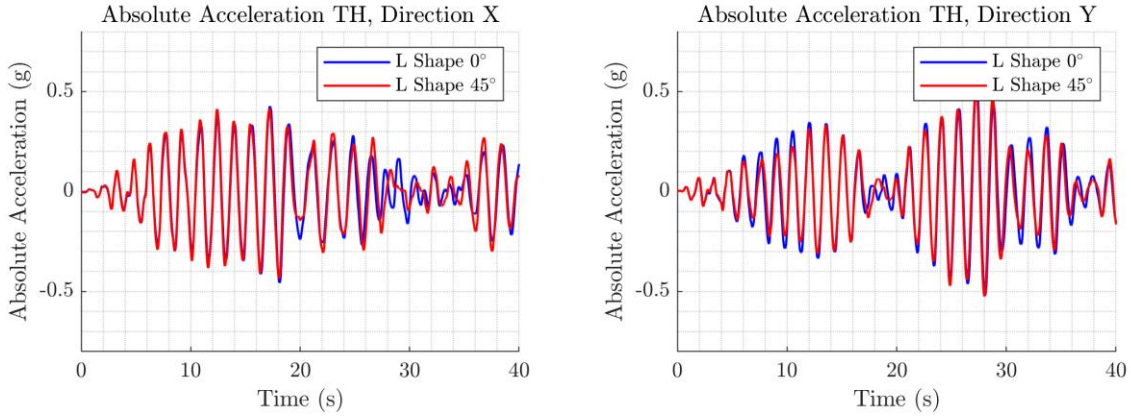

b) Scale = 1.00

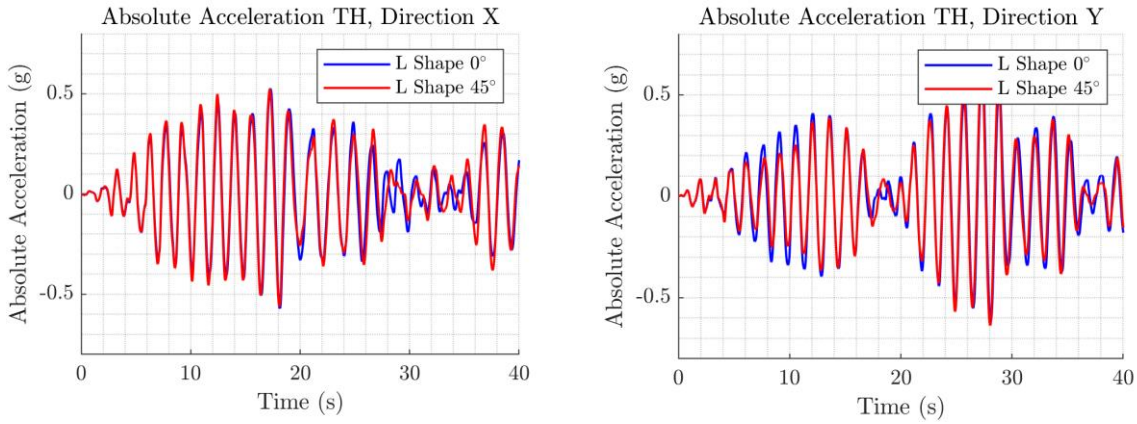

c) Scale = 1.25

Figure 3-64: 4 piles with L Shape configuration. Absolute acceleration TH.

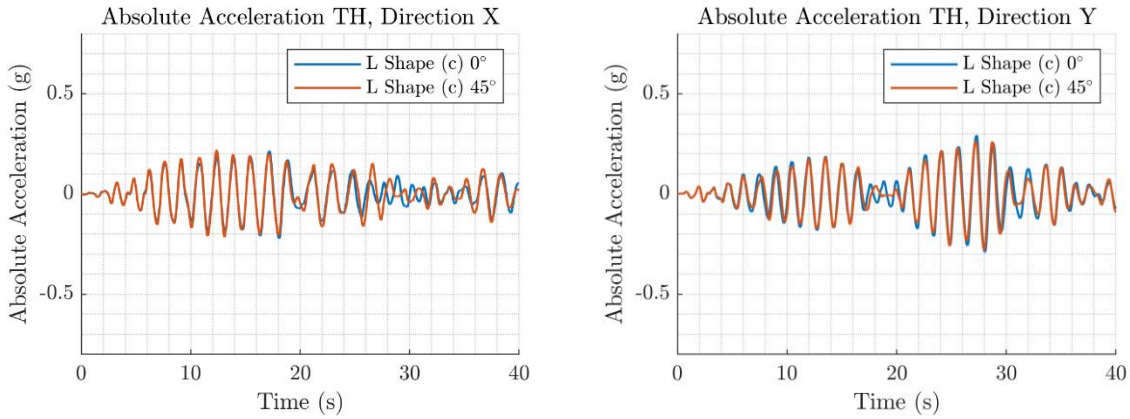

a) Scale = 0.50

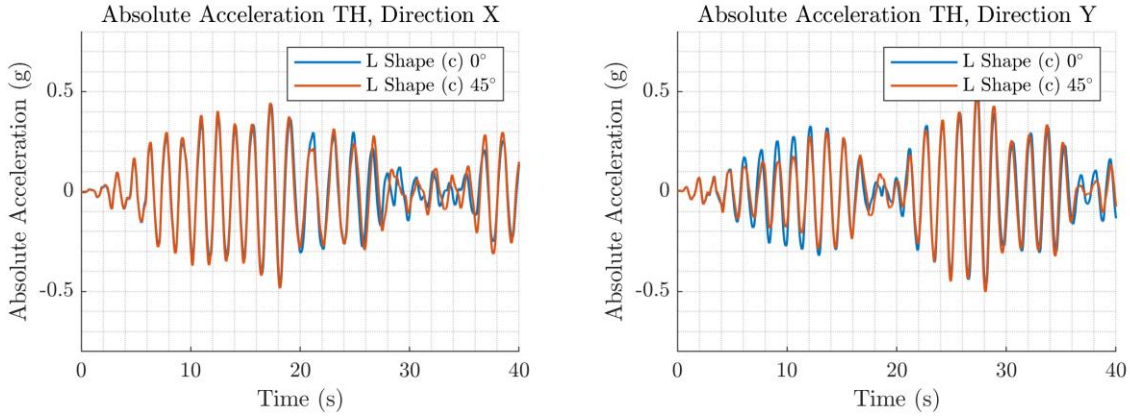

b) Scale = 1.00

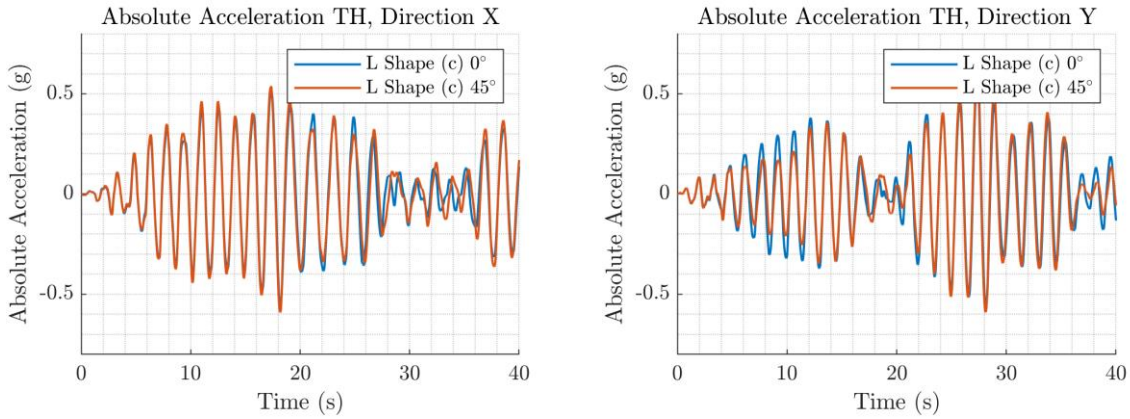

c) Scale = 1.25

Figure 3-65: 4 piles with L Shape (c) configuration. Absolute acceleration TH.

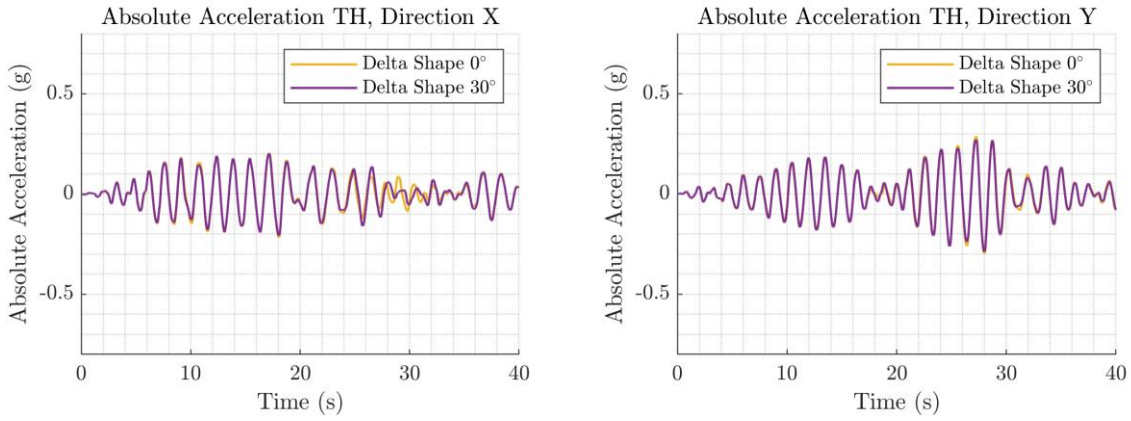

a) Scale = 0.50

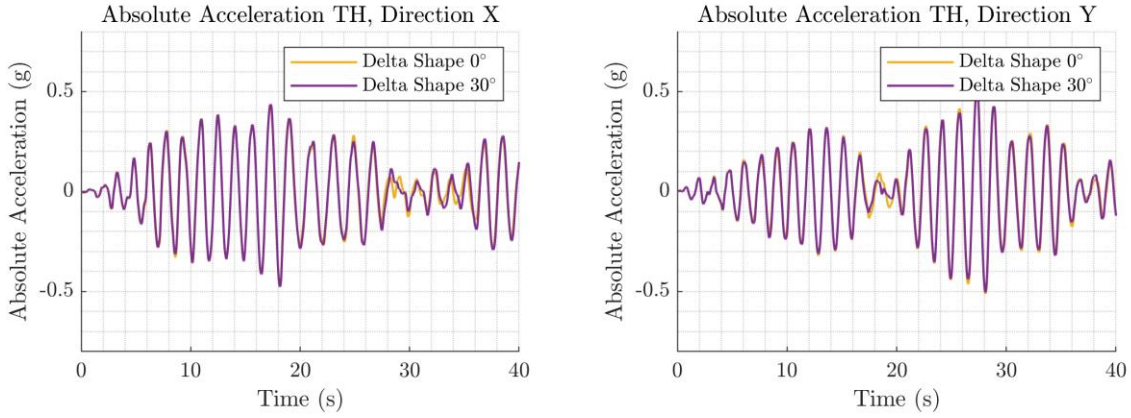

b) Scale = 1.00

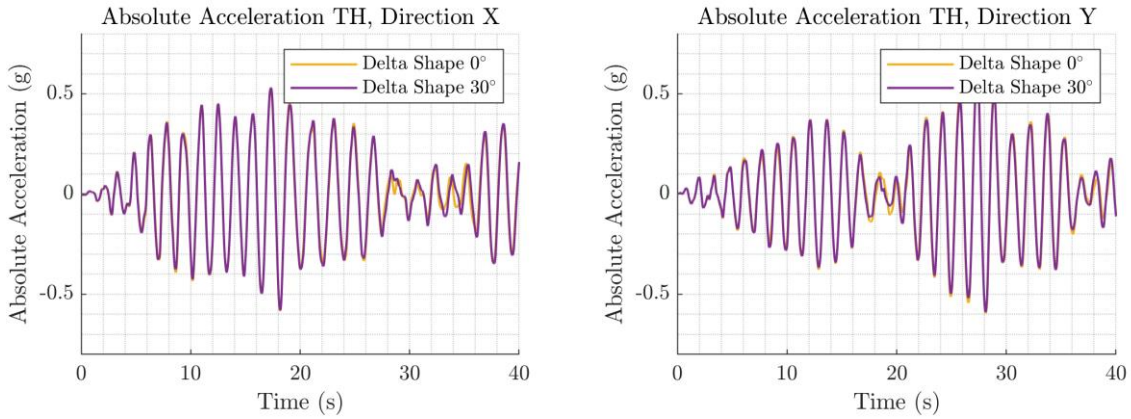

c) Scale = 1.25

Figure 3-66: 4 piles with Delta Shape configuration. Absolute acceleration TH.

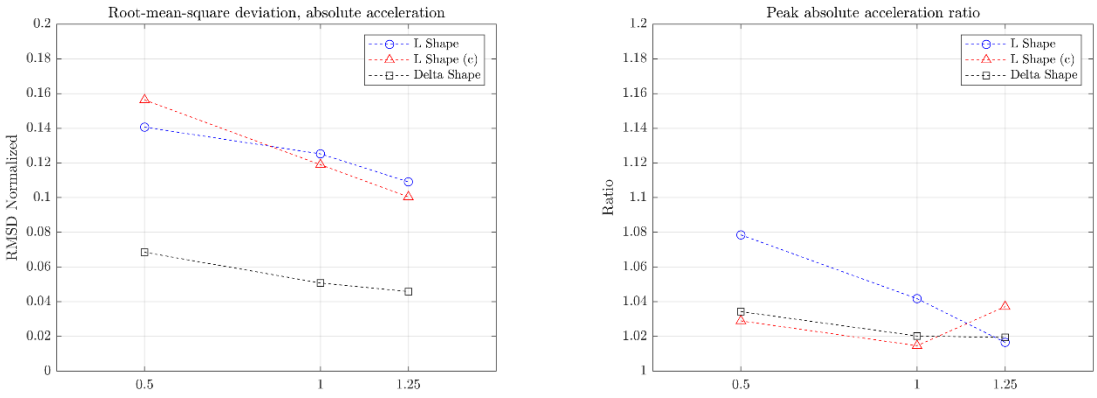

a) RMSD normalized **b) Peak absolute acceleration ratio**

Figure 3-67: Deviation for absolute acceleration group of piles

It can be noted again that the Delta Shape p-y spring configuration performs better than the L Shape configuration in terms of directionality.

3.5 P-Y SPRINGS HYSTERETIC RESPONSE

This section presents the hysteretic responses of select p-y springs. The stiffness and yield strength of the p-y springs vary with depth, soil type and water table location. Hysteretic responses of the p-y springs in the single pile model considering both components of the seismic record and the Delta Shape configuration are presented in Figure 3-68. In the X direction the level of forces and deformations is greater than in the Y-direction. It can also be noticed how at 0.5m depth, which corresponds to 0.8 pile diameters, the soil resistance is very low, and the lateral displacements are much larger than those observed at deeper springs. Then, at 3m depth, which corresponds to 5 pile diameters, the response is also nonlinear, and lateral displacements are smaller than those observed near the ground surface. Also, the strength of the soil column at this depth is greater than that at the vicinity of the surface. It is at around this depth that the largest energy dissipation occurs in the soil column. At 8m depth, which corresponds to 13.3

pile diameters, the p-y springs are linear, and the level of stress and lateral displacements are smaller. This is reflected in the moment diagrams presented in section 3.3.7. In Figure 3-69, the same results are shown, but for one pile of the 4-pile group model. The results obtained are similar to the case of the single pile model. It can be seen how the stiffness increases with depth and the deformation decreases.

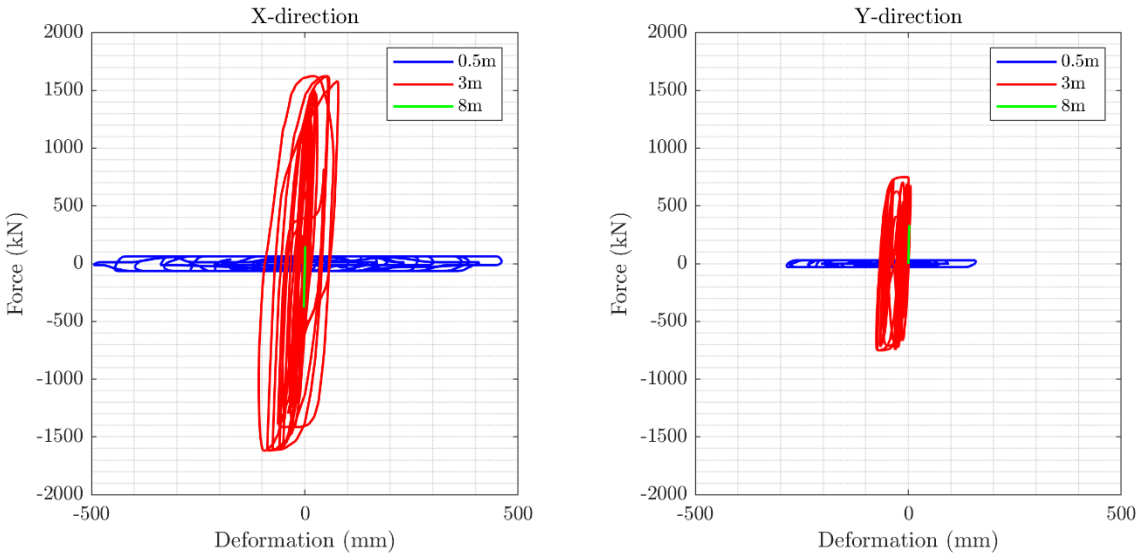

a) X-Direction **b) Y-Direction**

Figure 3-68: p-y springs hysteretic response along the pile. Single Pile model.

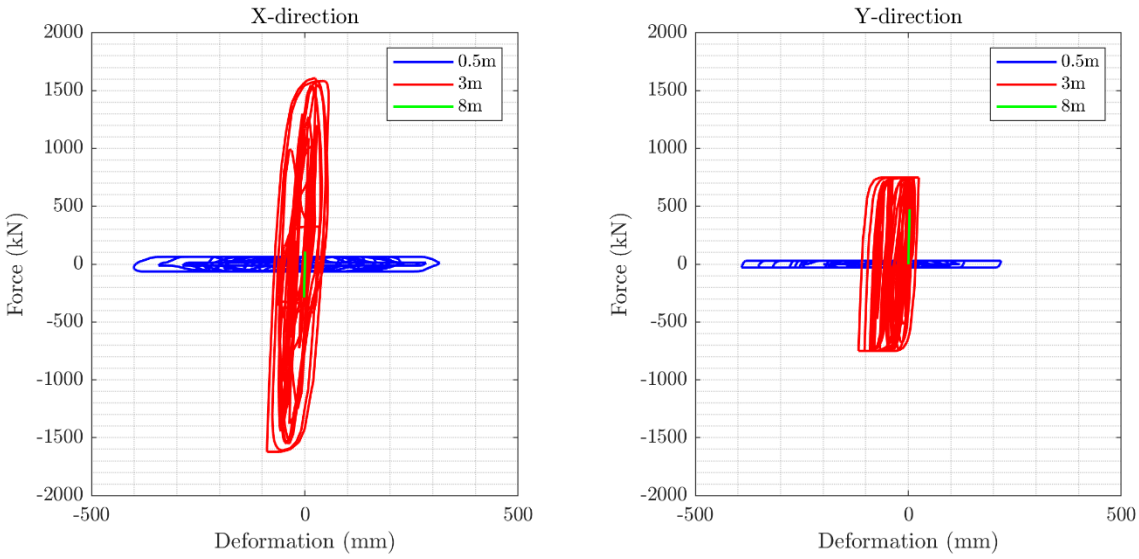

a) X-Direction **b) Y-Direction**

Figure 3-69: p-y springs hysteretic response along a pile. Group of 4 piles model.

3.6 CONCLUSIONS

In both the single pile and 4 pile models, it was found that the Delta Shape configuration has advantages over the L Shape and L Shape (c) configurations. Between using L Shape and L Shape (c) there are no major differences. The Delta Shape configuration performs better in terms of directionality and stress determination in the pile. However, when predicting peak displacements and accelerations there is no major difference between using the Delta Shape and L Shape (c) configurations.

4 SYSTEM-LEVEL MODEL AND GROUND MOTION INPUT

4.1 GENERAL DESCRIPTION

The building described in this section and used for the system-level analysis with and without piles is largely based on an existing apartment building located in Viña del Mar, Chile deigned in 2010 following the NCh433 (2009) standard. This building has twenty-three stories with one basement. The basement and first story are 2.7 m high. The remaining stories are 2.52 m in height. The total height of the building is 58.32 m. The building's structural system consists of an array of 200 to 300 mm thick reinforced concrete walls. These walls are connected by inverted-T reinforced concrete beams. The floor system is 170 mm and 160 mm thick reinforced concrete slabs. This is the typical structural system used in Chile for residential buildings. However, this building has the particularity of having pile foundations, whose use has become more popular in Chile in the past decade. The plan view of the basement, the first story, and the typical story of the building is shown in Figure 4-1, Figure 4-3,and Figure 4-4, respectively.

The building tower has eighty-seven 12m deep pre-drilled reinforced concrete piles 600, 1200 and 1500mm in diameter, as shown in Figure 4-1 and Figure 4-2. The piles are connected to a 1 m thick reinforced concrete pile cap. The perimeter walls of the basement have 0.5 m thick continuous footing. The basement columns have 3 m by 3 m square by 0.5 m deep isolated footings, see Figure 4-1.

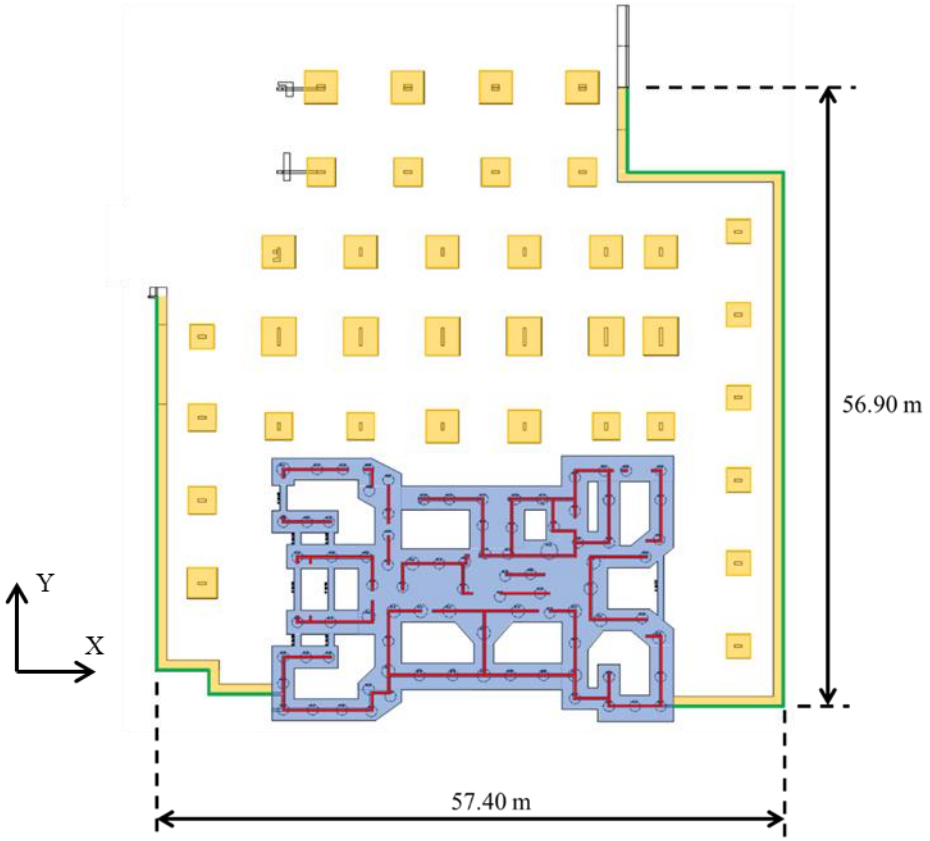

Figure 4-1: Foundations plan view

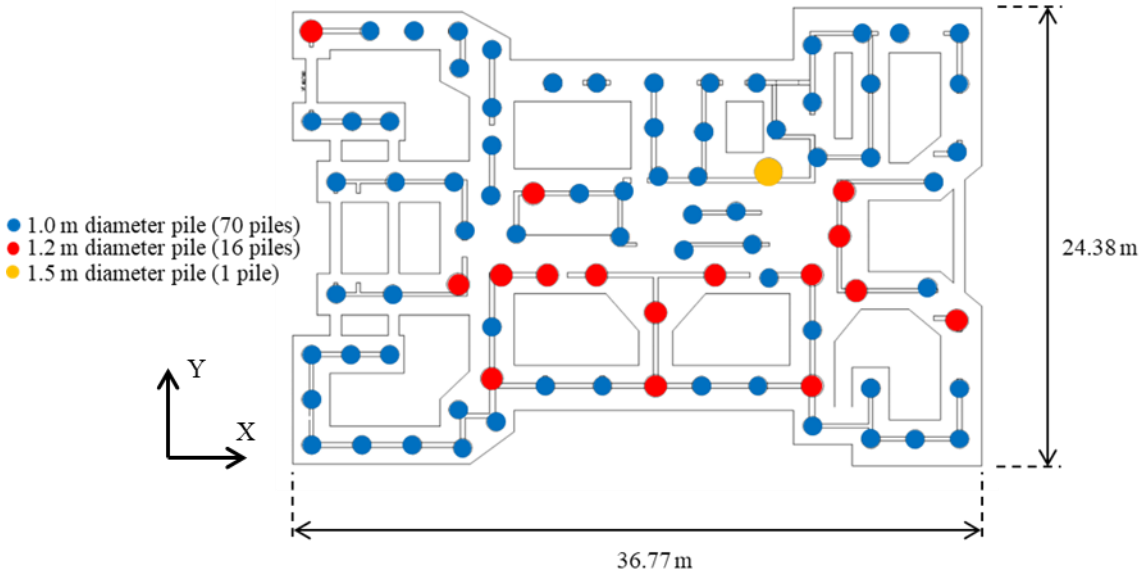

Figure 4-2: Building piles layout.

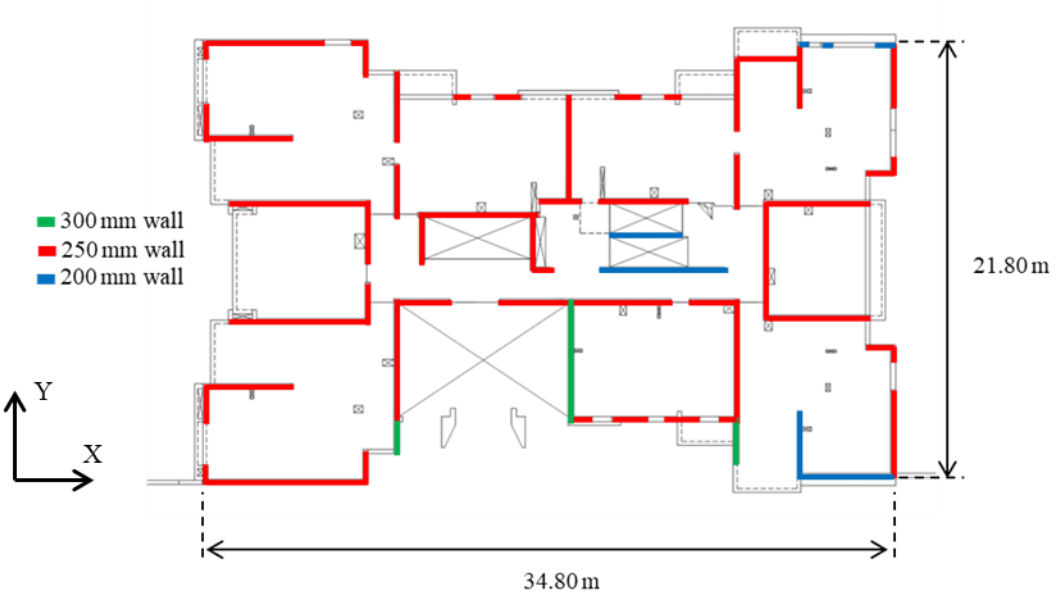

Figure 4-3: Structural walls in first story

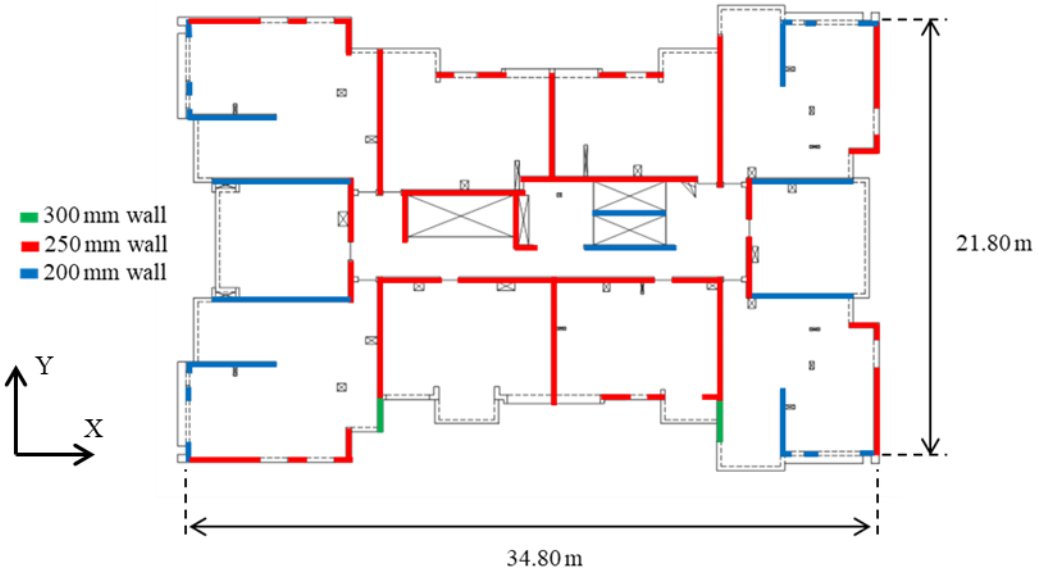

Figure 4-4: Structural walls in a typical story

The total area of the typical floor is 654 m2. The cross-section area of the X-direction and Y-direction structural walls in the typical floor is about 21 m2, which corresponds to approximately 3.2% of the total area of the typical floor.

The specified concrete for the walls is H-35 (f'_c=30 MPa) up to story 5 and H-30 (f'_c=25 MPa) for the walls from story 6 to the roof. The beams, slabs and foundations are H-25 concrete (f'_c=20 MPa). The specified reinforcing steel is A630-420H (f_y=420 MPa and f_u=630 MPa) throughout the structure. The materials for the structural elements of the building are shown in Table 4-1.

Table 4-1: Specified building materials.

Structural Elements	Concrete	Reinforcing steel
Wall (Basement to 5th story)	H-35	A630-420H
Wall (6th to roof)	H-30	A630-420H
Beams	H-25	A630-420H
Floors	H-25	A630-420H
Foundations	H-25	A630-420H

The reinforcing steel in the building walls varies in height. There is a reduction in steel on the 6th floor and a further reduction on the 10th floor.

4.2 MODEL

4.2.1 Model description

Two nonlinear 3D models of the structure were developed in ETABS 20. One model had a fixed-base, whereas the second incorporated the piles (SSI model), see Figure 4-5. The nonlinearity of the wall materials is considered using fiber shell elements. Floors are modeled with elastic shell elements. Rigid diaphragm is assigned to the upper floors and semi-rigid diaphragm to the podium floor (transfer diaphragm). Columns and piles are modeled as elastic frame elements.

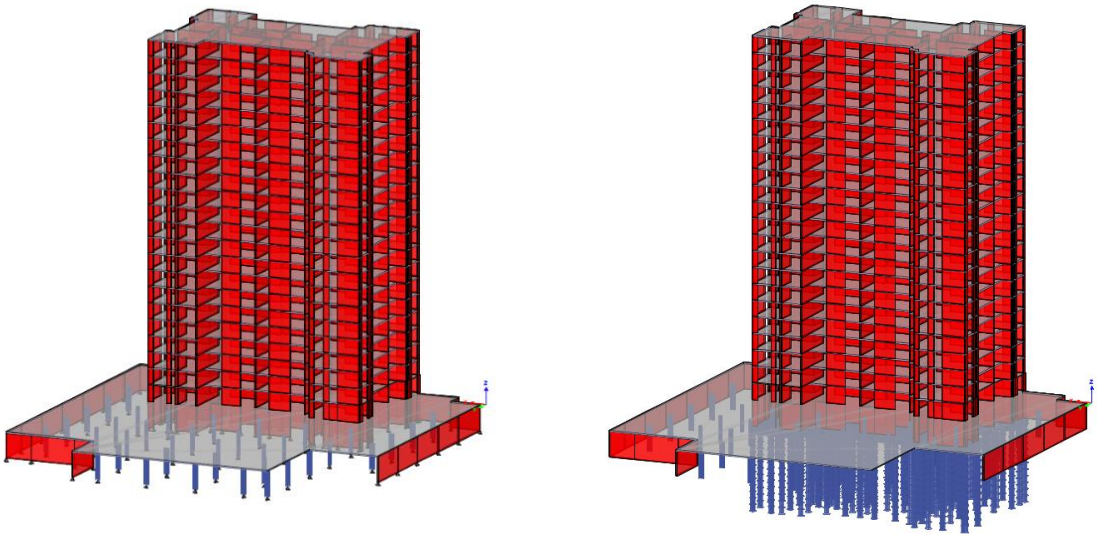

a) Fixed-base **b) Building on piles (SSI model)**

Figure 4-5: 3D ETABS Models

For soil-structure interaction, p-y springs, t-z springs, and q-z springs are considered to represent lateral soil resistance, vertical frictional resistance, and vertical tip resistance, respectively. The configuration used is the Delta Shape configuration as this has advantages in comparison with the L Shape configuration used typically, as discussed in chapter 3.

4.2.2 Gravitational loads

The gravity loads of the system were determined considering the provisions of the Chilean standard NCh1537 (1986). The values considered as live load (L) and superimposed dead load (SD) are presented in Table 4-2.

Table 4-2: Building gravitational loads.

Area	Dead Load, SD (kPa)	Live Load, L (kPa)
Apartment	1.0	2.0
Parking	1.0	5.0

The dead load (D) is composed of the self-weight of the structural elements and the superimposed dead load (SD). The total dead load of the superstructure is 150515 kN and the total live load is 41199 kN. The seismic mass considered in the analysis is considered as 100% of the dead load plus 25% of the live load according to ACHISINA (2017). The total seismic weight of the superstructure is 161 MN.

4.2.3 Nonlinear properties

In the nonlinear model, some simplifications were made to avoid stability problems in the analysis. First, the beams were not modeled explicitly since they correspond to beams with a very large aspect ratio (tall and short beams), so it is assumed that they fail in shear and do not contribute to the stiffness of the building in an intense earthquake. Secondly, a criterion was considered to incorporate nonlinear properties in the walls. Since this building has a high density of walls, nonlinear hinges were assigned only to those with an inertia greater than 1/25 of the inertia of the wall with the highest inertia in each direction of analysis. Thus, the walls considered nonlinear are shown in Figure 4-6. The rest of the walls were modeled as linear with stiffness modifiers. The stiffness modifiers present in the model are in accordance with the LATBSDC manual (2020) and are shown in Table 4-3.

Table 4-3: Structural elements stiffness modifiers.

Element	Axial	Flexural in plane	Flexural out of plane	Shear
Walls	1.00	0.35	0.25	0.20
Columns	1.00	0.70	-	0.40
Beams	1.00	0.30	-	0.40
Floors	1.00*	1.00*	1.00*	1.00*

* For the floors, in-plane, semi-rigid diaphragm is considered on the podium floor and rigid diaphragm on the upper floors. An out-of-plane stiffness equal to 1.0 was considered due to model stability issues.

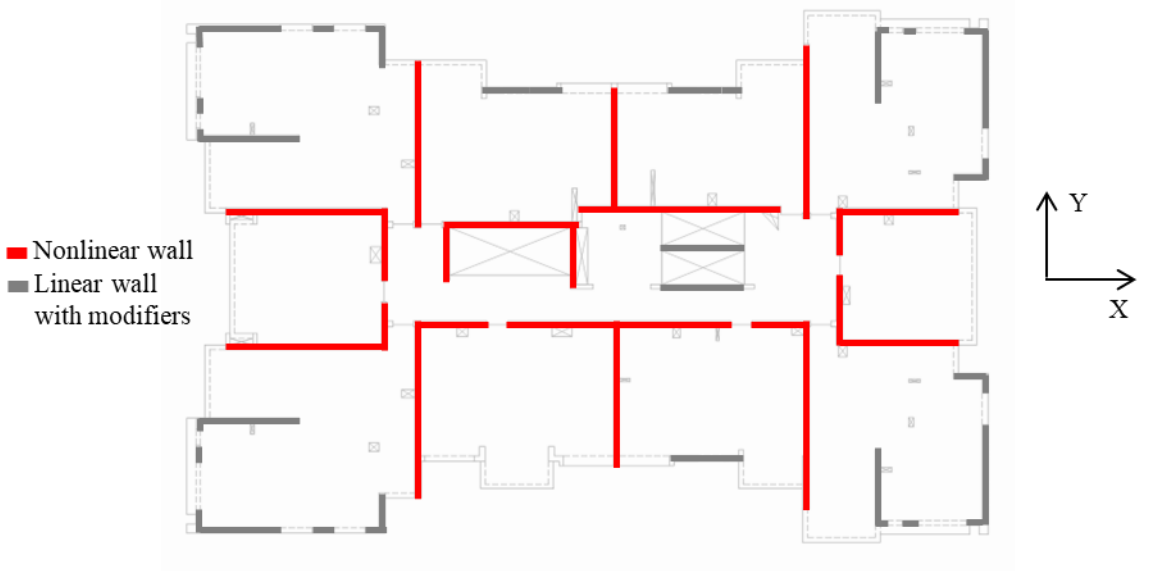

Figure 4-6: ETABS mode nonlinear walls typical story

The nonlinear material constitutive curves for the concretes are presented in Figure 4-7, Figure 4-8, and Figure 4-9.for each of the concrete types used in the model and listed in Table 4-1. Initial runs indicate that the strain demand in some fibers modeling the confined concrete boundary elements and corners would exceed the strain at the peak stress. Regularization of the stress-strain relationship, i.e., correction of the stress-strain constitutive relationship in the softening region to maintain an equal stress-displacement relationship (or equal fracture energy), resulting in very steep degradation that caused instability in the analyses. For this reason, the concrete was modeled without degradation; see Figure 4-7, Figure 4-8, and Figure

4-9. Such modeling assumption implies that the post-peak strain demands are not used to validate the building's performance but rather to establish the amount of confining reinforcement needed. Such modeling assumption is used in performance-based seismic design for the same purpose (Restrepo 2023).

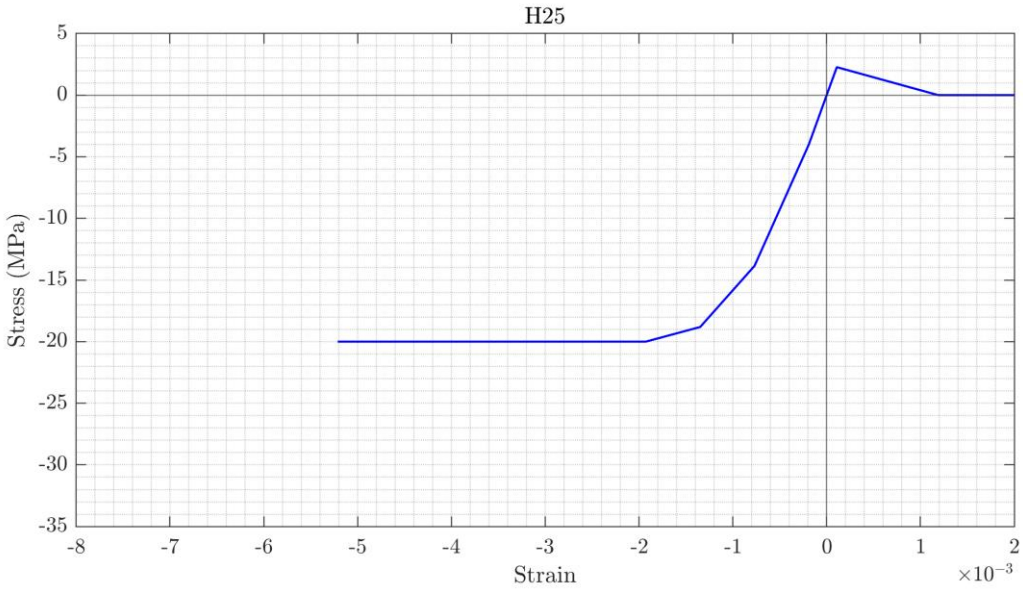

Figure 4-7: Concrete H-25 backbone stress-strain relationship

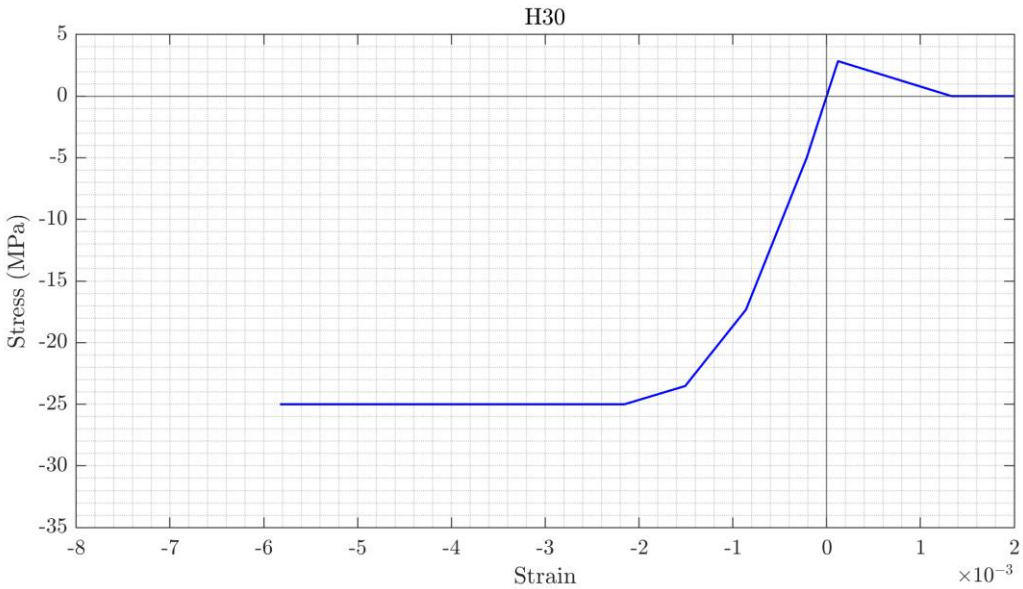

Figure 4-8: Concrete H-30 backbone stress-strain relationship

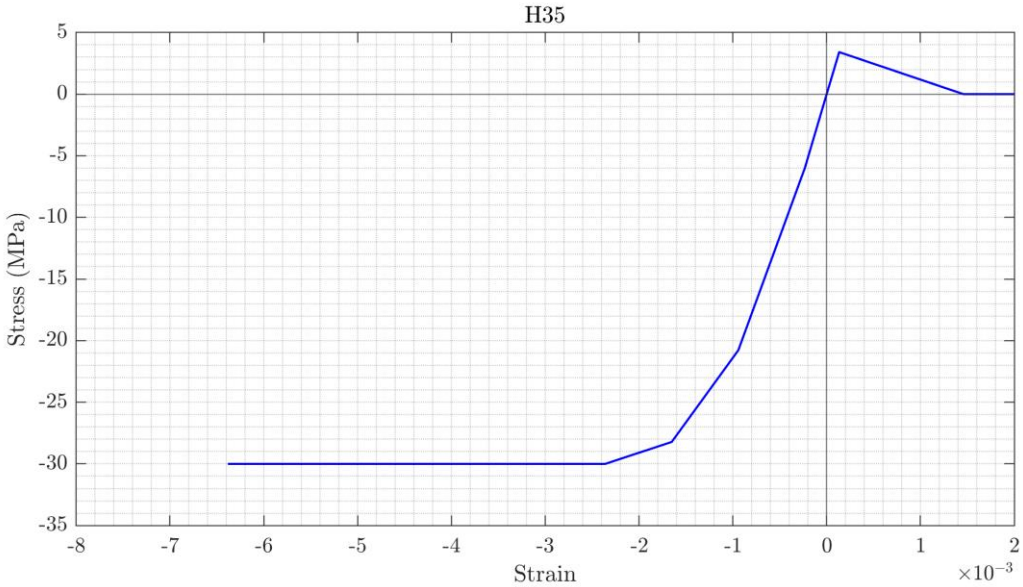

Figure 4-9: Concrete H-35 backbone stress-strain relationship

The nonlinear material constitutive curve for the reinforcing steel A630-420H is shown in Figure 4-10.

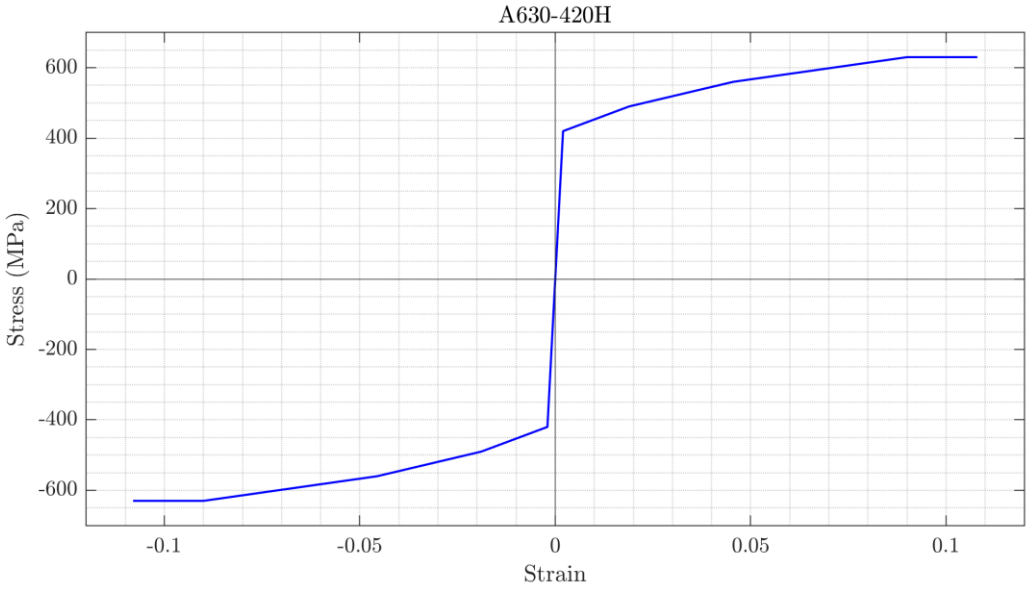

Figure 4-10: Reinforcing steel A630-420H backbone stress-strain relationship

4.2.4 Foundations modeling

As performed in chapter 3, the piles are modeled as elastic frame elements. The interaction between soil and piles is realized by the elements defined in 3.1, both vertically and horizontally. Delta Shape configuration is considered for the horizontal elements. In this case, to account for group effects on lateral load behavior, the p-y curves were modified by group factor according to Brown et al. (1998). The group factor was considered equal to 0.7 for all the piles. This is a simplification of the model, as Curras et al. (2001) show, since, in reality, a different group factor should be assigned for each pile depending on its position and loading direction. The minimum clear spacing between piles is 1.5 pile diameters.

The pile cap is modeled as H-25 elastic concrete frames. These elements respect the dimensions of the pile cap and are, therefore, relatively rigid. The pile cap serves the function of transferring the forces from the walls to the piles as well as connecting the piles to each other. The connection of the piles to the pile cap is modeled and enabled to transmit shear but not to transmit moment.

The isolated foundations of the parking lot columns were modeled according to Mylonakis et al. (2006). Unlike the springs used in the piles, the isolated foundations are modeled with equivalent linear springs, i.e., a linear spring with a linear viscous damper in parallel. The foundation is modeled with two horizontal springs, one vertical spring, two rotational springs (pitch and roll), and one torsional spring. The horizontal springs are in an L-Shape configuration. However, as mentioned in chapter 3, because these springs are linear, there is no difference between using this configuration or a Delta Shape configuration.

4.2.5 Modal analysis

The modal analysis results obtained from ETABS nonlinear models are presented below. Figure 4-11 and Figure 4-12 show the cumulative modal mass over the range of periods for the nonlinear model and the linear model with a fixed-base for the X- and Y-direction of analysis. Table 4-4 shows the periods of the structure for structure with and without SSI.

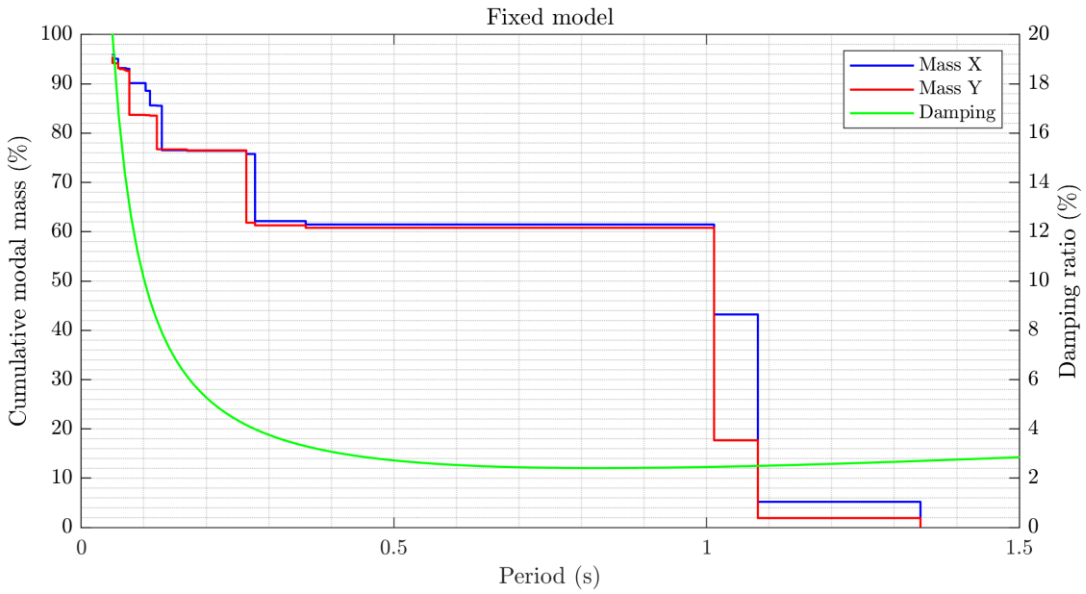

Figure 4-11: Fixed-base model cumulative modal mass and viscous damping

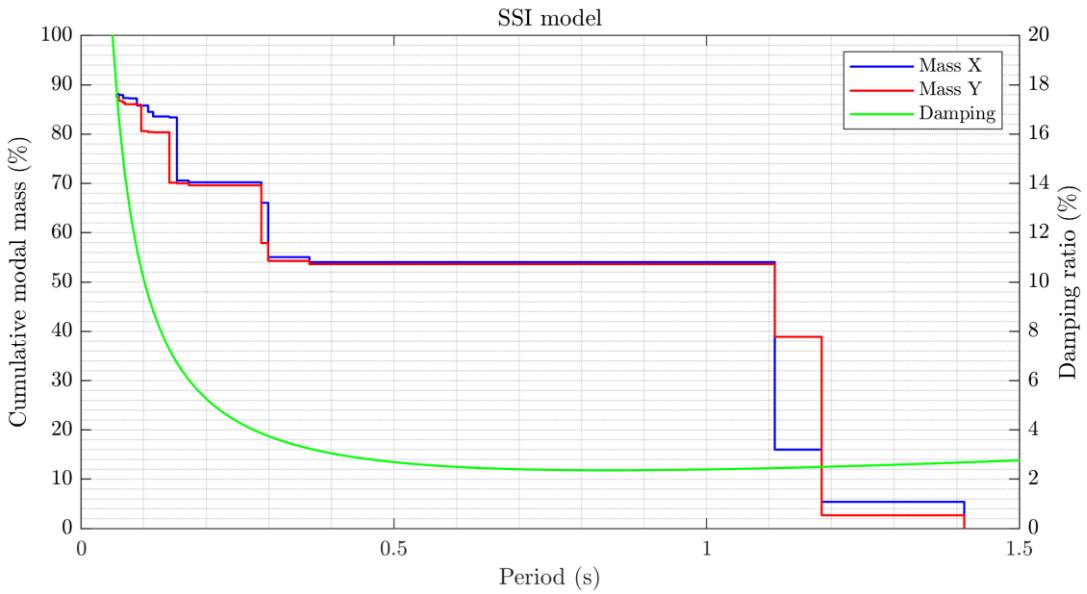

Figure 4-12: SSI model cumulative modal mass and viscous damping

Table 4-4: Building periods with and without SSI

Mode	T Fixed (s)	T SSI (s)	SSI/Fixed
XY	1.34	1.41	1.05
X1	1.08	1.11	1.02
Y1	1.01	1.18	1.17
X2	0.278	0.299	1.08
Y2	0.264	0.288	1.09

It can be noted that the first mode of the structure corresponds to a torsional mode, this occurs both in the structure with fixed-base and in the structure with SSI. By incorporating SSI in the structure, the periods increase by 8% on average. In addition, it can be noted that the modes of the building are not aligned in the same direction as the main directions of analysis since the modes present mass in both directions.

4.2.6 Damping

Rayleigh linear viscous damping is employed in the models. Although the inclusion of nonlinear materials allows some energy dissipation to be captured hysterically, there is still dissipated energy that is not correctly represented. The equation proposed by LATBSDC (2020) for the calculation of the damping ratio in the lowest translational mode.

$$0.025 \leq \xi = \frac{0.36}{\sqrt{H}} \leq 0.05 \tag{4-1}$$

Since there is not enough evidence to choose to consider a different criterion if SSI is included in the model, the same damping is selected for both the model with fixed-base and the one including SSI.

The damping was to be decisive in achieving stability and convergence in the model. Finally, a damping of 2.5% was assigned in the lowest translational mode and 20% damping at a frequency of 20 Hz. In this way, problems that high-frequency vibrations may generate were attenuated. Table 4-5 and Table 4-6 show the periods used to approximate the coefficients proportional to mass and stiffness for the Rayleigh damping.

Figure 4-11 and Figure 4-12 show the damping as a function of period together with the cumulative mass plot for each model.

Table 4-5: Fixed-base model damping

T (s)	ξ (%)	α (1/s)	β (s)
1.082	2.5	0.0032	0.183
0.05	20		

Table 4-6: SSI model damping

T (s)	ξ (%)	α (1/s)	β (s)
1.184	2.5	0.0032	0.176
0.05	20		

4.3 INPUT GROUND MOTION

The models described in the previous section were subjected to the two horizontal components of the ground motion recording by the CONZ station during the M_w 8.8 Maule earthquake of February 27, 2010. Section 3.3.3 shows the main characteristics of the ground motion. The CONZ station is located in the Inmaculada Conception School in the central business district of the city of Concepcion, where significant structural damage and a catastrophic collapse were recorded in medium-rise buildings of similar number of stories as the building in the case study (Boroschek et al. 2014, Zhang et al. 2017). It is noted that the building in the case study was designed with the post-Maule earthquake seismic design regulations that typically resulted in thicker structural walls, which incorporate confined boundary elements. To perform the nonlinear time-history analysis, the S63W(+) component of the ground motion was applied in the X-direction of the building, and the N27W(+) component of the ground motion was applied in the Y-direction.

4.4 SOLUTION STRATEGY

The nonlinear time-history analysis performed in ETABS 20 is a direct integration nonlinear time-history analysis. The time integration method used is the implicit method Hiber-Hughes-Taylor (1976), with γ equal to 0.5 and β equal to 0.2. The maximum time step selected for solving the equation of motion is 0.005 seconds. The model lateral mass was applied as a

nonlinear static load case, including 100% of the dead load plus 25% of the live load. The vertical mass was not included in the model. The damping defined in 4.2.6 was included.

Due to convergence problems, different convergence tolerances were selected in the models. For the model with fixed-base a tolerance of 1E-7 was chosen and for the model with SSI a tolerance of 1E-4 was used. With these values, convergence, and stability of the analysis were achieved.

4.5 ASSUMPTIONS AND SIMPLIFICATIONS

In this section, a summary of the principal assumptions and simplifications considered in the modeling process are shown.

- Use of fiber elements for modeling nonlinear walls. This element does not correctly capture the behavior of complex wall configurations. Other models as BTM are more suitable for this type of analysis. However, fiber elements are the type of elements used in the state of practice.
- Consider only nonlinear hinges were assigned on walls with a moment of inertia greater than 1/25 of the moment of inertia of the wall with the highest moment of inertia in each direction of analysis to reduce the possible sources of instabilities in the analysis.
- Beams not included in the modeling assuming that they will fail in shear due to their geometry and they will not contribute to the stiffness.
- The degradation in the concrete backbone curve is not considered to avoid instabilities in the analysis.

- Incorporation of higher damping on higher frequencies (20 Hz) to eliminate convergence issues.
- Modeling of piles and floors as elastic elements.
- Use of a constant group factor (p-multiplier) to incorporate the group effect on the piles.

4.6 CONCLUSIONS

Table 4-7 shows a summary of the analysis parameters for the model with fixed-base and the model considering SSI.

Table 4-7: Analysis models parameter summary

Model	Fixed-base	SSI
Superstructure total height H	58.32 m	58.32 m
Superstructure total weight W	160815 kN	160815 kN
First Period in X, T_{x1}	1.082s	1.109s
Second Period in X, T_{x2}	0.275s	0.299s
First Period in Y, T_{y1}	1.012s	1.184s
Second Period in Y, T_{y2}	0.264s	0.288s
Damping ratio T_1	2.50%	2.50%
Damping ratio 20Hz	20%	20%
Tolerance	1E-7	1E-4

These models have many simplifications and limitations due to the difficulty of achieving convergence in the results. This project was carried out considering the state of practice and not the state of the art. To have a more realistic model, all nonlinear walls should be considered, and another type of element should be used for modeling. Shell elements with fiber are not good for this type of building and should be considered as beam-truss mode (BTM) element, developed by Lu and Panagiotou (2014), to capture the behavior. A beam model that considers shear failure should also be included. The pile material in this model is being

considered linear, but a more detailed model could include the nonlinearity of the pile material. This model also does not consider separation between the soil and the piles, this could be incorporated using gap elements, but they should be calibrated according to experimental data. For verification of the building's performance, the concrete model should be more realistic by including the confinement of the walls and the degradation of the material strength. Tests should be performed for a more accurate calibration of concrete, reinforcing steel and soil spring. The pile group factor has also been simplified by using a constant value for all piles. This factor should be different for each pile depending on its location and loading direction, to date there is no consensus on this issue. Due to problems in the convergence of the model it was necessary to assign a higher damping than recommended, in a more detailed model this damping should be reduced.

However, this simplified model allows a comparison of the global behavior of the structure and to see how the SSI affects the analysis. A more detailed study of the behavior of particular elements would require a more detailed model.

5 SYSTEM-LEVEL RESULTS AND DISCUSSION

5.1 INPUT GROUND MOTION

The nonlinear time-history analysis was performed for a single ground motion record. This record corresponds to the 2010 Maule earthquake measured in the city of Concepción, Chile. This record is the same as the one considered in section 3.3.3. Only 2 horizontal components of the record were considered (S63W + and N27W +) and no vertical accelerations were included in the model because the software DeepSoil v7 (2020) does not perform analysis in the vertical direction of analysis, so it is not possible to obtain the vertical accelerations along the piles. At the end of the acceleration record, four seconds with zero acceleration have been included to obtain a free vibration response of the system, which results in a record of 44 seconds total duration.

The free field ground motion is obtained using DeepSoil v7 (2020) and the soil profile corresponds to the one described in section 3.3.2. Since the input corresponds to the ground level acceleration record, a deconvolution of the record is required to obtain the displacement response along the soil profile. Then, these displacements are input into the model with piles (SSI model) at the ends of the p-y springs (modeled using the Delta Shape configuration). The process is the same as the one performed in chapter 3 for the single pile and the 4-pile group.

5.2 CONVERGENCE AND RUN TIMES

As described in chapter 4, certain decisions had to be made in the model and analysis to achieve convergence. When considering other tolerance or damping values, an error was produced in which some of the walls of some of the intermediate floors of the building achieved

a false convergence. This false convergence resulted in a complete loss of wall stiffness and the deformations of the element went out of control. This generated a chain reaction that led other walls to fail in the same way, leading to a complete collapse of the model. It is worth mentioning that this error occurred in a random time step and with the wall in elastic range. Finally, by simplifying the model, it was possible to obtain the results shown in this section.

Figure 5-1 shows the percentage of completed analysis as a function of elapsed time for both the model with fixed-base and the model incorporating soil-structure interaction.

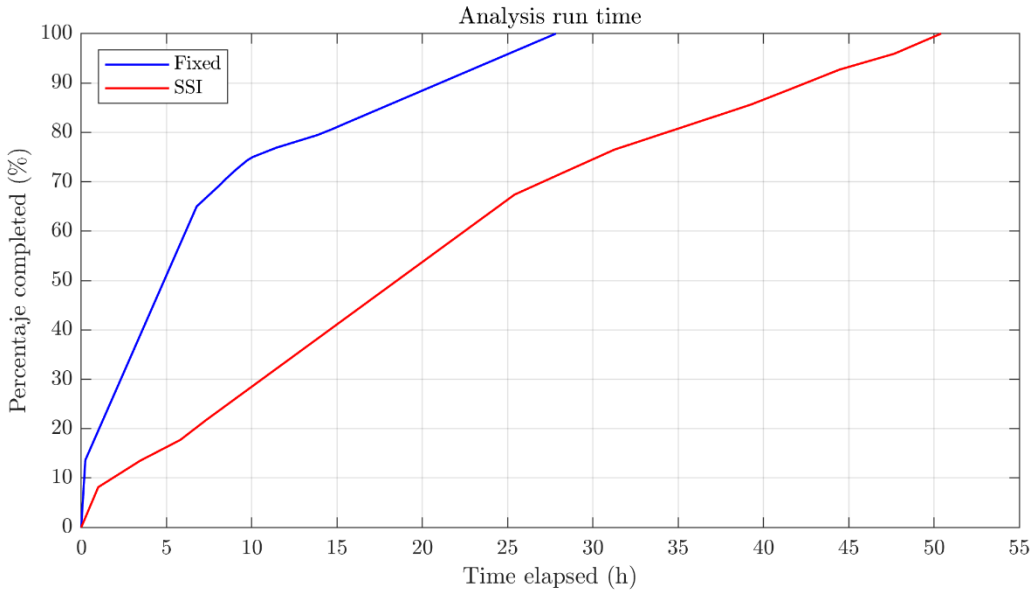

Figure 5-1: Analysis run time of fixed-base and SSI models.

The fixed-base model, despite having a more demanding tolerance, ran in a shorter time than the SSI model. The fixed-base model ran complete in 27.8 hours and the SSI model ran complete in 50.4 hours. This increase in analysis time may be due to the incorporation of the nonlinear soil springs.

5.3 TIME-HISTORY SERIES OF KEY ENGINEERING RESPONSE PARAMETERS

This section presents and discusses several time-history series of key engineering response parameters obtained from the nonlinear analysis of the building in the fixed-base and pile configurations. Figure 5-2 and Figure 5-3 present the time series for the building's roof drift ratio. The roof drift ratio was defined as the lateral displacement of the roof at center of mass of the roof diaphragm minus the lateral displacement at ground level divided by the roof height measured from the ground level. The drift ratios were computed for each of the two orthogonal directions. Since the building exhibits torsional response, the roof drift ratio had to be defined at a single point in the plan. This point was defined as the center of mass of the roof diaphragm. The roof ratio time-history series compared closely for the two building models, with the model with pules exhibiting slightly greater roof drift ratios. This comparison of the responses suggests that SSI had negligible effect on the specific building for the type of soil and input ground motion.

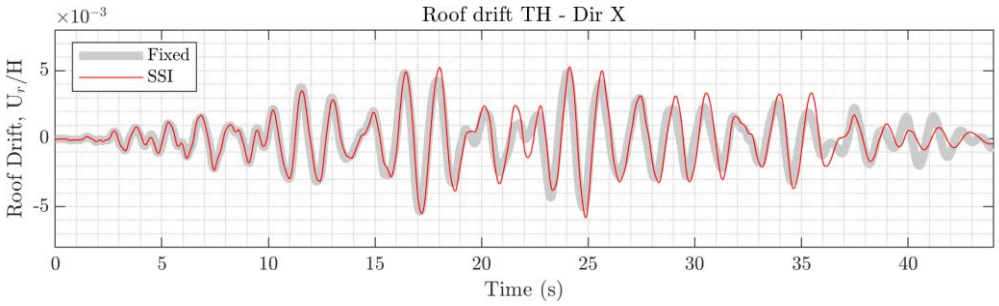

Figure 5-2: Roof drift time-history X-direction

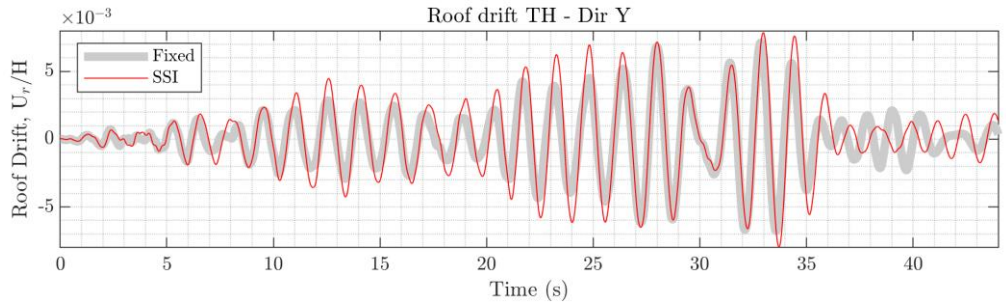

Figure 5-3: Roof drift time-history Y-direction

Figure 5-4 and Figure 5-5 plots the time series of the overturning moment in the X- and Y-directions (with the moment defined vectorially, it means that overturning in the X-direction was the result of the floor accelerations in the Y-direction, and vice-versa). In Figure 5-4 and Figure 5-5, the overturning moments have been normalized by the product of the superstructure's total weight listed in Table 4-7, and the roof height defined previously. The overturning moment was computed as the seismic mass of each story multiplied by the floor acceleration at the center of mass of the respective diaphragm, plus the story weight multiplied by the displacement of the center of mass of the diaphragm relative to the ground (to incorporate the P-Delta effect), for each direction of analysis. The inclusion of SSI had only a slight increase in the building overturning moments, which again suggests that for the specific building, type of soil, and input ground motion, SSI had a negligible effect.

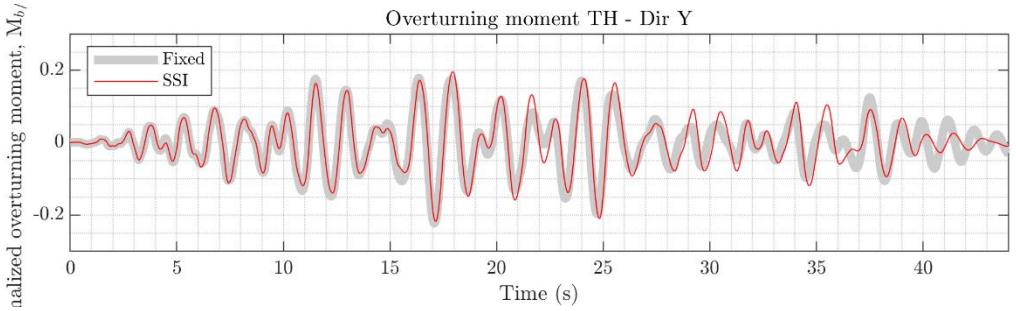

Figure 5-4: Overturning moment Y-direction time-history

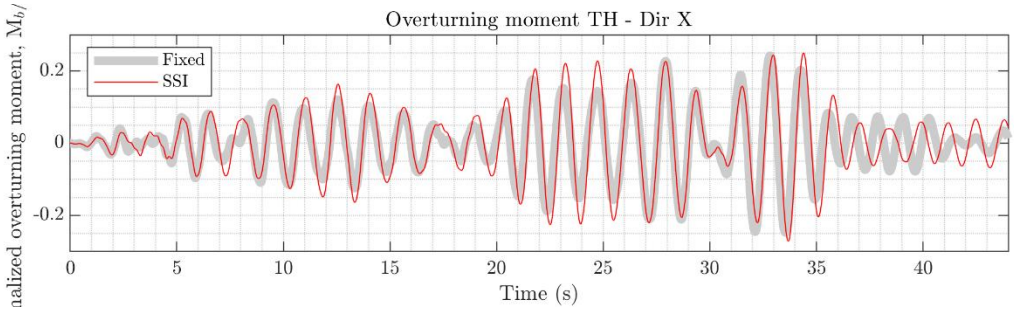

Figure 5-5: Overturning moment X-direction time-history

Figure 5-6 and Figure 5-7 plots the time series of the base shear in the X- and Y-directions. The base shear was computed as the seismic mass of each story multiplied by the floor acceleration at the center of mass of the respective diaphragm, for each direction of analysis. In Figure 5-6 and Figure 5-7 the base shears have been normalized by the superstructure's total weight listed in Table 4-7. The inclusion of SSI had only a slight increase in the building's base shear, which again suggests that for the specific building, type of soil, and input ground motion, SSI had negligible effect.

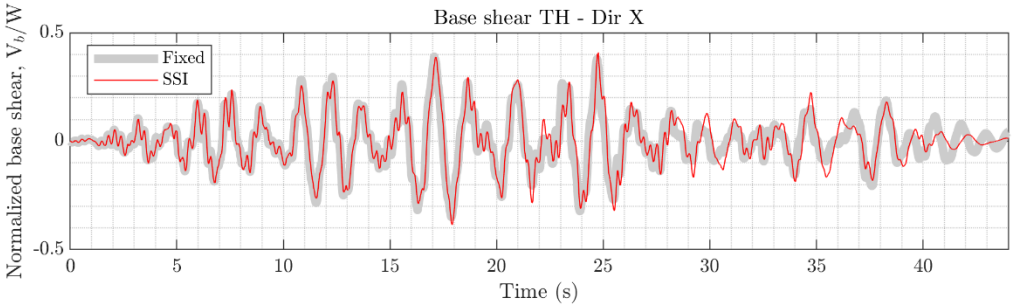

Figure 5-6: Base shear time-history X-direction

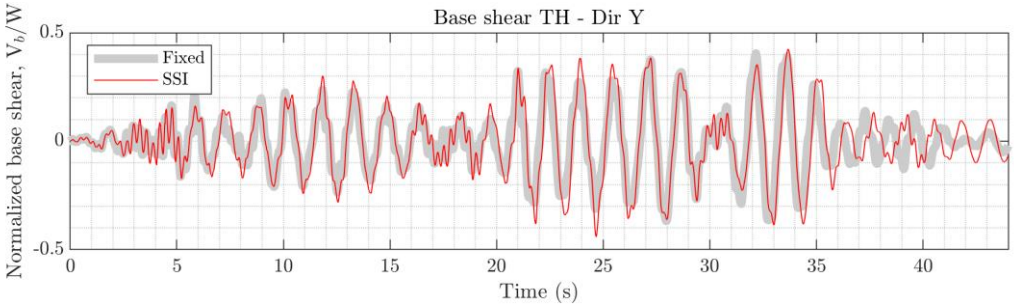

Figure 5-7: Base shear time-history Y-direction

5.4 HYSTERETIC RESPONSE

Figure 5-8 and Figure 5-9 plot the hysteretic response of the overturning moment and base shear, respectively, versus roof drift. All the parameters have been normalized in the plots in the same way the parameters were normalized in the time-history responses discussed previously. A comparison of the X- and Y-direction responses indicates that X-direction normalized overturning moment (induced by Y-direction floor accelerations) and the corresponding Y-direction roof drift ratio is greater than in the orthogonal direction. The envelope of the hysteretic response of the X-direction overturning moment and Y-direction rood drift ratio. The latter seems to qualitatively indicate that the building response caused by the Y-component of the input ground motion may have experienced a more inelastic response than in the orthogonal direction. Keep in context that the peak (i.e., max(max drift, -min drift)) roof drift ratios in both directions is less than 0.8%, which is the result of the dense array of structural walls found in Chilean practice. For such a drift ratio, one can qualitatively deduce there is limited yielding of the longitudinal reinforcement (though crushing of the confined concrete in boundary elements and wall corners could occur). Section 5.6 presents the roof pseudo-transfer function where the overall building nonlinear response can be detected.

Now, when the response of the fixed-base and model on piles are compared in Figure 5-8 and Figure 5-9, and particularly the envelope of the responses, a conclusion is reached that SSI has minimal effect on the overturning versus roof ratio response of this building for the type of soil and the input ground motion.

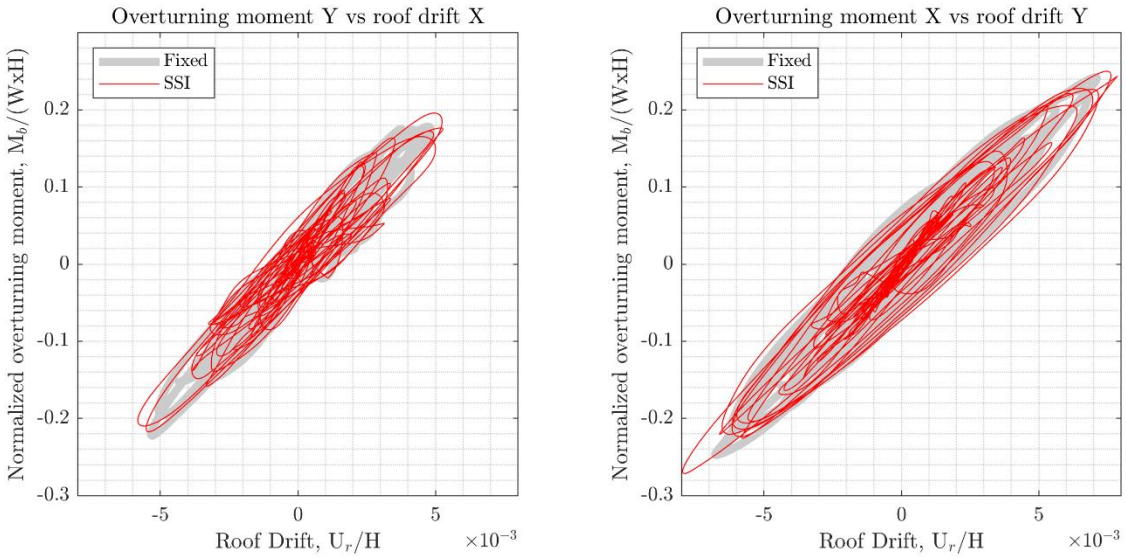

a) Overturning moment Y vs roof drift X-direction

b) Overturning moment X vs roof drift Y-direction

Figure 5-8: Normalized overturning moment vs roof drift

The hysteretic response of the base shear, depicted in Figure 5-9, exhibits a response that is much noisier than that observed for the overturning moment. This is because, whereas the overturning moment is greatly affected by the lower modes of response, the base shear is affected by lower and higher modes of response. Like in the analysis of overturning moment versus roof drift ratio, SSI has a minimal effect on the base shear versus roof drift ratio response of this building for the type of soil and the input ground motion.

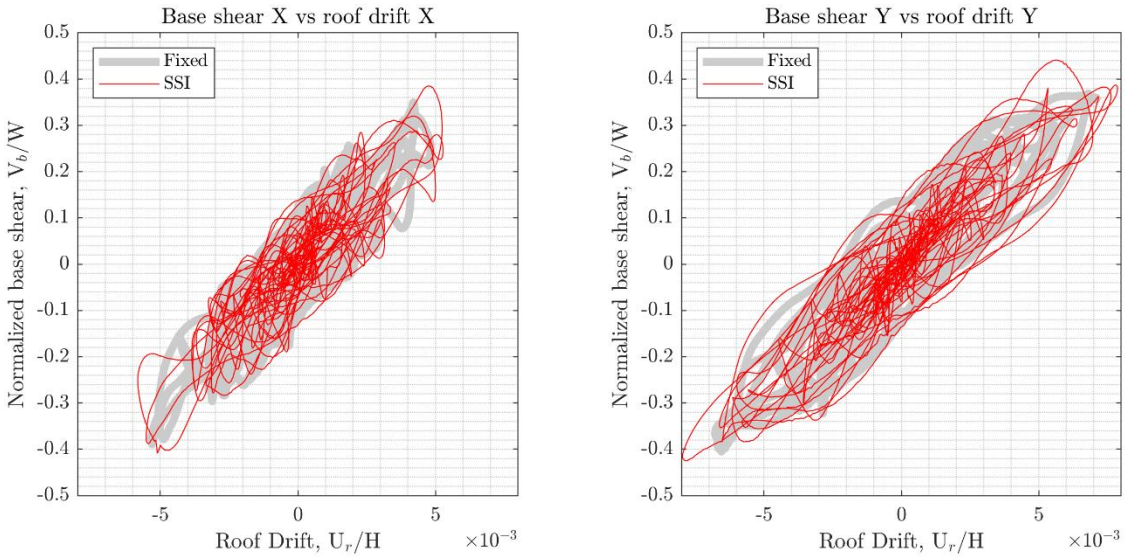

a) X-direction **b) Y-direction**

Figure 5-9: Normalized base shear vs roof drift

5.5 RESPONSE ENVELOPES

Figure 5-10, Figure 5-11, Figure 5-12, and Figure 5-13 show the envelopes for overturning moment, base shear, relative displacement, and interstory drift ratio, respectively. In all figures, the responses have been normalized for clarity.

It can be seen that there are no significant differences in overturning moments along the height of the building. In the Y-direction, at the base, the overturning moment is slightly higher when considering SSI than when modeling with a fixed-base.

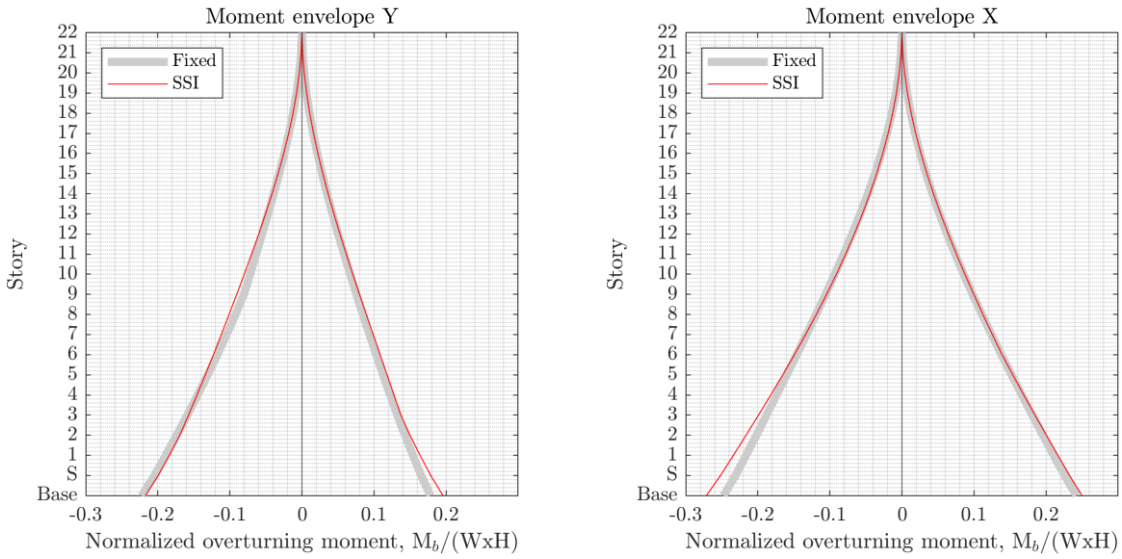

a) Y-direction **b) X-direction**

Figure 5-10: Bending moment envelope

With the envelope shear, slightly higher stresses are again observed when incorporating SSI. This is especially noticeable at the base of the building.

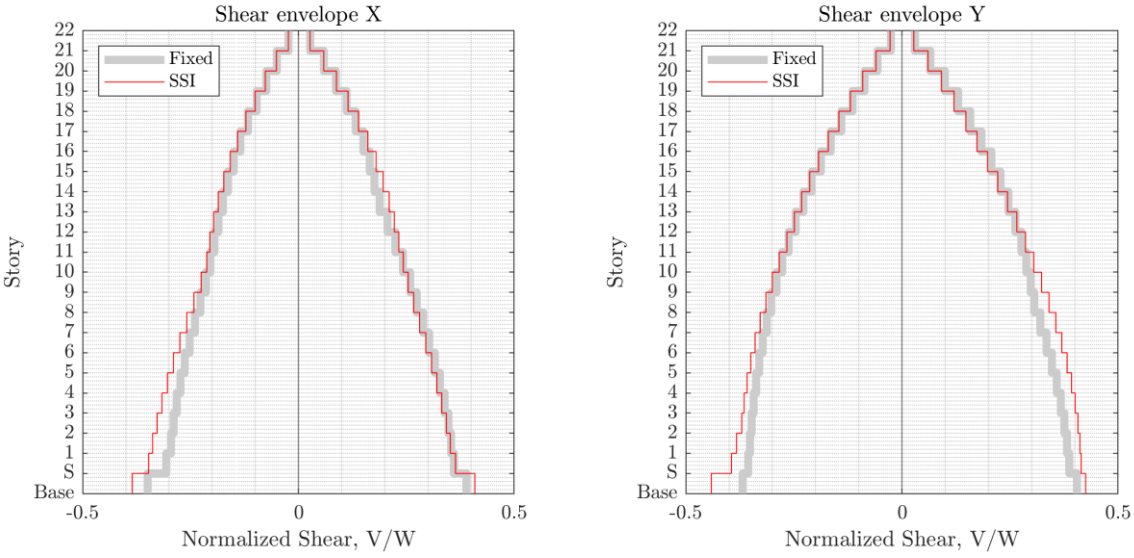

a) X-direction **b) Y-direction**

Figure 5-11: Shear force envelope

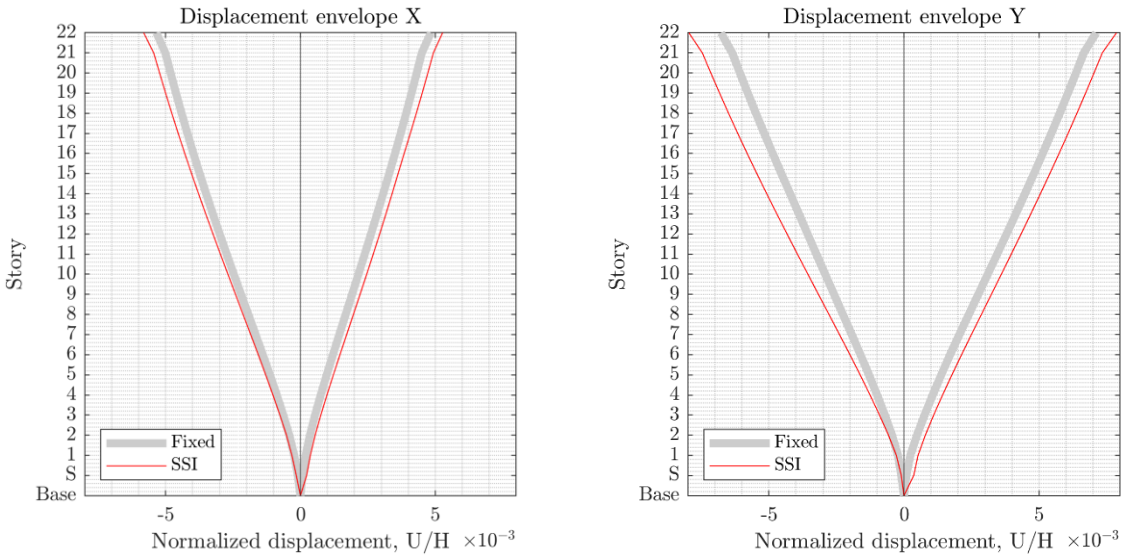

a) X-direction **b) Y-direction**

Figure 5-12: Maximum relative displacement

The maximum relative displacements obtained are larger when SSI is included in all floors in both the X- and Y-directions.

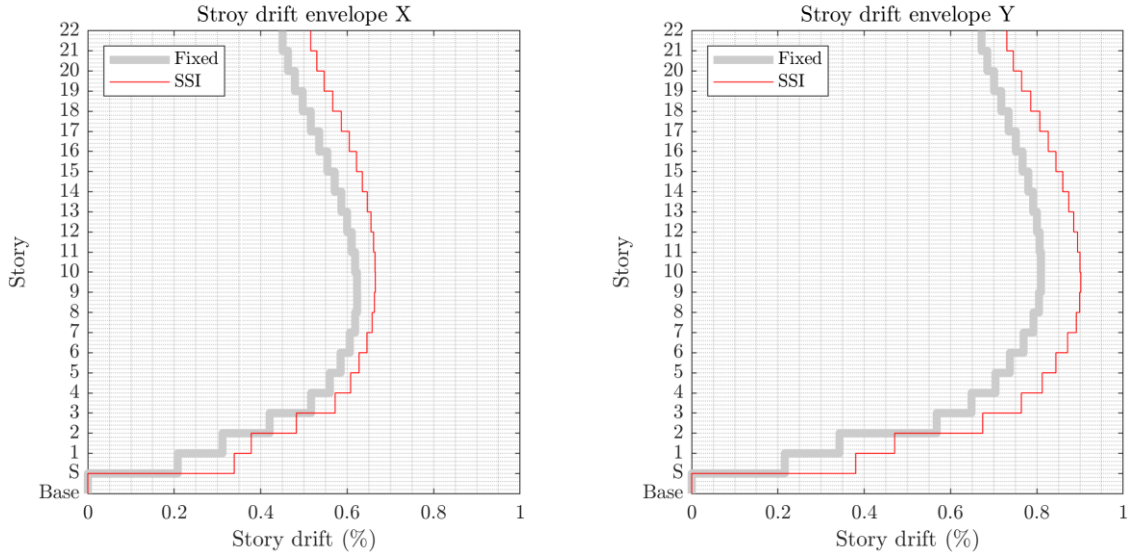

a) X-direction **b) Y-direction**

Figure 5-13: Maximum interstory drift ratio

With respect to the interstory drift ratio, something similar to the maximum relative displacement of the structure is observed. When SSI is included, the displacements are increased.

5.6 PSEUDO-TRANSFER FUNCTION

With the accelerations obtained at the roof of the structure, a spectrum of pseudo-accelerations is constructed considering a damping ratio equal to 0. Then, if this spectrum of pseudo-accelerations of the roof of the structure is divided by the spectrum of pseudo-accelerations at ground level (with a damping ratio equal to 0) a pseudo-transfer function of the system is obtained since it relates the input at ground level with the response of the roof of the building as a function of the period (Chen et al. 2017). The pseudo-transfer functions in the X and Y directions of analysis are shown in Figure 5-14 and Figure 5-15, respectively, together with vertical lines indicating the periods obtained from the modal analysis carried out with the initial stiffness for all lateral load-resisting elements (i.e., assuming no cracking occurred). It can be noted that the first peak in the figures corresponds to the second translational mode of vibration of the structure. The first mode obtained in the modal analysis of the building does not coincide with the corresponding period (i.e., this is the predominant period during the response to the input ground motion) determined from the pseudo-transfer function. This is because there is damage to the in the way of cracking and even plasticity.

In the X-direction, the key predominant periods were 1.24 and 1.25 seconds for the fixed-base and SSI models, respectively. This implies that the predominant lateral building stiffness decreased to 76% and 79% of the initial stiffness during the excitation. There is also a

small peak at 1.57 and 1.59 seconds in the fixed base and SSI model, suggesting that during the response, the predominant period lengthened to those values. For such a moderate reduction in lateral stiffness (i.e., secant stiffness) of 76% and 79%, one could conclude that the building behaved predominantly linear in this direction. The small peaks suggest that the lateral stiffness decreased 47% and 49% during the excitation in the fixed-base and SSI models, respectively, which could indicate some limited plasticity.

In the Y-direction, the predominant periods were 1.26 seconds for both models, with small predominant periods extending to 1.77 seconds. Such periods result in lateral stiffness of 64% and 88% for the key predominant period and 33% and 44% when the longest predominant periods were observed. Such values indicate that the building may have experienced moderate plasticity in a few walls, as it is discussed in the following section.

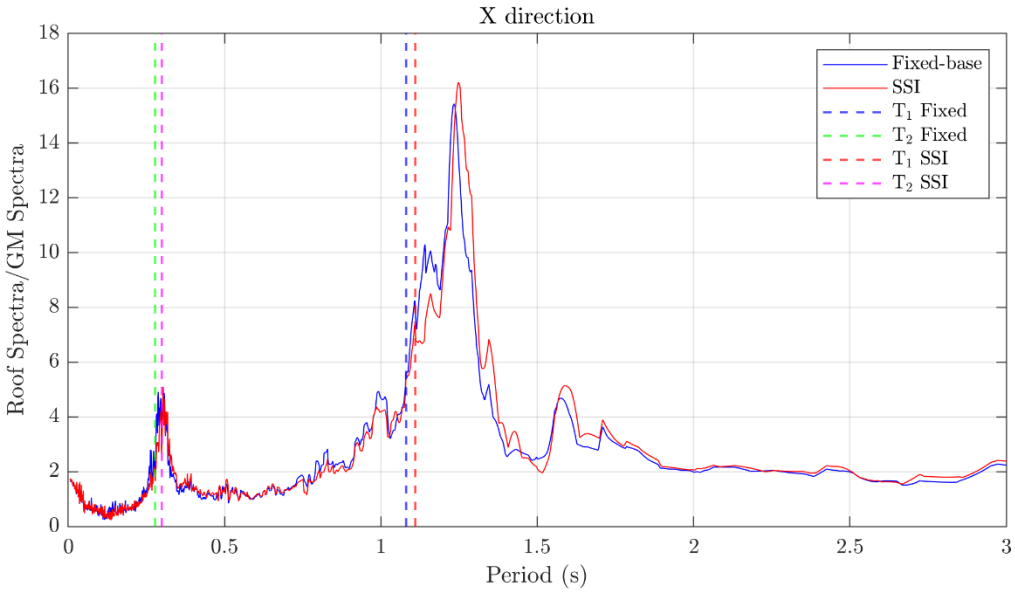

Figure 5-14: Pseudo-transfer function X-direction

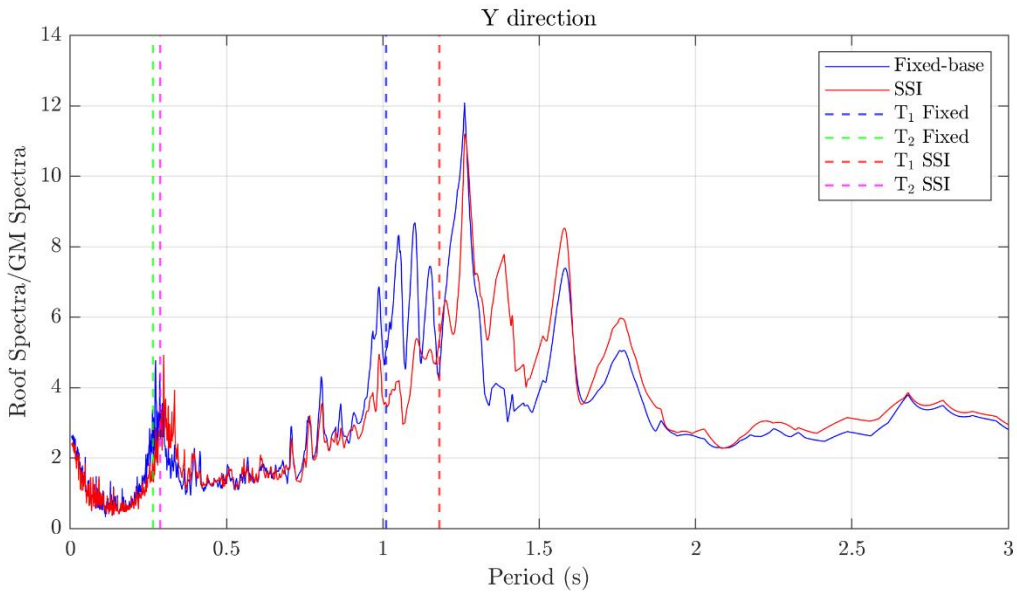

Figure 5-15: Pseudo-transfer function Y-direction

5.7 OBSERVED PLASTICITY IN STRUCTURAL WALLS

The highest plasticity in the building occurs in the first story. Figure 5-16 shows the walls of the first story which its longitudinal reinforcement steel reaches the yielding strength for the model with fixed-base and the model with pile (SSI model). The location of the maximum reinforcement steel strain is marked with a blue dashed line. For both models the maximum strain is around 2% or ten times the yield strain of the longitudinal reinforcement. Figure 5-17 shows the walls of the first story in which the concrete exceeded the strain at the compressive strength for both models. The location of the minimum concrete strain is marked in the figure with a blue dashed line. For both models the minimum strain is around -1%, or about five times the strain of the concrete at its maximum strength. The latter implies that should this be an average of several runs, the confinement in corners and boundary elements should be revised and detailed to match the strain demand computed from the analysis. Comparing the

model with fixed-base and SSI, there are no major differences in the plasticity generated in the walls.

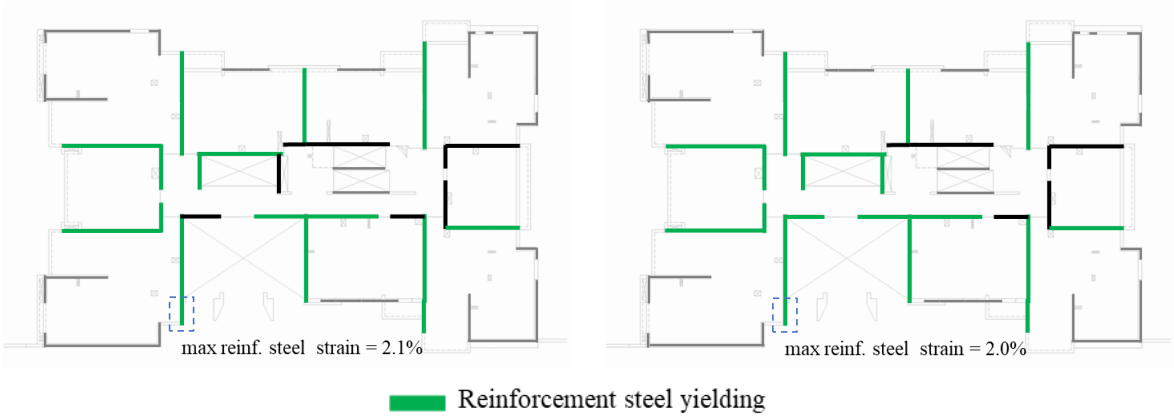

a) Fixed-base **b) SSI**

Figure 5-16: Walls reinforcement steel yielding in tension. First story.

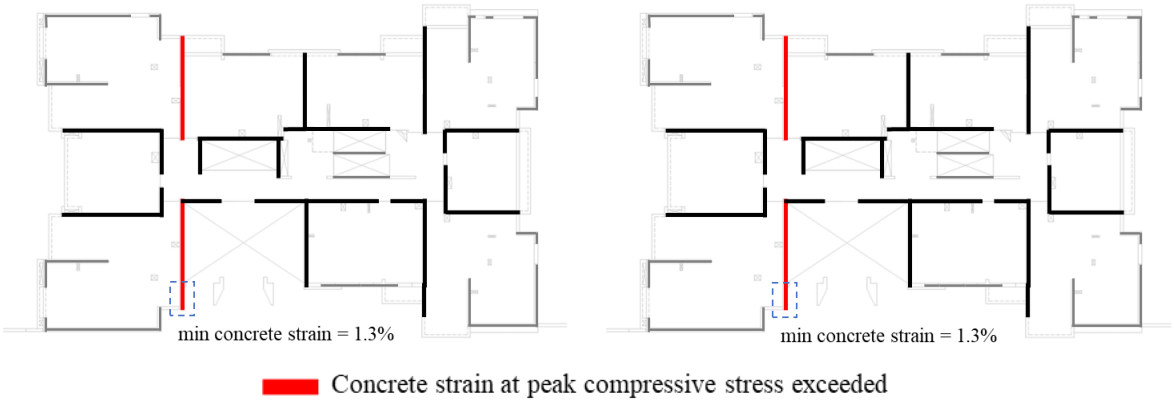

a) Fixed-base **b) SSI**

Figure 5-17: Walls concrete compressive strength reached. First story.

5.8 PILES RESPONSE ENVELOPES

In this section the bending moments and axial forces response envelopes of the piles of the building are analyzed. Since the building has 87 piles, only the results of two representative piles are shown. One of the piles corresponds to a pile close to the center of mass of the building

tower and the other is a pile located at one of the corners of the building tower. Both piles have a diameter of 1 m. The location of the selected piles is shown in Figure 5-18.

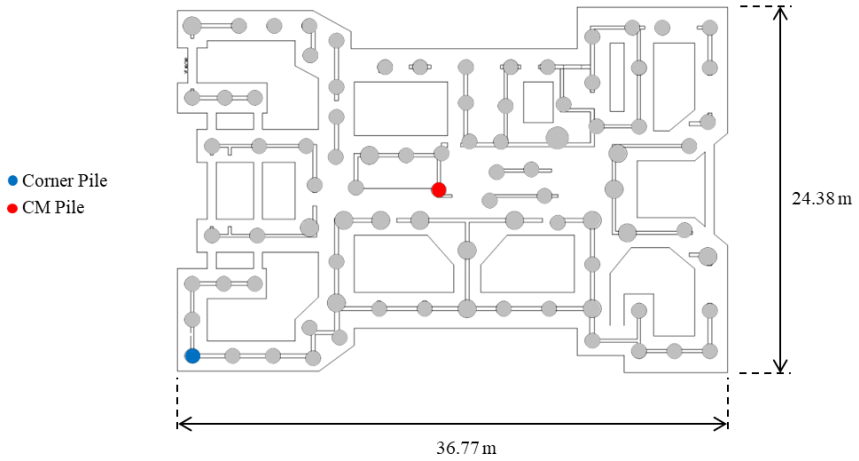

Figure 5-18: Selected piles for analyzing bending moments and axial force.

Figure 5-19 and Figure 5-20 show the bending moment envelopes for the selected pile close to the center of mass and the corner pile respectively. It can be noted that the maximum bending moments are obtained in the X direction. In addition, in the X direction of analysis the negative moments are large and on the contrary the positive moments are small. The moments obtained in the corner pile are slightly larger than the moments obtained in the central pile. This small difference may be due to the torsion in the building. However, since a constant p-multiplier for all piles is considered in this model, the difference due to the group effect in the piles cannot be appreciated.

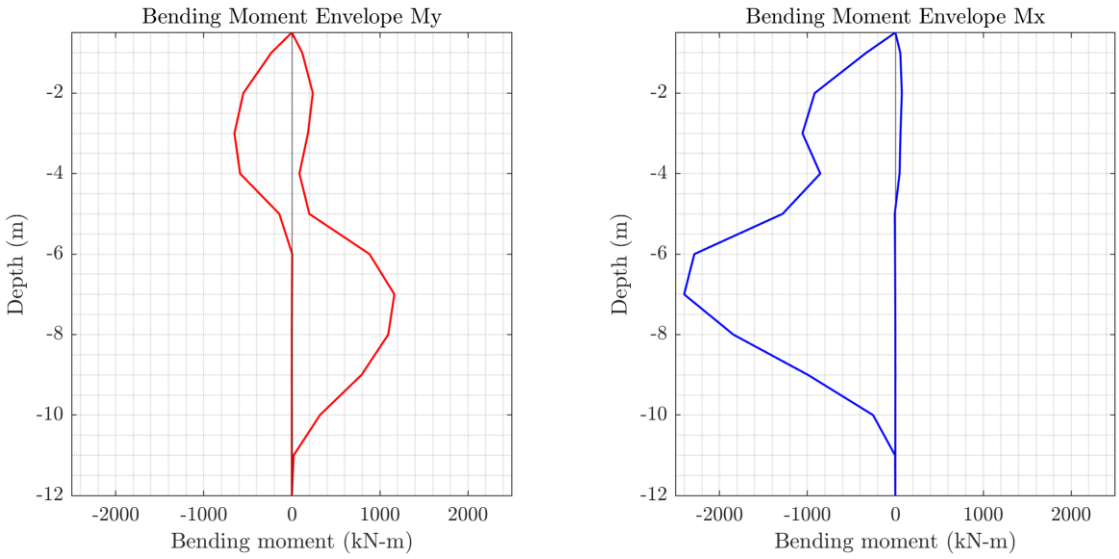

a) Y direction **b) X direction**

Figure 5-19: Bending moment envelopes for the pile close to the center of mass.

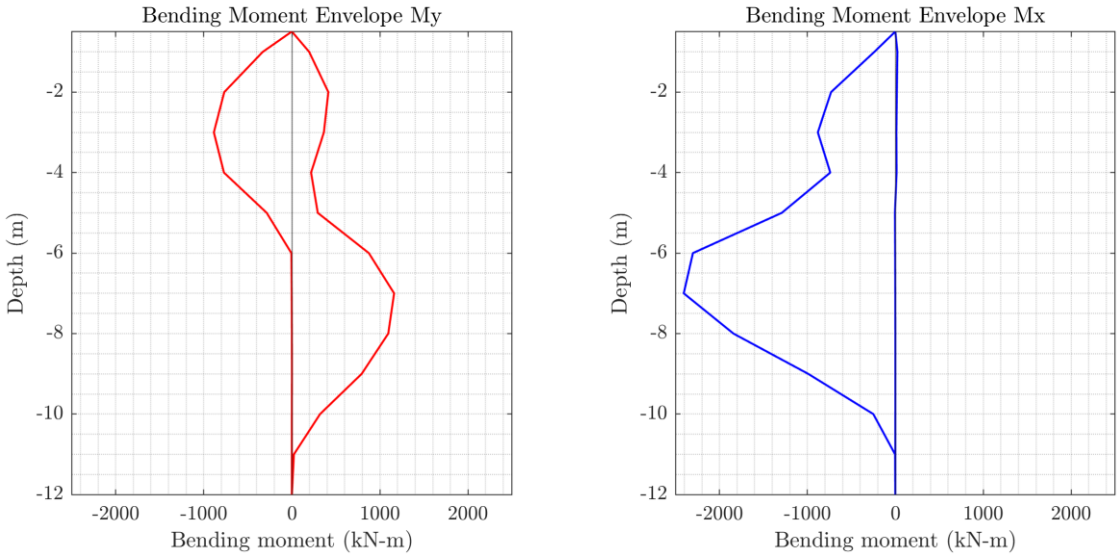

a) Y direction **b) X direction**

Figure 5-20: Bending moment envelopes for the corner pile.

Figure 5-21 shows the envelopes of axial force for the center of mass pile and the one located in the corner. It can be noted that tension is generated in both cases, however the tension and compression obtained in the corner pile is higher than in the center of mass. These differences are due to the rocking effect of the building.

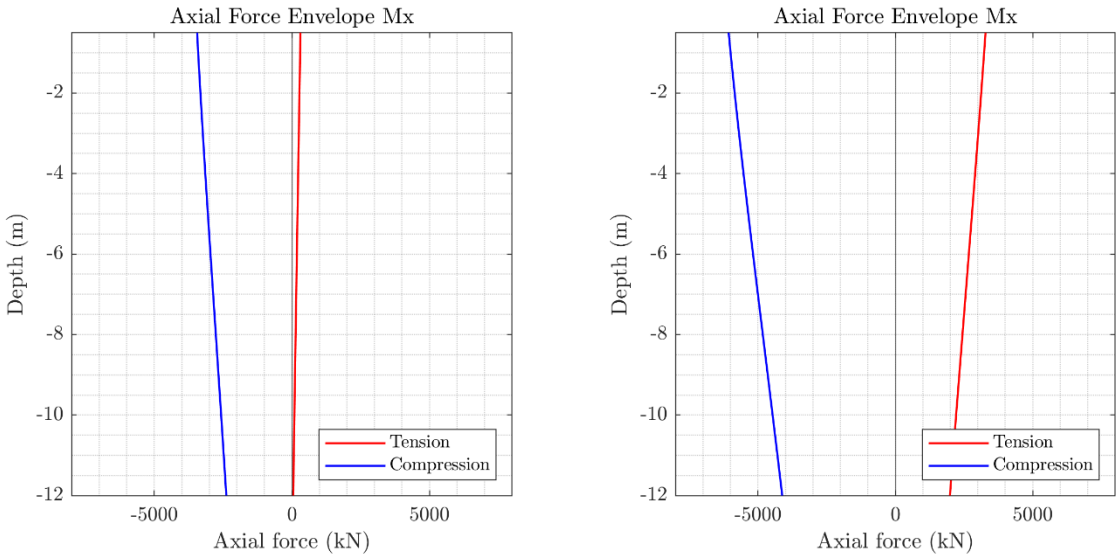

a) Center of mass **b) Corner**

Figure 5-21: Piles axial force envelopes.

5.9 P-Y SPRINGS HYSTERETIC RESPONSE FOR ONE PILE OF THE BUILDING

In this section, the p-y springs hysteretic curves of an arbitrarily selected building pile close to the center of mass of the building are presented. The pile corresponds to one of 1m diameter and 12m depth. Hysteretic curves of the p-y springs for depths of 4.5m (4.5 pile diameters), 6.5m (6.5 pile diameters), 8.5m (8.5 pile diameters) and 10.5m (10.5 pile diameters) are presented in Figure 5-22. It can be noted that the results obtained are different from those obtained in section 3.5 since in this case the p-y springs have a practically linear behavior in all depths. It should be noted that the building piles are started at a depth of 3.7m (basement height, 2.7m, plus pile cap thickness, 1m). Therefore, the soil present at this depth is stiffer and more resistant than the soil located at ground level. On the other hand, in the case of the single pile model and the group of 4 piles, the piles are buried at ground level. In addition, the building piles have a larger diameter, which implies higher strength and stiffness of the p-y curves. Despite the above, some nonlinearity in the p-y springs at 4.5m depth of the pile analyzed can be appreciated.

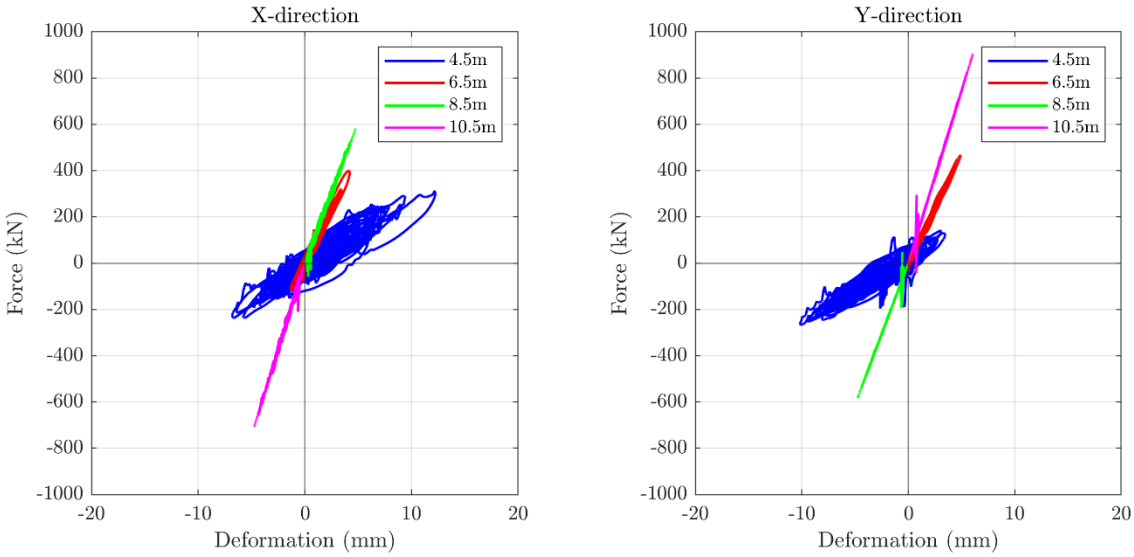

a) X-direction **b) Y-direction**

Figure 5-22: p-y springs hysteretic curves of a building pile

5.10 SUMMARY AND CONCLUSIONS

Table 5-1 and Figure 5-23 summarize the ratios of the key engineering response parameters obtained in the analysis.

Table 5-1: Summary of key engineering parameter ratios

Engineering parameter	Fixed-base	SSI	Ratio SSI/FB
Normalized overturning Moment Y	0.223	0.217	0.98
Normalized overturning Moment X	0.248	0.271	1.10
Normalized base shear X	0.389	0.409	1.05
Normalized base shear Y	0.405	0.441	1.09
Roof drift ratio X	0.005	0.006	1.09
Roof drift ratio Y	0.007	0.008	1.13
Max interstory drift ratio X	0.623	0.665	1.07
Max interstory drift ratio Y	0.810	0.902	1.11

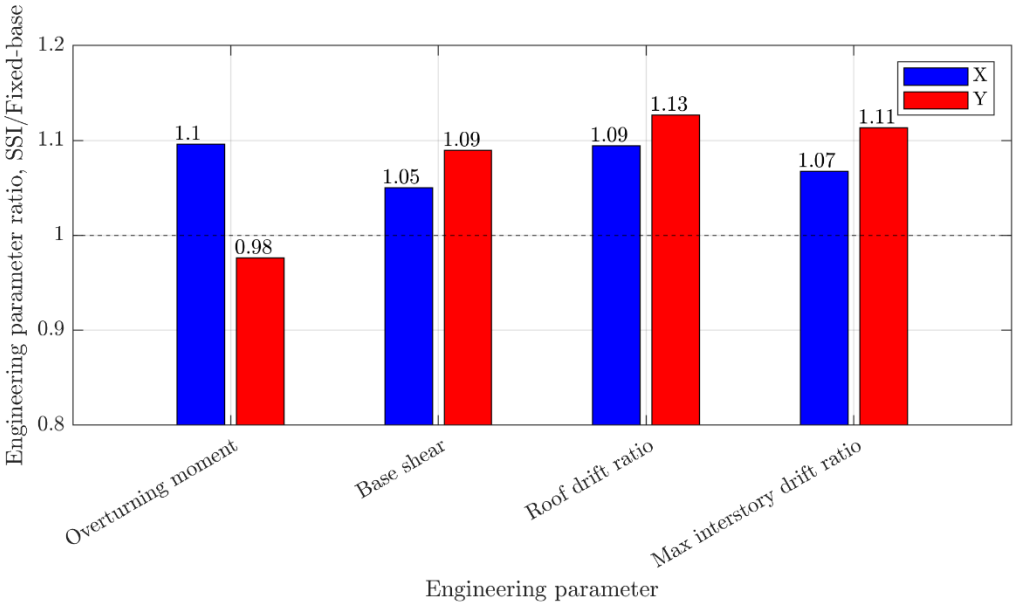

Figure 5-23: Summary of key engineering parameter ratios

In general, the response with both models is very similar, with the responses obtained with SSI being slightly greater than the responses obtained considering the structure with fixed-base. Therefore, in this case study it can be concluded that for the specific building, soil type, input ground motion, and modeling assumptions, SSI is practically negligible.

6 CONCLUSIONS

From the results obtained in this thesis, important conclusions regarding the modeling of soil-structure interaction are generated, specifically when considering piles. It was possible to analyze how the response of a building is modified by incorporating SSI in the model.

Considering an L-Shape configuration, as is typically done in practice, can cause model biases that may not be negligible. Considering only two springs in a 3D model to represent the lateral interaction of a pile with the soil implies an overestimation of the force when loading it diagonally. The L-Shape configuration presents an important directionality. Using models such as Delta Shape or Penta Shape configurations helps to reduce this error. However, it was found that the use of other configurations in the case studied does not generate large differences in the prediction of maximum displacement against an input ground motion.

A case study was performed on a typical Chilean mid-rise building designed with dense array of structural walls following NCh433 (2009). The building is founded on piles on a typical soil profile found in the central business district of Concepcion. To compare the effects of SSI on the building's response, nonlinear fixed-base and on pile models were developed in the program ETABS 20. The models were subjected to the strong input ground motion recorded in the central business district of Concepcion during the 27 February 2010 M_w 8.8 Maule earthquake. Medium and high-rise buildings designed before the earthquake in this part of the city exhibited significant structural damage, including the catastrophic collapse of one medium-rise building. The nonlinear time-history analysis of the fixed-base and on piles models resulted in very similar structural responses, with the model on piles resulting in slightly greater

demands than those recorded for the fixed-base model. In conclusion, for this specific building, soil profile, input ground motion, and modeling assumptions, SSI effects resulted in a slight increase in demands of key engineering response parameters, but the increase did not justify the incorporation of SSI in the analysis.

APPENDIX

APPENDIX 1: API P-Y CURVES CALCULATIONS

This appendix shows the procedure for the calculation of the p-y curves using the equations of the API manual (2000). Since the soil profile considered in this thesis is only composed of sands, the equations of section 6.8.6 and 6.8.7 of the API manual are used.

First, the ultimate resistance p_u is determined with equations 6.8.6-1 and 6.8.6-2 of the API manual:

$$p_u = \min\left((C_1 \cdot H + C_2 \cdot D) \cdot \gamma \cdot H \;;\; C_3 \cdot D \cdot \gamma \cdot H\right) \qquad \text{(A1-1)}$$

Where H is the depth, D is the pile diameter, γ is the effective soil weight. The coefficients C_1, C_2 and C_3 are obtained using figure 6.8.6-1 of the API manual.

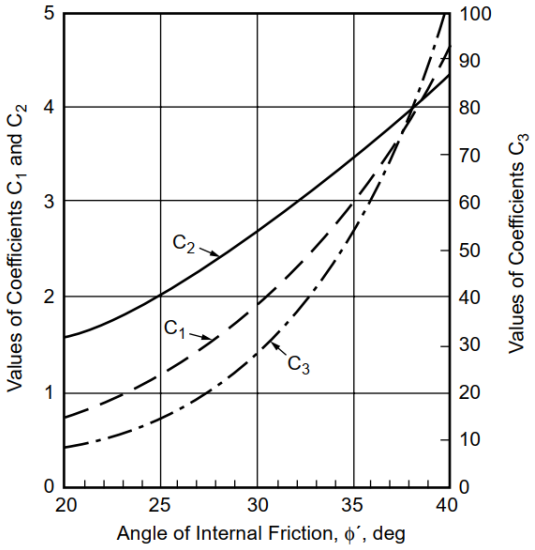

Figure A1-1: Coefficients C_1, C_2 and C_3 API (2000) figure 6.8.6-1

Then, the p-y curve is calculated using the equation shown in section 6.8.7 of the API manual.

$$P = A \cdot p_u \cdot \tanh\left(\frac{k \cdot H}{A \cdot p_u} \cdot y\right) \quad \text{(A1-2)}$$

Where A is the factor to account for cyclic loading condition equal to 0.9, p_u is the ultimate bearing capacity determined as shown above, k is the initial subgrade capacity determined using figure 6.8.7-1 of the API manual, H is the depth, P is the lateral resistance and y is the lateral deflection.

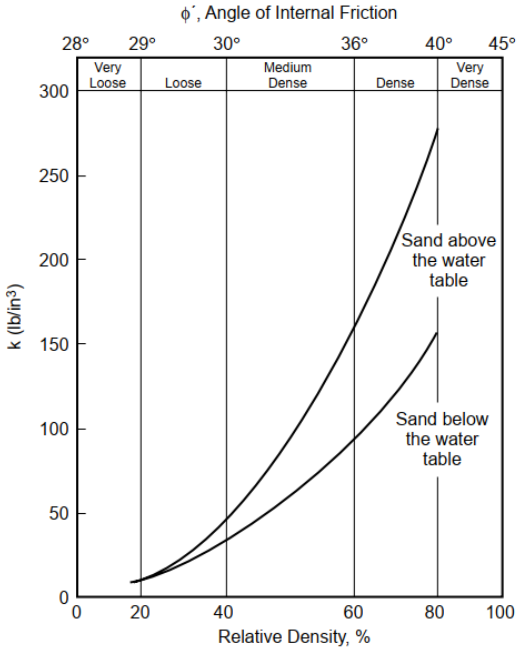

Figure A1-2: Initial modulus of subgrade reaction *k* API (2000) figure 6.8.7-1

An example of the calculation of the p-y curves for 1m, 1.2m and 1.5m diameter piles at a depth of 5 meters is shown below. The parameters of the piles and the soil are shown in Table A1-1.

Table A1-1: Piles and soil parameters for p-y curves calculation

Pile	Diameter (m)	Depth (m)	Below water table?	Soil effective weight (kN/m^3)	Internal friction angle (°)
1	1.0	5	Yes	9	37
2	1.2	5	Yes	9	37
3	1.5	5	Yes	9	37

Table A1-2 shows the coefficients obtained using figure 6.8.6-1 and the values of ultimate bearing capacity obtained.

Table A1-2: Ultimate bearing capacity p_u calculation

Pile	Soil effective weight (kN/m3)	C_1	C_2	C_3	Ultimate bearing capacity p_u (kN/m)
1	9	3.6	3.8	69	981
2	9	3.6	3.8	69	1015
3	9	3.6	3.8	69	1067

Table A1-3 shows the values of initial modulus of subgrade obtained using figure 6.8.7-1.

Table A1-3: Initial modulus of subgrade reaction *k* dtermination

Pile	Internal friction angle (°)	Initial modulus of subgrade reaction k (kN/m^3)
1	37	30580
2	37	30580
3	37	30580

Finally, using equation A1-2 and the parameters from tables Table A1-1, Table A1-2, and Table A1-3, the p-y curves for each pile at 5m depth can be generated. The p-y curves obtained are shown in Figure A1-3.

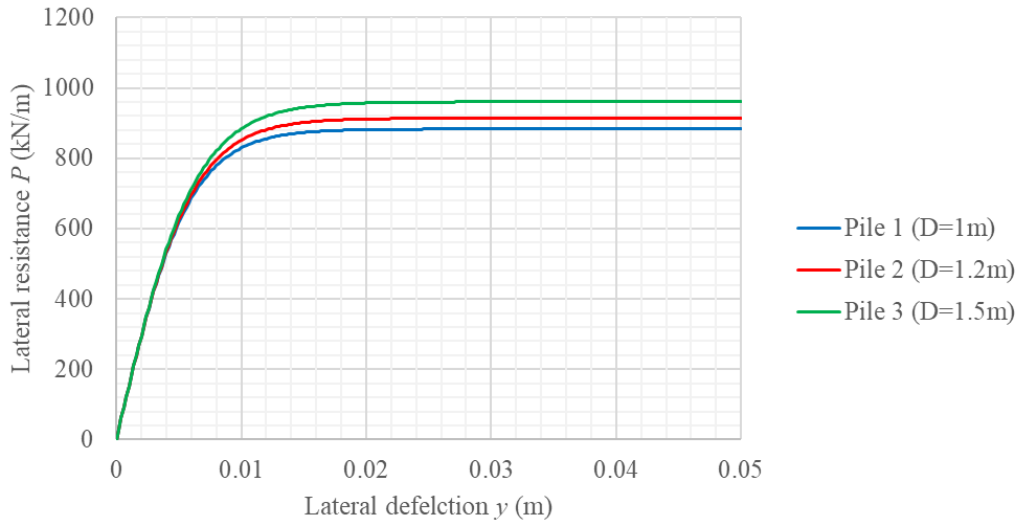

Figure A1-3: API (2000) p-y curves for piles of 1m, 1.2m, and 1.5m diameter at 5m depth

This is the process to generate the p-y curves according to API (2000). These curves are used in the ETABS modeling as the backbone curves for the hysteresis behavior of p-y springs.

REFERENCES

ACHISINA, 2017. Diseño Sísmico Basado en Desempeño: Un procedimiento alternativo para el análisis y diseño sísmico de edificios. *Asociación Chilena de Sismología e Ingeniería Antisísmica.*

ACI, 2019. Building Code Requirements for Structural Concrete (ACI 318-19) and Commentary. *American Concrete Institute*. Farmington Hills, Mich.

Anand, V. and Kumar, S.S., 2018. November. Seismic soil-structure interaction: a state-of-the-art review. In *Structures* (Vol. 16, pp. 317-326). Elsevier.

API, 2000. Recommended Practice for Planning, Designing and Constructing Fixed Offshore Platforms – Working Stress Design. *American Petroleum Institute*. 21st Edition.

ASCE, 2010. Minimum design loads for buildings and other structures. ASCE/SEI 7-10. *American Society of Civil Engineers*.

ASCE, 2016. Minimum design loads for buildings and other structures. ASCE/SEI 7-16. *American Society of Civil Engineers*.

ATC, 1978. Tentative provisions for the development of seismic regulations for buildings. ATC 3-06. *Applied Technology Council*.

Berger, E., Mahi, S.A. and Pyke, R., 1977, May. Simplified method for evaluating soil-pile-structure interaction effects. In *Offshore Technology Conference*. OnePetro.

Biggs, J. M., 1964. Introduction to Structural Dynamics. *Mc Graw & Hill*.

Blandon, C., 2007. Seismic Analysis and Design of Pile Supported Wharves [Ph. D. Thesis] (Doctoral dissertation, Pavia: Universita degli Studi di Pavia).

Boulanger, R.W., Curras, C.J., Kutter, B.L., Wilson, D.W. and Abghari, A., 1999. Seismic soil-pile-structure interaction experiments and analyses. *Journal of geotechnical and geoenvironmental engineering*, *125*(9), pp.750-759.

Boroschek, R., Bonelli, P., Restrepo, J.I., Retamales, R. and Contreras, V., 2014. Lessons from the 2010 Chile earthquake for performance based design and code development. *Performance-based seismic engineering: Vision for an earthquake resilient society*, pp.143-157.

Chen, M.C., Astroza, R., Restrepo, J.I., Conte, J.P., Hutchinson, T. and Bock, Y., 2017. Predominant period and equivalent viscous damping ratio identification for a full-scale building shake table test. *Earthquake Engineering & Structural Dynamics*, *46*(14), pp.2459-2477.

Ciampoli, M. and Pinto, P.E., 1995. Effects of soil-structure interaction on inelastic seismic response of bridge piers. *Journal of structural engineering*, *121*(5), pp.806-814.

CSI, 2016. CSI Analysis Reference Manual for SAP2000, ETABS, SAFE and CSiBridge. Berkeley, California.

Curras, C.J., Boulanger, R.W., Kutter, B.L. and Wilson, D.W., 2001. Dynamic experiments and analyses of a pile-group-supported structure. *Journal of Geotechnical and Geoenvironmental Engineering*, *127*(7), pp.585-596.

Darandeli, M., 2001. Development of a new family of normalized moduli reduction and material damping curves [Ph. D. Thesis] (Doctoral dissertation, Austin: University of Texas at Austin).

De Carlo, G., Dolce, M. and Liberatore, D., 2000, January. Influence of soil-structure interaction on the seismic response of bridge piers. In *Proceedings of the 12th World Conference on Earthquake Engineering* (pp. 1-8). Upper Hut, New Zealand: New Zealand Society for Earthquake Engineering.

Durante, M.G., Di Sarno, L., Mylonakis, G., Taylor, C.A. and Simonelli, A.L., 2016. Soil–pile–structure interaction: experimental outcomes from shaking table tests. *Earthquake Engineering & Structural Dynamics*, *45*(7), pp.1041-1061.

Elgamal, A., Yan, L., Yang, Z. and Conte, J.P., 2008. Three-dimensional seismic response of Humboldt Bay bridge-foundation-ground system. *Journal of structural engineering*, *134*(7), pp.1165-1176.

EN 1998-5; 2004. Eurocode 8: design of structures for earthquake resistance - part 5: foundations, retaining structures and geotechnical aspects. EN 1998-5. Brussels: European Committee for Standardization.

FEMA; 2015. NEHRP recommended seismic provisions for new buildings and other structures. FEMA P-1050. Washington DC: Federal Emergency Management Agency.

Filonenko-Borodich, M.M., 1940. Some Approximate Theories of the Elastic Foundation. *Uchenyie Zapiski Moskovskogo Gosudarstvennogo Universiteta Mekhanica,* Vol. 46, pp. 3–18.

Gajan, S. and Kutter, B.L., 2009. Contact interface model for shallow foundations subjected to combined cyclic loading. *Journal of Geotechnical and Geoenvironmental Engineering*, *135*(3), pp.407-419.

Gazetas, G. and Dobry, R., 1984. Simple radiation damping model for piles and footings. *Journal of Engineering Mechanics*, *110*(6), pp.937-956.

Gazetas, G. and Mylonakis, G., 2001, March. Soil-structure interaction effects on elastic and inelastic structures. In Fourth International Conference on Recent Adavances in Geotechnical Earthquake Engineering and Soil Dynamics. Symposium in Honor of Professor WD Liam Finn. San Diego, California.

Gazetas, G. and Stokoe, K.H., 1991. Free vibration of embedded foundations: theory versus experiment. *Journal of geotechnical engineering*, *117*(9), pp.1382-1401.

Gomez, R., 1982. Rigideces Dinamicas de Grupos de Pilotes. Ph. D. Dissertation, National Autonomous University of Mexico (UNAM).

Hashash, Y.M.A., Musgrove, M.I., Harmon, J.A., Ilhan, O., Xing, G., Numanoglu, O., Groholski, D.R., Phillips, C.A., and Park, D, 2020. DEEPSOIL 7, User Manual. Urbana, IL, Board of Trustees of University of Illinois at Urbana-Champaign.

Hassani, N., Bararnia, M. and Amiri, G.G., 2018. Effect of soil-structure interaction on inelastic displacement ratios of degrading structures. *Soil Dynamics and Earthquake Engineering*, *104*, pp.75-87.

Hetényi, M. and Hetbenyi, M.I., 1946. Beams on elastic foundation: theory with applications in the fields of civil and mechanical engineering (Vol. 16). Ann Arbor, MI: University of Michigan press.

Hilber, H.M., Hughes, T.J.R. and Taylor, R.L., 1976. Improved Numerical Dissipation Algorithms in Structural Dynamics. *Univ. of California, USA*.

Horvath, J.S., 1993. Beam-column-analogy model for soil-structure interaction analysis. *Journal of geotechnical engineering*, *119*(2), pp.358-364.

Hussien, M.N., Tobita, T., Iai, S. and Karray, M., 2016. Soil-pile-structure kinematic and inertial interaction observed in geotechnical centrifuge experiments. *Soil Dynamics and Earthquake Engineering*, *89*, pp.75-84.

INN, 1986, NCh1537.Of1986. Cargas permanentes y sobrecargas de uso, Instituto Nacional de Normalización, Santiago, Chile.

INN, 2009, NCh433.Of1996 Mod.2009. Diseño sísmico de edificios, Instituto Nacional de Normalización, Santiago, Chile.

IS 1893-3; 2014. Criteria for earthquake resistant design of structures - part 3: bridges and retaining walls. IS 1893-3. New Delhi: Bureau of Indian Standards.

IS 1893-4; 2015. Criteria for earthquake resistant design of structures - part 4: industrial structures including stack-like structures. IS 1893-4. New Delhi: Bureau of Indian Standards.

Jarernprasert, S., Bazan-Zurita, E. and Bielak, J., 2013. Seismic soil-structure interaction response of inelastic structures. *Soil Dynamics and Earthquake Engineering*, *47*, pp.132-143.

JSCE 15; 2007. Standard specifications for concrete structures - design. JSCE 15. Tokyo: Japan Society of Civil Engineers.

Kausel, E. and Roesset, J. M., 1974. Soil Structure Interaction Problems for Nuclear Containment Structures. *Electric Power and the Civil Engineer, Proc. of the ASCE Power Div. Conf.*, Boulder, Colorado.

Kausel, E., 2010. Early history of soil–structure interaction. *Soil Dynamics and Earthquake Engineering*, *30*(9), pp.822-832.

Kaynia, A. M. and Kausel, E., 1982. Dynamic Behavior of Pile Groups. *Proc. 2nd Int. Conf. on Numerical Methods in Offshore piling.* Austin, Texas.

Kaynia, A.M. and Kausel, E., 1991. Dynamics of piles and pile groups in layered soil media. *Soil Dynamics and Earthquake Engineering*, *10*(8), pp.386-401.

Kerr, A.D., 1965. A study of a new foundation model. *Acta Mechanica*, *1*(2), pp.135-147.

LATBSDC, 2020. An alternative procedure for seismic analysis and design of tall buildings located in the Los Angeles region. *Los Angeles Tall Buildings Structural Design Council*. 2020 Edition.

Lu, Y. and Panagiotou, M., 2014. Three-dimensional cyclic beam-truss model for nonplanar reinforced concrete walls. *Journal of Structural Engineering*, *140*(3), p.04013071.

Luco, J. E., 1974. Impedance Functions for a Rigid Foundation on a Layered Medium. *Nuclear Eng. and Design*, Vol. 31, pp. 204-217.

Lysmer, J., Udaka, T., Seed, H. B. and Hwang, R. N., 1974. LUSH A Computer Program for Complex Response Analysis of Soil Structure Systems. *UCB/EERC-74/ 4*, U.C. Berkeley.

Martakis, P., Taeseri, D., Chatzi, E. and Laue, J., 2017. A centrifuge-based experimental verification of Soil-Structure Interaction effects. *Soil Dynamics and Earthquake Engineering*, *103*, pp.1-14.

Martel, R. R., 1940. Effect of Foundation on Earthquake Motion. *Civil Engineering*.

Miranda, E. and Bertero, V.V., 1994. Evaluation of strength reduction factors for earthquake-resistant design. *Earthquake spectra*, *10*(2), pp.357-379.

Mononabe, N. and Matsuo, H., 1929. On the determination of earth pressure during earthquakes. *Proc. of the world eng. Conf.*, Vol. 9, p.176.

Mylonakis, G. and Gazetas, G., 2000. Seismic soil-structure interaction: beneficial or detrimental? *Journal of earthquake engineering*, *4*(3), pp.277-301.

Mylonakis, G., Nikolaou, S. and Gazetas, G., 2006. Footings under seismic loading: Analysis and design issues with emphasis on bridge foundations. *Soil Dynamics and Earthquake Engineering*, *26*(9), pp.824-853.

Nova, R. and Montrasio, L., 1991. Settlements of shallow foundations on sand. *Géotechnique*, *41*(2), pp.243-256.

NZS 1170.5; 2004. Structural design actions - part 5: earthquake actions - New Zealand. NZS 1170.5. Wellington: Standards New Zealand.

Okabe, S., 1926. General theory of earth pressure. *Journal of the Japanese Society of Civil Engrs*, Tokyo, Japan.

Priestley, M. J. N., 1974. Mangere Bridge Foundation Cylinder Load Tests. *Ministry of Works and Development Central Laboratories*. Report no. 488. Wellington, New Zealand: Ministry of Works and Development.

Randolph, M.F., 1991. Analysis of the dynamics of pile driving. In *Advanced geotechnical analyses* (pp. 233-282). CRC Press.

Raychowdhury, P. and Hutchinson, T.C., 2009. Performance evaluation of a nonlinear winkler-based shallow foundation model using centrifuge test results. *Earthquake Engineering & Structural Dynamics*, *38*(5), pp.679-698.

Raychowdhury, P., 2011. Seismic response of low-rise steel moment-resisting frame (SMRF) buildings incorporating nonlinear soil–structure interaction (SSI). *Engineering Structures*, *33*(3), pp.958-967.

Reese, L.C., Cox, W.R., and Koop, F.D., 1974, May. Analysis of laterally loaded piles in sand. In *Offshore Technology Conference*. OnePetro.

Restrepo, J.I., 2023, Personal communication.

Roesset, J.M., 2013. Soil structure interaction the early stages. *Journal of Applied Science and Engineering*, *16*(1), pp.1-8.

Sáez, E., Lopez-Caballero, F. and Modaressi-Farahmand-Razavi, A., 2013. Inelastic dynamic soil–structure interaction effects on moment-resisting frame buildings. *Engineering structures*, *51*, pp.166-177.

Sanhueza, E and Verdugo, R., 2010.Peritaje estructural edificio Alto Rio ciudad de Concepción, Informe Final. *N° 644.424-04*.

Seed, H.B. and Idriss, I.M., 1970. Soil moduli and damping factors. *Dynamic Response Analyses, Univ. of California, EERC*, pp.70-10.

Shao, B., 2022. LS-DYNA for Civil/Structural applications [Webinar]. [Online] Oasys LS-DYNA Environment. [Accessed 03 June 2023]. Available from: https://www.youtube.com/watch?v=fkv506akSlc&ab_channel=OasysLS-DYNAEnvironment

Stewart, J., Crouse, C.B., Hutchinson, T.C., Lizundia, B., Naeim, F. and Ostadan, F., 2012. Soil-structure interaction for building structures. Grant/Contract Reports (NISTGCR), National Institute of Standards and Technology, Gaithersburg, MD.

Terzaghi, K., 1955. Evalution of conefficients of subgrade reaction. *Geotechnique*, *5*(4), pp.297-326.

Van Nguyen, Q., Fatahi, B. and Hokmabadi, A.S., 2016. The effects of foundation size on the seismic performance of buildings considering the soil-foundation-structure interaction. *Structural Engineering and Mechanics*.

Van Nguyen, Q., Fatahi, B. and Hokmabadi, A.S., 2017. Influence of size and load-bearing mechanism of piles on seismic performance of buildings considering soil–pile–structure interaction. *International Journal of Geomechanics*, *17*(7), p.04017007.

Wang, S., Kutter, B.L., Chacko, M.J., Wilson, D.W., Boulanger, R.W. and Abghari, A., 1998. Nonlinear seismic soil-pile structure interaction. *Earthquake spectra*, *14*(2), pp.377-396.

Whitman, R. V., 1970. Soil-Structure Interaction. *Seismic Design for Nuclear Power Plants*. Edited by Robert J. Hanson, The M.I.T. Press, Cambridge, Mass.

Winkler, E., 1867. *Die Lehre von der Elasticitaet und Festigkeit: mit besonderer Rücksicht auf ihre Anwendung in der Technik, für polytechnische Schulen, Bauakademien, Ingenieure, Maschinenbauer, Architecten, etc*. H. Dominicus.

Wolf, J. P., 1985. Dynamic Soil Structure Interaction. Prentice Hall.

Wolf, J. P., 1988. Soil-Structure-Interaction Analysis in Time Domain. Prentice Hall.

Zangeneh, A., Svedholm, C., Andersson, A., Pacoste, C. and Karoumi, R., 2018. Identification of soil-structure interaction effect in a portal frame railway bridge through full-scale dynamic testing. *Engineering structures*, *159*, pp.299-309.

Zhang, P., Restrepo, J.I., Conte, J.P. and Ou, J., 2017. Nonlinear finite element modeling and response analysis of the collapsed Alto Rio building in the 2010 Chile Maule earthquake. *The Structural Design of Tall and Special Buildings*, *26*(16), p.e1364.